THE ROLE OF CYCLIN B3 IN MAMMALIAN MEIOSIS

by

Mehmet Erman Karasu

A Dissertation

Presented to the Faculty of the Louis V. Gerstner Jr.

Graduate School of Biomedical Sciences,

Memorial Sloan Kettering Cancer Center

In Partial Fulfillment of the Requirements for the Degree of

Doctor of Philosophy

New York, NY

November, 2018

Scott Keeney, PhD
Dissertation Mentor

Date

DEDICATION

I would like to dedicate this thesis to my parents, Mukaddes and Mustafa Karasu.

I have been so lucky to have their support and unconditional love in this life.

ABSTRACT

Cyclins and cyclin dependent kinases (CDKs) lie at the center of the regulation of the cell cycle. Cyclins as regulatory partners of CDKs control the switch-like cell cycle transitions that orchestrate orderly duplication and segregation of genomes. Similar to somatic cell division, temporal regulation of cyclin-CDK activity is also important in meiosis, which is the specialized cell division that generates gametes for sexual production by halving the genome. Meiosis does so by carrying out one round of DNA replication followed by two successive divisions without another intervening phase of DNA replication. In budding yeast, cyclin-CDK activity has been shown to have a crucial role in meiotic events such as formation of meiotic double-strand breaks that initiate homologous recombination. Mammalian cells express numerous cyclins and CDKs, but how these proteins control meiosis remains poorly understood. Cyclin B3 was previously identified as germ cell specific, and its restricted expression pattern at the beginning of meiosis made it an interesting candidate to regulate meiotic events. Although its first characterization in mammalian cells was nearly 20 years ago, the functions of cyclin B3 have remained elusive.

This thesis examines the role of mouse cyclin B3 in mammalian meiosis. Generation of highly specific monoclonal antibodies enabled characterization of cyclin B3 expression during spermatogenesis. Cyclin B3-deficient mice were generated by CRISRP-Cas9 mediated genome engineering. Unexpectedly, male mice lacking cyclin B3 did not show any detectable meiotic defects. However, mutant females were unable to produce progeny, indicating that cyclin B3 is

essential for female fertility. Moreover, although expression patterns in spermatogenesis led to the expectation of a function for cyclin B3 during meiotic prophase, cyclin B3-ablated ovaries and follicular oocytes were structurally similar to controls, suggesting that meiotic prophase and development of oocytes up to entry into meiosis I are normal. Cyclin B3-deficient oocytes were also able to enter meiosis I when cultured ex vivo. However, they failed to complete the meiosis division I and arrested at the metaphase I to anaphase I transition with hallmarks of defective activation of the anaphase promoting complex/cyclosome (APC/C). Specifically, the arrested oocytes displayed high levels of securin and cyclin B1, high maturation promoting factor (MPF) activity and little or no separase activation. The arrested mutant oocytes could be rescued by inhibiting MPF activity or by injecting mRNA encoding wild-type cyclin B3 or a mutant form lacking its destruction box. Lastly, cyclin B3 homologs from frog, zebrafish and fruitfly could rescue the arrest in cyclin B3 ablated oocytes suggesting evolutionarily conserved roles for this cyclin, and opening up further possibility to study cyclin B3 in more experimentally tractable organisms such as frogs. Together, these studies establish a critical role for cyclin B3 in fine-tuning APC/C activity to promote the unique cell division program of oocyte meiosis.

BIOGRAPHICAL SKETCH

Mehmet Erman Karasu was born on November 8, 1988 in Izmir, Turkey. Erman grew up in Bornova, Izmir and graduated from Izmir Science High School in 2006. He obtained his Bachelor of Science degree in Molecular Biology and Genetics from Bilkent University (Ankara/Turkey). During his undergraduate education, Erman did several internships around the world, including SURP program in Gerstner Sloan Kettering Graduate School in 2010. In 2011, Erman moved to New York and started the doctoral program at Louis V. Gerstner Jr. Sloan Kettering Graduate School. In 2012, he joined the laboratory of Dr. Scott Keeney in Molecular Biology Program at Memorial Sloan Kettering Cancer Center, where he conducted his doctoral dissertation on investigating the role of cyclin B3 in mammalian meiosis.

ACKNOWLEDGEMENTS

First and foremost, I would like to acknowledge and thank my mentor Scott Keeney for his guidance, support and patience. This thesis has been a long and not a smooth journey for me. For the first couple of years, I was not able to make any progress. However, he always stood by me and told me that I can complete this work. I was so lucky to work alongside such a talented and intelligent scientist. I am sincerely grateful that Scott took his time to teach me how to do science properly.

I would like to thank my thesis committee members, Drs. Andrew Koff and Dirk Remus. In particular, I would like to thank Dr. Koff for the characterization of cyclin B3 in mammals and giving me unlimited access to Koff lab antibodies. I would like to thank Dr. John Petrini agreeing on for the chairman position in my thesis committee. I would like to also thank Dr. Debra Wolgemuth not only being my external committee member, but also for the several nice reviews and research papers regarding cyclins during the spermatogenesis.

I would like to thank Keeney lab members, who made the Keeney Lab as a fun place to come and do science every day, including weekends. It was quite a joy to work with all of them and I will definitely miss each one of them in the future. I believe that they were not only colleagues to me but also close friends. I was so lucky to be a part of this amazing group of people. I cannot thank every one of them enough for all the support and assistance on this journey.

I would like to thank particularly Boeke who worked on a gene that I identified in a yeast two-hybrid screen. Boeke took the project from the beginning

and completed it, without him, we might not have heard of the gene called *Ankrd31.*

I would like to thank my “French lab” as well. Nora Bouftas and Dr. Katja Wassmann are the ones I worked with to investigate cyclin B3 in oocytes. The Wassmann group hosted me for 7 months in Paris and taught me how to work with oocytes. Without their collaboration, chapter 3 would not be in this thesis. I cannot thank them enough for their assistance and patience with me.

I would like to thank Corentin Claeys Bouuaert and Ryo Hayama for the discussion on the thesis chapters. In particular, I would like to thank Corentin for critical reading and for his help in editing thesis chapters.

Finally, I would like to thank all my friends and family who have been with me on this journey. I would not have been able to finish this thesis without your support. I love you all.

TABLE OF CONTENTS

LIST OF FIGURES

ABBREVIATIONS:

CDK: Cyclin dependent kinases

SAC: Spindle assembly checkpoint

APC/C: Anaphase promoting complex/cyclosome

IP: Immnunoprecipitation

WB: Western blot

IHC: Immunohistochemistry

IF: Immunofluoresence

Em: Endonuclease mediated

CSF: Cytostatic factor

MPF: Maturation promoting factor

GV: Germinal vesicle

GVBD: Germinal vesicle breakdown

PBE: Polar body extrusion

Introduction

Cell cycle

Cells are the minimal units of life and arise from division of a pre-existing mother cell. To coordinate cell division with the segregation of their genetic material, eukaryotic cells have evolved a cycle that consists of four distinct phases, G1, S, G2 and M (Howard and Pelc, 1986; Nigg, 2001). The cells replicate their chromosomes and other organelles in S phase and distribute these components to daughter cells in M phase. M and S phases are separated by the gap phases, G1 and G2. Cells reside in G1 until they decide to initiate cell division or to exit the cell cycle and stay in the non-dividing stage called G0. Once the cells commit to the cell cycle, there is no return. After DNA replication, cells stay in G2 until conditions are satisfied to enter mitosis (Malumbres and Barbacid, 2005)(Figure 1.1A).

M phase is divided into 5 stages: prophase, prometaphase, metaphase, anaphase and telophase. In prophase, sister chromatids start to condense into compact chromosomes and make connections with the kinetochores. During metaphase, sister chromatids are attached to microtubules coming from the opposite poles of the spindle and align at the cell equator. Once all the chromosomes are aligned and have made the correct interactions with the tubules, the cells are ready to segregate the chromosomes. In anaphase, cells segregate the chromosomes to opposite poles. Finally, during telophase, the

separated chromosomes decondense and nuclear envelope starts to form around the chromosomes. This is followed by cytokinesis, in which the cytoplasm and the organelles are distributed to the daughter cells. These distinct phases of the cell cycle are almost universal, except for a few unusual cases such as early embryonic divisions in frogs that do not have defined G1 and G2 phases (Murray, 1989). The transition between each phase is tightly regulated to ensure a faithful cell division, which is under the control of cell cycle kinases (Malumbres and Barbacid, 2005; Murray, 2004).

Cyclin-CDK complexes in mitosis

The progression through the cell cycle is ensured by activation and inactivation of serine/threonine kinases known as cyclin dependent kinases (CDKs). In the human or mouse genomes, 11 CDKs and 9 CDK-like proteins have been identified (Malumbres and Barbacid, 2005). CDKs are not active by themselves and need to be activated by their regulatory subunits, called cyclins. Cyclins were identified in the 80s from the extracts of star fish oocytes, based on the cyclic pattern of their expression (Evans et al., 1983). The first CDK (Cdc2, Cdc28 respectively), on the other hand, was identified in genetic screens for fission and budding yeast mutants with the defects in the cell cycle (Russell and Nurse, 1986). Cyclins carry a conserved domain of about 150 amino acids (aa), called the cyclin box. This domain consists of five helical regions and is responsible for binding to CDK and cyclin-CDK substrates (Nurse, 1990). Analysis of the human genome yields at least 29 genes encoding proteins that carry a cyclin box

domain (Malumbres and Barbacid, 2005). However, it is still not known whether all these genes are expressed and degraded cyclically. Among those, the most extensively studied families are cyclin D, E, A and B. Their roles are discussed below. Although the main role of a cyclin is in the context of the cell cycle, there is a growing body of studies related to cyclin function independent of cell division, which will not be further discussed in this thesis (Lim and Kaldis, 2013). I will discuss the cyclin types D, E, A and B based on their ordered appearance during the cell cycle (Figure 1.1B).

Cyclin D

Three D-type cyclin genes have been identified in the mammalian genome, cyclin D1 (*Ccnd1*), D2 (*Ccnd2*) and D3 (*Ccnd3*). D-type cyclins govern cell cycle progression from G1 to S phase (Kozar et al., 2004; Sherr, 1994; Sherr and M., 1999). Upon mitogenic signaling, D-type cyclins start to accumulate and bind to CDK4 and CDK6. CDK4-cyclin D and CDK6-cyclin D complexes phosphorylate a number of retinoblastoma (RB) proteins such as pRb, p107 and p130 to drive the cells through G1 phase (Malumbres and Barbacid, 2005). pRb proteins sequester E2F family proteins, thereby suppressing transcription of genes important for DNA replication and cell cycle progression, including E-type cyclins (Cobrinik, 2005). Moreover, pRb proteins have multiple phosphorylation sites that could be targeted by CDKs. CDK4-cyclin D and CDK6-cyclin D complexes can phosphorylate a number of sites on pRb proteins, which prevents the interaction between pRb proteins and E2F. E2F can subsequently promote transcription of

the genes including *cyclin E*, *cyclin A* and *Cdk1* (Ezhevsky et al., 1997; Sachdeva and O'Brien, 2012). (Figure 1.C)

Individual D-type cyclin knock-out mice were generated, and found to be viable. However, each deletion resulted in a distinct phenotype. Briefly, *Ccnd1*-deficient animals showed a reduction in body size and neurological disorders, *Ccnd2*-deficient animals had problems in pancreatic beta cells and had hypoplastic testes and *Ccnd3*-deficient animals had altered immune cell development (Kozar et al., 2004; Sicinska et al., 2003; Sicinski et al., 1996; Sicinski et al., 1995). Distinct phenotypes indicate that D-type cyclins are not redundant in certain biological processes.

Cyclin E

After initial phosphorylation and inactivation of pRB proteins by CDK4/6- cyclin D complexes, E-type cyclins start to express, which form complexes with CDK2. CDK2-cyclin E complexes drive cells from G1 to S phase (Möröy and Geisen, 2004). Mammals have two cyclin E genes, cyclin E1 (*Ccne1*) and cyclin E2 (*Ccne2*). Cyclin E1 and E2 share ~50% amino acid similarity in the entire protein sequence and both of them are co-expressed in cells (Möröy and Geisen, 2004). CDK2-cyclin E complexes further phosphorylate pRb proteins, which leads to irreversible inactivation of pRb proteins (Malumbres and Barbacid, 2001). Cyclin E is also essential for the loading of mini chromosome maintenance protein complex (MCM) onto origins of DNA replication (Geng et al., 2007). Moreover,

other proteins involved in histone biosynthesis, pre-mRNA splicing, centrosome duplication and gene expression control are also substrates for CDK2-cyclin E complexes (Yu and Sicinski, 2004). Knock-out alleles of *Ccne1* and *Ccne2* were generated. Individual deletions of the genes resulted in viable mice with no major defects in cell proliferation (Geng et al., 2003; Parisi et al., 2003). However, *Ccne2* knock-out mice showed interesting fertility phenotypes. *Ccne1* and *Ccne2* double knock out mice died during early embryogenesis, indicating the essential roles of cyclin E family in cell proliferation (Geng et al., 2003). The role of E-family cyclins was further investigated by generating conditional deletions of *Ccne1* and *Ccne2* in testis tissues and the implications will be discussed later in the introduction.

Cyclin A and B

Similar to cyclin E, the mammalian genome encodes two cyclin A genes, cyclin A1 (*Ccna1*) and cyclin A2 (*Ccna2*). Whereas *Ccna1* expresses specifically during spermatogenesis, *Ccna2* is ubiquitously expressed in all tissues (Pines and Hunter, 1990; Ravnik and Wolgemuth, 1996; Sweeney et al., 1996; Wang et al., 1990; Yang et al., 1997). Later in S phase, *Ccna2* transcription starts upon inactivation of pRB, and cyclin A2 forms a complex with CDK2. CDK2-cyclin A complexes further phosphorylate different substrates, for example proteins involved in DNA replication such as Cdc6 and Mcm4, to ensure the completion of S phase (Sherr and Roberts, 1999). At the end of S phase, cyclin A2 also forms complexes with CDK1 and further phosphorylates protein substrates to exit S

phase and enter G2 phase (Wolgemuth and Roberts, 2010). During G2 phase, cyclin A2 is subjected to ubiquitin-mediated proteasomal degradation. Mice lacking *Ccna1* exhibit sterility as expected from the expression pattern (which will be discussed in detail later) (Liu et al., 1998). Mice lacking *Ccna2* died in embryonic development (Murphy et al., 1997). Since *Ccna2* is expressed in all dividing cells, it may not be surprising to find that *Ccna2* is essential for cell cycle progression.

In G2, B type cyclins start to accumulate and form complexes with CDK1 and drive cells from G2 to the end of M phase (Satyanarayana and Kaldis, 2009). There are three different B type cyclins in mammals, cyclin B1 (*Ccnb1*), B2 (*Ccnb2*) and B3 (*Ccnb3*). *Ccnb3* is germ-cell specific, like *Ccna1*, and will be the main topic of this thesis. *Ccnb1* and *Ccnb2* are ubiquitously expressed in the cells from all tissues, similar to *Ccna2* (Brandeis and Hunt, 1996). CDK1-cyclin B complexes regulate several important events during G2-M transition and progression through mitosis, which will be discussed below. Individual targeted mutations of *Ccnb1* and *Ccnb2* were generated (Brandeis et al., 1998). Deletion of *Ccnb1* resulted in embryonic lethality in mice, however, mice lacking *Ccnb2* were viable and fertile with no major phenotype, indicating that *Ccnb1* might compensate for *Ccnb2 in vivo*. Moreover, a recent study indicated that the role of *Ccnb1* can also be compensated by *Ccnb2* during oocyte maturation, which will be discussed below (Li et al., 2018).

Regulation of cyclins in mitosis through proteasomal degradation

The sequential expression of cyclins drives a unidirectional and irreversible progression through the cell cycle in a highly coordinated and controlled manner. In addition to transcription regulation, cyclin/CDK activity is controlled at the level of subcellular localization, post-translational modification and proteolysis (reviewed in (Bloom and Cross, 2007)).

Cell cycle-related, or other proteins are targeted for proteasomal degradation by modification with a highly conserved small protein called ubiquitin. Ubiquitin-mediated proteasomal degradation is coordinated by three enzymes, the ubiquitin-activating enzyme E1, the ubiquitin- conjugating enzyme E2, and the ubiquitin ligase E3. First, E1 enzyme activates the ubiquitin in an ATP dependent manner and transfers it to E2 enzyme. E3 enzyme then catalyzes the transfer of ubiquitin from E2 to the substrate. Poly-ubiquitin attachments mark the protein for proteolysis by the 26 S proteasome (Barford, 2015; Peters, 2006; Pines, 2011).

Two E3 ubiquitin protein ligases are responsible for degrading most of the cell cycle proteins: SCF (Skp1/Cullin/F-box) and the anaphase promoting complex/cyclosome (APC/C) (Cardozo and Pagano, 2004; Heim et al., 2017; Morgan, 2007). SCF is important to degrade cell cycle proteins in G1 and S phases, while APC/C mediates the degradation of mitotic cyclins and triggers chromosome segregation.

APC/C complexes recognize specific degron-containing proteins and promote their proteasomal degradation in a precise order. There are three major degron motifs found in APC/C substrates: the destruction box (D box), KEN box, and the ABBA motif (Glotzer et al., 1991; Littlepage and Ruderman, 2002; Pfleger and Kirschner, 2000). Another motif, called CRY motif, has also been reported (Alfieri et al., 2016; Burton and Solomon, 2001; Burton et al., 2011; Diaz-Martinez et al., 2015; Glotzer et al., 1991; Pfleger and Kirschner, 2000; Yamaguchi et al., 2016). Cyclins carry D-box motifs, containing the arginine at position one and leucine at position four (RxxL). Although a canonical D-box motif is present in many proteins, different sequence versions are also found such as the cyclin B3 D-box motif, RxxF (Gallant and Nigg, 1994). The KEN box, as the name implies, contains a lysine, glutamate and an asparagine, and the ABBA motif is composed of the sequence [ILVF]x[ILMVP][FHY]x[DE] (for Acm1, Bub1, BubR1 and cyclin A) (Di Fiore et al., 2015; Littlepage and Ruderman, 2002). Some proteins contain more than one destruction motif, which increases the affinity of the substrates to APC/C(Davey and Morgan, 2016). For the faithful progression of the cell cycle, it is important to regulate activation of APC/C complexes and also orderly degradation of the substrates.

Meiosis

Meiosis is a specialized cell division in which germ cells undergo one round of chromosome replication followed by two rounds of chromosome segregation to

create gametes (or spores, in yeast). There are unique challenges that meiotic cells need to deal with, in contrast to mitotic cell division. One interesting feature is that there are two chromosome segregation events that occur without an intervening S phase. Another unique aspect of the meiosis is the sister chromatid segregation (Zickler and Kleckner, 2015). In the first round of the segregation, instead of sister chromatids, homologous chromosomes are separated. The sister chromatids separate in the second division. (Figure 1.2)

Meiotic recombination starts with the formation of programmed DNA double strand breaks (DSBs), which occurs uniquely in meiotic prophase I. These DSBs, repaired by homologous recombination, give rise to physical linkages between homologous chromosomes, called chiasmata (Lam and Keeney, 2015). (Figure 1.2) The proper execution of meiotic recombination events that lead to formation of chiasmata is critical for the proper orientation and segregation of homologous chromosomes during the first meiotic division. Thus, failure in homologous recombination or precocious progression into the cell cycle would result in improper segregation of homologous chromosomes, giving rise to aneuploidy in the gametes (Reviewed in (Page and Hawley, 2003; Petronczki et al., 2003)). For this reason, it is critical that homologous recombination is initiated and completed in a timely manner, in coordination with the cell cycle.

Meiotic prophase can be divided into four different stages based on cytological markers: leptonema, zygonema, pachynema and diplonema (Page and Hawley,

2003; Zickler and Kleckner, 2015). In leptonema, chromatin starts to condense and DSBs are formed. As the DSBs are repaired by recombination, the homologs find each other and start to synapse, which defines the zygonema stage. During pachynema, the homologs are fully synapsed, and a subset of the recombination sites are resolved into crossovers. In diplonema, the homologs disassemble from each other and crossover sites become cytologically visible as chiasmata. In mice, 200 to 300 breaks are eventually converted to about 25 crossovers, and the system is controlled to ensure that each pair of chromosomes gets at least one crossover (Cole et al., 2012).

Double strand break formation

The evolutionarily conserved protein Spo11, a type II topoisomerase-like protein, introduces programmed double strand breaks genome-wide (Bergerat et al., 1997; Keeney et al., 1997). The enzymatic activity of Spo11 needs nine other proteins in budding yeast : Mre11, Rad50, Sae2, Ski8, Mer2, Rec102, Rec104, Rec114, Mei4 (Ajimura et al., 1993; Alani et al., 1990; Arora et al., 2004; Cool and Malone, 1992; Gardiner et al., 1997; Ivanov et al., 1992; Johzuka and Ogawa, 1995; Kee et al., 2004; Malone et al., 1997; Menees and Roeder, 1989). The individual deletion of those ten genes in budding yeast results in the absence of DSB formation and consequently synapsis problems and reduced spore viability (Reviewed in (Lam and Keeney, 2015)).

The orthologs of *Rec114*, *Mei4* and (*MER2*) *Iho1* were identified in mouse and deletion of individual genes causes the absence of DSBs genome-wide, indicating *Mei4*, *Rec114* and *Iho1* are also essential for DSB formation (Kumar et al., 2010; Kumar et al., 2018; Stanzione et al., 2016). Moreover, a mutagenesis screen has revealed that *Mei1* (meiosis defective 1) is also essential for DSB formation but there is no indication of how this gene contributes to the initiation of meiotic recombination in the mouse (Libby et al., 2002). Considering the complexity of the mouse genome compared to yeast genome, it is likely that presently unknown proteins are involved in DSB formation together with SPO11.

Homolog synapsis through synaptonemal complexes

Synapsis between homologs is another important step which occurs during meiotic prophase I and is mediated by a proteinaceous structure called the synaptonemal complex (SC) (Reviewed in (Fraune et al., 2012)). The assembly of SC proteins on the chromosomes starts at the leptotene stage; SYCP2 and SYCP3 initiate the formation of fibrous cores along the chromosomes, called the axial elements (AE) of SC, mediated by meiosis-specific cohesin complex proteins, including SMC1ß, RAD21L, REC8 and STAG3 which in turn play a role in holding sister chromatids together (Herrán et al., 2011; Ishiguro et al., 2011; Lee and Hirano, 2011; Prieto et al., 2001; Revenkova et al., 2004; Xu et al., 2005; Yang et al., 2006; Yuan et al., 2000). In zygonema, the AEs of the homologs, now referred to as lateral elements, are interconnected by the central region (CR) that is composed of transverse filaments (TFs) and the central

element (CE). SYCP1 is the major component of TFs. Moreover, four identified proteins, SYCE1, SYCE2, SYCE3 and TEX12, have been shown to specifically localize to CE (Costa et al., 2005; Hamer et al., 2006; Schramm et al., 2011). In zygonema, another meiotic phenomenon called bouquet formation occurs, in which the telomeres become attached to nuclear envelope to form a cluster. Telomere clustering is thought to be another mechanism promoting homolog recognition and pairing (reviewed in (Jan et al., 2012; Scherthan, 2001)). In pachynema, the synapsis between homologs is fully completed. The full chromosome synapsis and proper meiotic DSB repair are dependent on the proper formation of the CE structure. In diplonema, the SC starts to disassemble (Dix et al., 1996; Dix et al., 1997).

Meiotic recombination and crossover designation

Meiotic recombination is another unique and essential feature of meiotic prophase I. Moreover, meiotic recombination and the synapsis of the homologs are highly intertwined events. The introduction of DSBs genome-wide is important for subsequent meiotic events such as the pairing of homologs and meiotic recombination. Once breaks formed, RAD51 and DMC1, two recombinases, are recruited to break sites along with AEs during leptonema (Shinohara and Shinohara, 2004). At the leptonema/zygonema transition, other proteins such as RPA, BLM, MSH4 and MSH5 are involved in the repair of breaks, functioning by localizing in between the AE of homologs and mediating the initial contact between homologs (Moens et al., 2002; Snowden et al., 2008).

In late pachynema, only around 25 of those breaks sites recruit MLH1, which further mature into cross-over sites (Baker et al., 1996). MLH1 can also interact with the CE of the SC and mark the chiasmata sites in the diplotene stage (Froenicke et al., 2002).

Cyclin-CDK complexes in meiotic prophase I in budding yeast

In budding or fission yeast, the cell cycle is governed by a single CDK: Cdc28 or Cdc2, respectively (Hartwell et al., 1970; Nurse and Thuriaux, 1980). As in mitosis, the temporal regulation of CDK by different cyclins is critical for the events occurring in meiosis. Cdc28, along with B type cyclins Clb5 and Clb6 regulates the initiation of replication during S-phase in both mitosis and meiosis (Benjamin et al., 2003; Stuart and Wittenberg, 1998). Mer2 (essential DSB protein) is phosphorylated by Cdc28 (CDK1 in budding yeast) -Clb5/6 (CDK-S phase) on Ser30 and Ser270 (Henderson et al., 2006). This phosphorylation is essential for the initiation of meiotic recombination and for Mer2's interaction with other proteins involved in DSB formation such as Rec114, Mei4 and Xrs2 (Henderson et al., 2006). The further characterization of Mer2 phosphorylation has also revealed that Ser30 phosphorylation primes for Ser29 phosphorylation by Dbf4- dependent kinase Cdc7-Dbf4 (DDK) (Sasanuma et al., 2008; Wan et al., 2008). Moreover, phosphorylation of both Ser29 and Ser30 residues is required for Mer2's role in the initiation of meiotic recombination (Sasanuma et al., 2008; Wan et al., 2008). Further research identified the physical association of DDK with the replisome components, which mediates the chromatin bound

phosphorylation of Mer2 on Ser 30 (Murakami and Keeney, 2014).These studies explicitly demonstrate the contribution of cyclin-CDK complexes to the initiation of meiosis in budding yeast.

Besides Clb5 and Clb6, Clb1, Clb3 and Clb4 are also important for the progression of the meiotic divisions. It has been shown that the restricted expression pattern of Clb3 is important for microtubule- kinetochore interactions during the first meiotic division (Carlile and Amon, 2008; Miller et al., 2012). In one study (Miller et al., 2012), Clb3 which is normally expressed later in meiosis was overexpressed early by using the copper-inducible *CUP1* promoter. The early expression of Clb3 resulted in premature microtubule–kinetochore interactions that led to segregation of sister chromatids instead of homologous chromosomes. These data suggest that temporal regulation of cyclin-CDK activity is essential not only for the initiation of meiotic recombination but also during later steps of meiosis in budding yeast.

Although studies from budding yeast have made major advancement in understanding the role of cyclin-CDK complexes in meiotic progression, specific roles of different cyclin-CDK complexes and their regulation in mammalian cells are not well understood. Next, I review mammalian meiosis and explore how cyclin-CDK complexes can be involved in the regulation of the meiotic events.

Meiosis in mammals

Mammalian meiosis is known as spermatogenesis in males or oogenesis in females and is restricted to germline tissues (testes and ovaries, respectively). Spermatogenesis occurs in the testicular seminiferous tubules, where the location of the cells depends on their stage through meiosis. Primordial spermatogonia, mitotically dividing cells, start to differentiate at the basal site, in the periphery of the tubules. Spermatocytes and spermatids are found progressively closer to the lumen. At the end of the process, mature spermatozoa are released into the lumen. In most mammals, the time required to generate mature spermatozoa takes ~30-40 days (Clermont, 1972). Spermatogenesis starts at the time of puberty and continues during the reproductive lifetime of the animal (Griswold, 2016). In females, the process called oogenesis is initiated during the fetal development but is arrested around the time of the birth. Oogenesis resumes around the puberty which takes months or years depending on the species (Feng et al., 2014). Oogenesis, produces only a limited number of mature gametes that are used during the reproductive lifetime of the animal. Although both developmental programs produce haploid gametes, stark differences exist between the two programs such as the timing of entry into meiosis or the duration of meiotic prophase.

Oogenesis

In mouse oogenesis, the cells stop proliferation and enter meiosis I around 13.5 days post coitum (dpc). They subsequently progress through meiotic prophase I

and around birth enter a specialized, prolonged arrest called dictyate (Speed, 1982). By this time, a large proportion of oocytes pool undergo degeneration by atresia as a quality control mechanism (Tingen et al., 2009). Starting around the time of birth, oocytes surrounded by somatic granulosa cells form primodial follicles. After birth, these follicles enter a growth phase, in which the oocytes increase their volume over 100 fold and reach a final size of ~80 µm in diameter (granulosa cells proliferate generating several cell layers as the oocyte volume increases). These arrested oocytes with the intact nucleus are called germinal vesicle stage (GV). Starting from puberty, arrested oocytes resume their meiosis I prophase following luteinizing hormone- (LH) surge, which is marked by germinal vesicle breakdown (GVBD), equivalent to nuclear envelope breakdown (NEBD) in mitosis. Following GVBD, oocytes progress through the first meiotic division, which is an asymmetric cell division and marked by the extrusion of the first polar body (PB). Oocytes then enter the second meiotic division phase, where they are arrested for the second time and complete meiotic maturation (Masui and Markert, 1971). (Figure1.3) Depending on the mouse strain, the first meiotic division can take 6 hours to 10 hours, which is almost 10 times longer than a typical mitotic cycle (Polański, 1997). Established *in vitro* protocols allow us to examine oocyte maturation and enable us to manipulate the oocyte further as well. The molecular players coordinating the oocyte maturation will be discussed below.

Resumption of meiosis I

Studies from oocytes have shown that the GV-GVBD transition is highly regulated and driven by an increase in cyclin B and CDK activity (identified as maturation promoting factor (MPF) discussed below) (Chesnel and Eppig, 1995; Kanatsu-Shinohara et al., 2000). In GV oocytes, CDK1 activity is inhibited by WEE1/MYT1 kinases. and CDC25A phosphatases, specifically phosphorylation on Thr14- Tyr15 is inhibiting kinase activity of CDK1 (Solc et al., 2010). Upon hormonal stimulation or removal of the cumulus cells in *in vitro* culture, the balance is tilted to increase CDC25A phosphatase resulting in dephosphorylation of Thr14- Tyr15 on CDK1 and activation of CDK1.

On the other side, restraining the nuclear accumulation of cyclin B levels also contributes to keeping the oocytes in the GV stage. Overexpression of cyclin B in GV arrested oocytes prematurely progressed into meiotic prophase (Ledan et al., 2001; Reis et al., 2006). Moreover, APC/C^{CDH1} proteasomal degradation of cyclin B in the nucleus keeps cyclin B levels under control (Holt et al., 2010; Reis et al., 2006). Upon the meiotic resumption, activation of cyclin B-CDK1 leads to phosphorylation of APC/C^{CDH1}, which inhibits activity of the APC/C^{CDH1} and promotes further accumulation of cyclin B1.

M phase regulation through cyclin-CDK complexes and Metaphase I to Anaphase I transition

Throughout metaphase I, cyclinB-CDK1 (MPF) activity is increasing gradually and regulates events such as spindle formation, chromosome condensation and compaction (Figure1.2). Historically, MPF was identified as a transferable activity from cycling Xenopus oocytes to immature oocytes and shown that it is sufficient to drive the meiotic transition (Masui and Markert, 1971; Smith and Ecker, 1971). Later, MPF activity was demonstrated in other organisms and in vitro cell cycle arrested cells (Gerhart et al., 1984; Kishimoto, 1988; Kishimoto et al., 1984; Sunkara et al., 1979; Tachibana and Yanagishima, 1987). During oocyte maturation, MPF activity increases during pro-metaphase. At the metaphase I to anaphase I transition, MPF activity drops suddenly but recovers quickly to drive the cells to the next chromosome segregation. MPF activity stays high in the oocytes until the end of MII and later it cycles during the embryonic cell cycles (Figure 1.3) (reviewed in (Kishimoto, 2018)).

Thus, once the bivalents are aligned on the metaphase I plate and the correct microtubule- kinetochore interactions are ensured, two main substrates, securin and cyclin B1, need to be degraded by APC/C^{CDC20} to activate separase, which in turn cleaves the RAD21/REC8 subunits of the cohesion ring on the chromosome arms, resulting in the segregation of homologs (Burton and Solomon, 2001; Herbert et al., 2003; Hilioti et al., 2001) (Figure1.4).

APC/C is a 1.5 megadalton complex composed of 15 to 17 subunits, depending on the organism (Pines, 2011). Its activity fluctuates during the cell cycle, primarily based on its association with either CDC20 or CDH1 (Pines, 2011; Primorac and Musacchio, 2013; Sivakumar and Gorbsky, 2015). During mitosis, APC/C is activated by binding to CDC20 and is dependent on phosphorylation by CDK1-cyclin complexes. Recent biochemical studies showed that CDK1 phosphorylates internal loop domain of APC/C subunit called APC1. When the loop is not phosphorylated, it prevents CDC20-N terminal domain to access to the APC/C. Upon phosphorylation, this inhibition by the loop is relieved, CDC20 interacts with the core subunit of APC/C and activates APC/C (Fujimitsu et al., 2016; Qiao et al., 2016). APC/C^{CDC20} activation leads to the destruction of cyclin B and the separase inhibitor securin, which triggers chromosome segregation (Heim et al., 2017; Pines, 2011; Primorac and Musacchio, 2013; Sivakumar and Gorbsky, 2015). Cyclin B degradation and drop in CDK1 activity deactivates APC/C^{CDC20}. In turn, APC/C^{CDH1} is activated, which drives mitotic exit and suppresses cyclin-CDK complexes till the end of G1 (Heim et al., 2017). In meiosis I transition though, APC/C is inactivated to allow rapid accumulation of cyclin B to maintain high MPF activity during anaphase exit, which prevents cells to exit from the cell cycle. However, a failure to degrade either cyclin A2 or cyclin B1 at the metaphase-to-anaphase transition prevents exit from meiosis I in mouse oocytes, which indicates the importance of APC/C activity during the transition (Herbert et al., 2003; Polanski et al., 1998; Touati et al., 2012).

Spindle assembly checkpoint mediated control of APC/C activity

Cells have evolved a control mechanism to prevent chromosome segregation in the case of incorrect kinetochore- microtubule attachment, named spindle assembly checkpoint (SAC) (reviewed in (Polański et al., 2012)) (Figure1.5). Briefly, a group of proteins from MAD (for Mitotic arrest deficient) and BUB (for Budding uninhibited by benzimidazole) signal unattached kinetochores to the APC/C (Musacchio and Salmon, 2007; Vogt et al., 2008). SAC is composed of MAD2, MAD1 BUB1, BUBRI, BUB3 and MPS1 (Musacchio and Hardwick, 2002). In the case of inappropriate kinetochore- microtubule attachments, MAD2, BUBR1 and BUB3 bind to CDC20 and form mitotic checkpoint complex (MCC) and sequester it from APC/C (reviewed in (Bury et al., 2016)). Although SAC control is not as efficient in oocytes as in cultured cells (Kyogoku and Kitajima, 2017), it can keep the APC/C inactive until the kinetochore and microtubules attachments are satisfied.

Spermatogenesis

Spermatogenesis shows the following unique features. After differentiation to B-type spermatogonia, spermatocytes enter meiotic prophase in which they spend an extended period of time (~10-12 days). Cells pass sequentially through pre-leptotene, leptotene, zygotene, pachytene and diplotene stages. Among those stages, spermatocytes stay in the pachytene stage for ~6-7 days, which is one of the unique features of spermatogenesis. After that, the cells experience two sequential quick M phases to produce haploid spermatids. With respect to cell

cycle progression, it is not clear how Cdk-cyclin complexes control the timing of specific phases during spermatogenesis. However, several studies have demonstrated the regulated expression of cyclins during spermatogenesis (below).

Regulated cyclin expression during spermatogenesis

Among the cyclins presented in Figure 1.6, two cyclins show meiosis-specific expression, *Ccna1* and *Ccnb3* (reviewed in (Wolgemuth and Roberts, 2010)). Although the putative CDK partners for each cyclin have not been fully determined, the expression of CDK1, 2, 4, 5, 6 and 16 have been detected in testis tissue (Mikolcevic et al., 2012; Session et al., 2001; Wolgemuth and Roberts, 2010).

Phenotypes of cyclin-CDK knock outs and their implications on spermatogenesis

Since cyclin-CDK complexes are shown as the master regulators of the cell cycle, they have been subject to knockout experiments in mouse. For example, *Ccnb2, Ccnd1*, *Ccnd2*, *Ccnd3*, *Cdk4* and *Cdk6* knockouts result in completely fertile or slightly less fertile males (Beumer et al., 2000; Brandeis et al., 1998; Malumbres et al., 2004). *Ccna2*, *Ccnb1*, *Cdk1* and *Cdk5* knockouts result in embryonic lethality, which precludes the characterization of a potential role in spermatogenesis (Beumer et al., 2000; Brandeis et al., 1998; Ko et al., 2001; Santamaría et al., 2007).

Knocking-out meiosis-specific *cyclin A1*, the expression of which is restricted to late pachytene and diplotene, causes infertility in male mice (Liu et al., 1998). The examination of testis cells reveals that meiotic cells are arrested at a late stage of meiotic prophase I (late diplotene) (Liu et al., 1998). Later findings suggest that *Ccna1* plays a role in phosphorylation of H3 Serine 10 at the centromeres and the recruitment of aurora B kinase to pericentromeric regions (Nickerson et al., 2007), but the specific cause of the arrest is not fully understood.

A knock-out of *Cdk2*, the putative catalytic partner of *Ccna1*, also results in the meiotic arrest in males although at a different stage of meiotic prophase (pachytene) (Berthet et al., 2003; Ortega et al., 2003; Viera et al., 2009). In these cells, DSBs are formed but pairing of homologs and the repair of DSBs is incomplete, indicating that *Cdk2* plays an important role subsequent to programmed DSB formation. Furthermore, the different phenotypes of the *Cdk2* and *Ccna1* mutants suggest that although *Cdk2* is known as the putative *Ccna1* partner, there may be other cyclins that form a complex with *Cdk2* in early meiotic prophase. These examples support the idea that different cyclin-CDK complexes play a defined role during different stages of meiosis.

Mice lacking either *Ccne1* or *Ccne2* were viable with no major defects (Geng et al., 2003). However, *Ccne2* knock out males showed spermatogenesis and

fertility problems. Although slightly smaller testes were also observed in *Ccne1* knock-out mice, this did not affect the fertility of *Ccne1* knock out males. The embryonic lethality of *Ccne1* and *Ccne2* double knock outs impaired the elucidation of the roles of E-type cyclins during spermatogenesis. However, this was elegantly addressed by a recent study from the Wolgemuth lab (Martinerie et al., 2014). In the study, the authors were able to generate *cyclin E1* and *E2* double knockout spermatocytes by utilizing a conditional knock out allele of cyclin E1. Analysis of the *cyclin E2* single knockout showed that cyclin E1 levels were elevated in spermatocytes to compensate the absence of cyclin E2. The additional testes-specific deletion of cyclin E1 resulted in severe meiotic defects such as abnormal pairing, synapsis of homologous chromosomes, unrepaired DSBs and defects in CDK2 localization, which reveals the important roles for E-type cyclins during early-mid meiotic prophase in mammals. Moreover, this study also sheds light on why the phenotype of *Cdk2* mutants differ from *Ccna1* mutants in which the spermatocytes are arrested at the end of the meioitic prophase I. Double deletion of E-type cyclins phenocopied the *Cdk2* deletion in spermatogenesis, suggesting that cyclin E-CDK2 complexes have more prominent roles in early meiotic events than cyclin A-CDK2. However, the substrates of cyclin E-CDK2 during spermatogenesis have not yet been uncovered.

Cyclin B3

Discovery of *Ccnb3*

Ccnb3 was first identified in a chicken cDNA library and amino acid sequence comparisons revealed common features to other B-type cyclins (Gallant and Nigg, 1994). Cyclin B3 also shows properties similar to A-type cyclins, such as nuclear localization, but forms its own family distinct from A and B type cyclins (Gallant and Nigg, 1994; Gunbin et al., 2011). Later, cyclin B3 was detected in other organisms such as worms, flies, mouse and human (Kreutzer et al., 1995; Lozano et al., 2002; Nguyen et al., 2002; Sigrist et al., 1995).

Expression and targeted mutants of *Ccnb3* in metazoans

Ccnb3 is present through metazoans and diverse expression patterns are observed in different organisms. For example, *Ciona intestinalis Ccnb3* counteracts zygotic genome activation in the embryo, thus maternal *Ccnb3* mRNA diminishes at the time of zygotic transcription onset (Treen et al., 2018). In *Xenopus laevis* oocytes, no cyclin B3 protein was detected in oocytes and during the first embryonic divisions by western blot analysis (Hochegger et al., 2001), but this may also have been due to low expression levels relative to other B-type cyclins in this system. It has not yet been addressed whether *Ccnb3* has a role in meiotic or embryonic cell cycle progression in the frog. *Drosophila melanogaster Ccnb3* is dispensable for mitotic divisions, but is essential for female fertility (Jacobs et al., 1998). Besides its unique meiotic role, *Ccnb3* was shown to play a redundant role in mitosis by cooperating with *Ccnb* and *Ccna*,

but neither *Ccnb3* nor *Ccnb* is required for mitosis (Sigrist and Lehner, 1997). In flies, cyclin B3 promotes anaphase onset in early embryonic divisions (Yuan and O'Farrell, 2015), and loss of cyclin B3 perturbs exit from meiosis I (Jacobs et al., 1998). Moreover, *Drosophila* cyclin B3 is degraded depending on the APC/C in mitosis, with delayed timing relative to cyclin A and B (Sigrist et al., 1995; Yuan and O'Farrell, 2015). *C. elegans* and *Drosophila* cyclin B3 associate with CDK1 (Jacobs et al., 1998; van der Voet et al., 2009), and *in vitro* kinase activity was detected for *C. elegans* CDK1-cyclin B3 complexes (van der Voet et al., 2009).

Expression and targeted mutants of *Ccnb3* in mammals

Mammalian *Ccnb3* is uniquely and specifically expressed during meiosis; expression was detected during a small window of meiotic prophase, through leptonema and zygonema by in-situ mRNA hybridization in both spermatogenesis and oogenesis (Nguyen et al., 2002). This was interesting to us because these are the stages in meiosis when most of the DSBs are formed and homologous chromosomes start to pair. Moreover, the relevance of this restricted expression window for *cyclin B3* has been tested in a mouse model where ectopic human *Ccnb3* was expressed through meiotic prophase beyond the zygotene stage (Refik-Rogers et al., 2006). Prolonged expression of *Ccnb3* in testis perturbed spermatogenesis leading to reduced fertility and increased apoptosis during spermatogenesis. This suggests that the temporally restricted expression and destruction of *cyclin B3* could be important for proper spermatogenesis.

Interestingly, cyclin B3 protein has increased sharply in size in placental mammals due to the extension of a single exon, potentially required for novel protein-protein interactions. Cyclin B3 may therefore exert additional, unknown roles during cell division in mammals. Cyclin B3 was found to interact with CDK2, although no associated kinase activity was detected (Refik-Rogers et al., 2006). In female mice, cyclin B3 was speculated to be required for meiotic initiation because cyclin B3 mRNA becomes substantially upregulated as oogonia cease mitotic proliferation and enter meiotic prophase I (Miles et al., 2010). RNAi-mediated knock-down of cyclin B3 to ~30% of wild-type levels in cultured mouse oocytes perturbed progression through meiosis I (Zhang et al., 2015), although the molecular basis of the inhibition of meiotic progression in these experiments was not defined and off-target effects of the RNAi could not be excluded, so the function of cyclin B3 in oocyte meiosis remained unclear. Given that *Ccnb3* expression pattern is restricted to early meiotic prophase in mammals, I set out to test the hypothesis that *Ccnb3* is important to coordinate early meiotic events (such as DSB formation, recombination, and homolog pairing) to meiotic cell cycle progression.

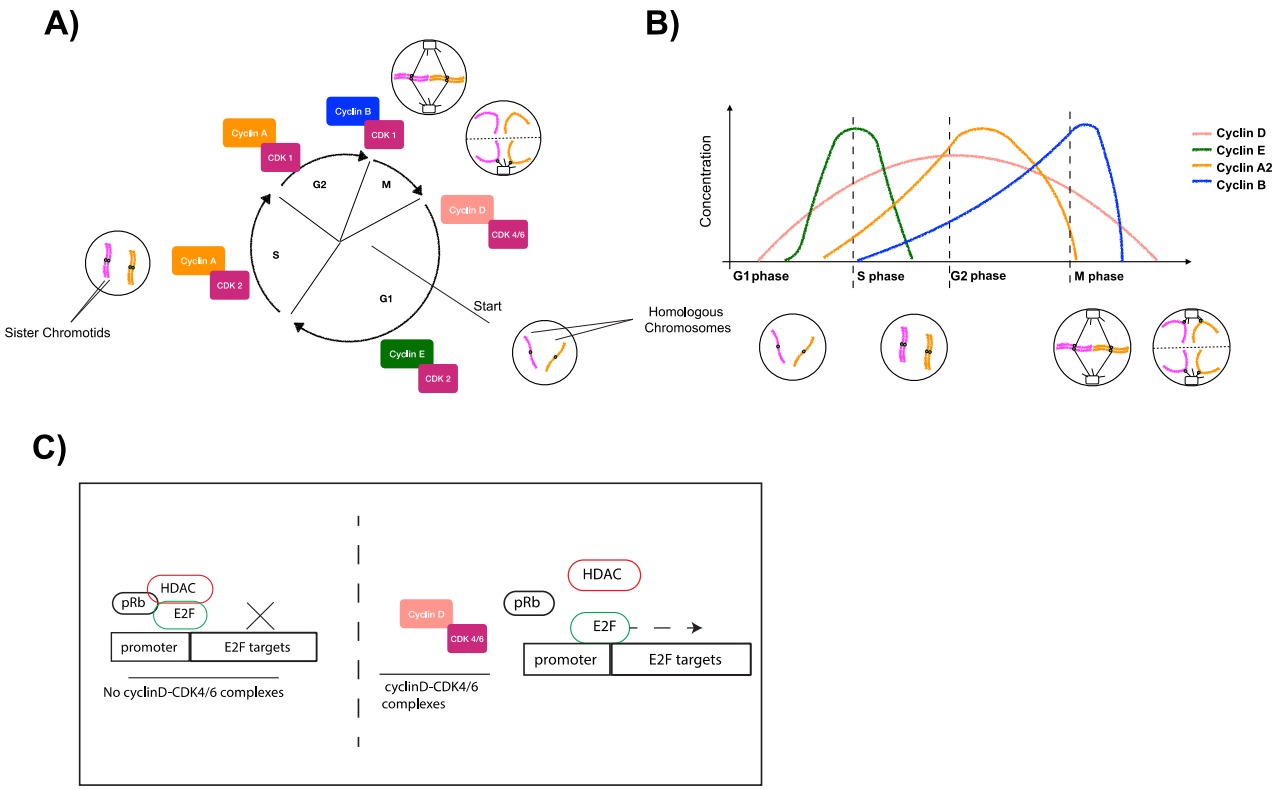

Figure1.1: The generic cell cycle and cyclin expression during mitosis.
A) The diagram represents the different phases of the cell cycle. The cell starts to express cyclinD- CDK4/6 complexes in G1. Phosphorylation of Rb proteins leads to expression of cyclin E-CDK2 complexes, which drives the cells from G1 to S phase. During S phase, chromosomes are replicated (shown in magenta and orange) and cyclin A-CDK2 complexes ensures S phase completion. At the end of S phase, cyclinA-CDK1 complexes takes place and prepares the cells to G2 phase. At the transition from G2-M phase, cyclin B- CDK1 complexes regulate several important events and drive the cells through M phase.
B) The graph shows the accumulation and degradation of cyclins during the mitotic cell stages
C) The diagram describes the events during G1 phase, which results in activating E2F targets by phosphorylating pRb with cyclinD- CDK4/6 complexes.

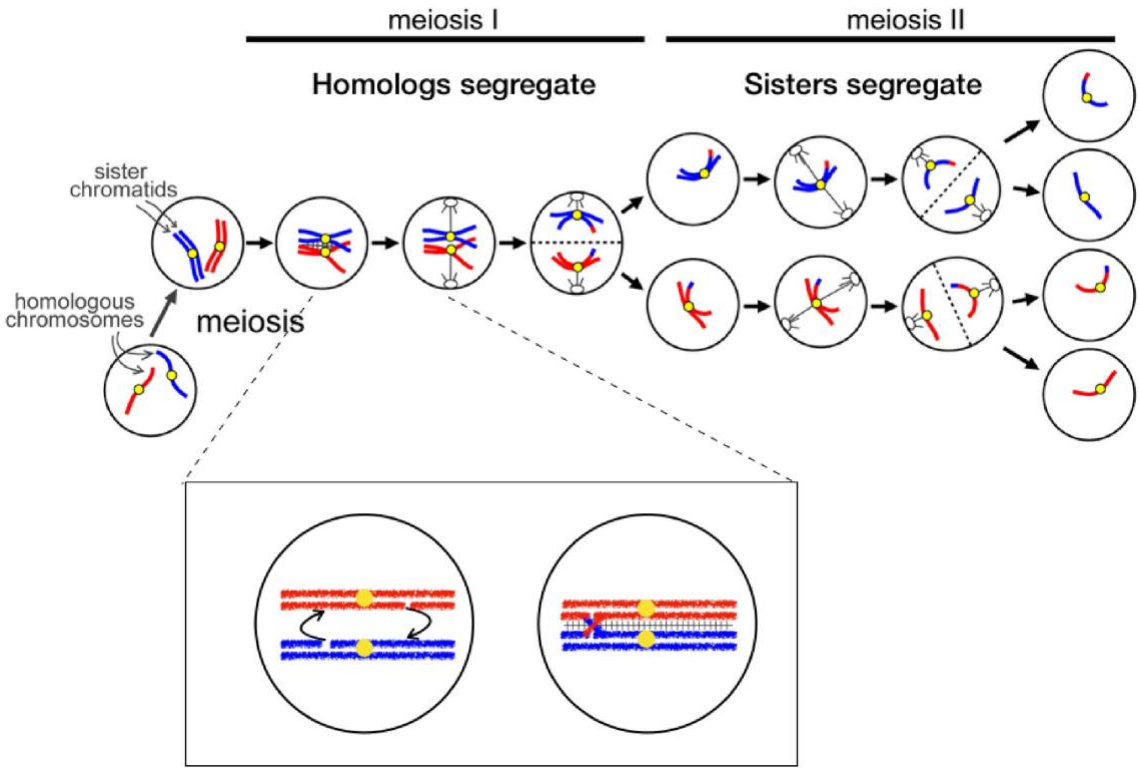

Figure 1.2: Diagram for meiotic cell cycle.
In meiosis, the genome content of the parental cell (2n) is reduced in half by undergoing two consecutive rounds of division following one round of DNA replication (premeiotic S phase). After replication,each homologous chromosome consists of a pair of sister chromatids. Meiosis I is a reductional division in which homologous chromosomes are segregated. At the beginning of the meiosis, DSBs are introduced genome wide.(shown in bottom panel) Through DSB repair by homologous recombination, each paternal and maternal homolog pair and physically connect them, thereby allowing their correct segregation onto daughter cells. (Adapted from Esther de Boer's Thesis, Wageningen Universiteit, (de Boer, 2007))

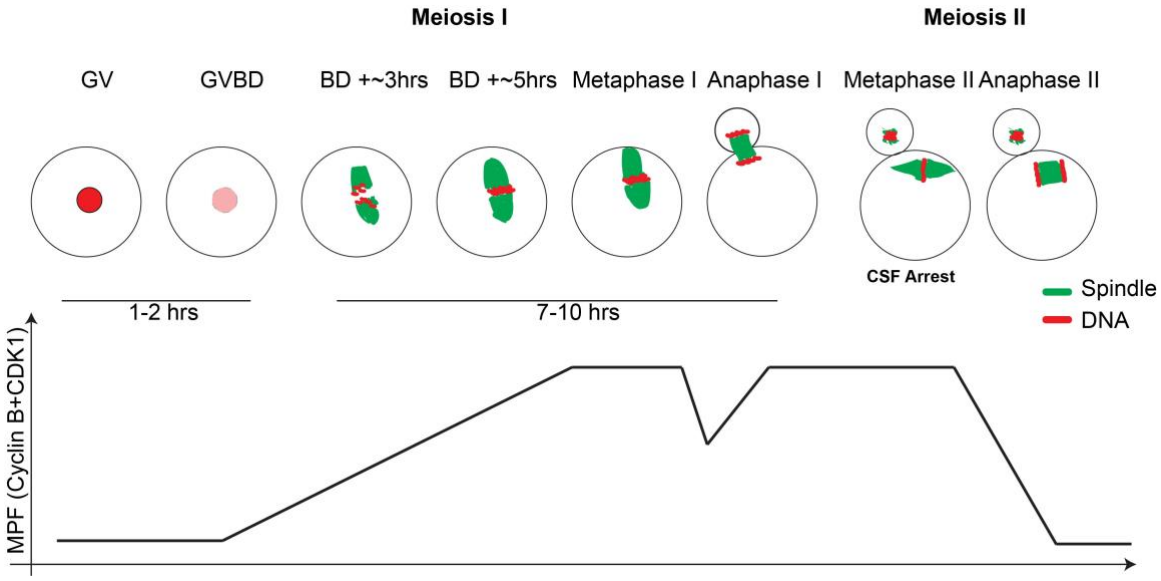

Figure1.3: Maturation of GV stage oocytes and MPF regulation during the maturation.
The upper panel represents the dynamics of the spindle (green labeled) and chromosomes (red labeled) during the oocyte maturation. In vitro culture conditions, GV stage oocyte starts to resume their meiosis, which is associated with GVBD (takes 1-2 hours). After GVBD, by increasing MPF activity, spindles are formed around the chromosomes and chromosomes start to congress and gets condensed. 7-10 hours after GVBD, oocytes go through the first division, associated with asymmetrical cytokinesis called (PBE). After MI division, MPF activity starts to rise again and inhibits the oocytes going through S phase, leading them to go immediately to metaphase II. Oocytes are arrested in this stage, CSF arrest, until they are fertilized by the sperm. Upon fertilization, oocytes can complete its chromosome segregation.
The lower graph shows MPF activity during the oocyte maturation. (Adapted from (Polański et al., 2012))

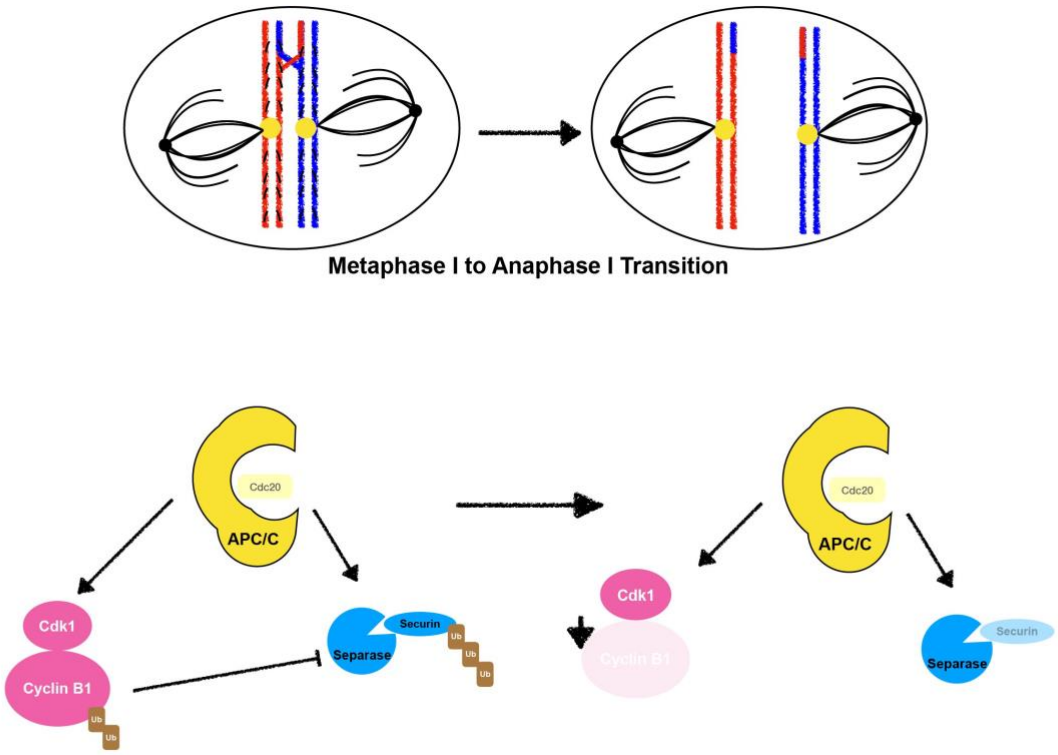

Figure1.4: APC/C mediated degradation of cyclin B1 and securin. Once the chromosomes are aligned on the metaphase plate and kinetochore-microtubule attachments are satisfied, APC/C^{CDC20} catalyzes the ubiquitination of cyclin B1 and Securin, which promotes the proteasomal degradation of these subunits. Once Separase inhibition is relieved, Separase can cleave the cohesion on the chromosome arms and chromosomes can be separated.

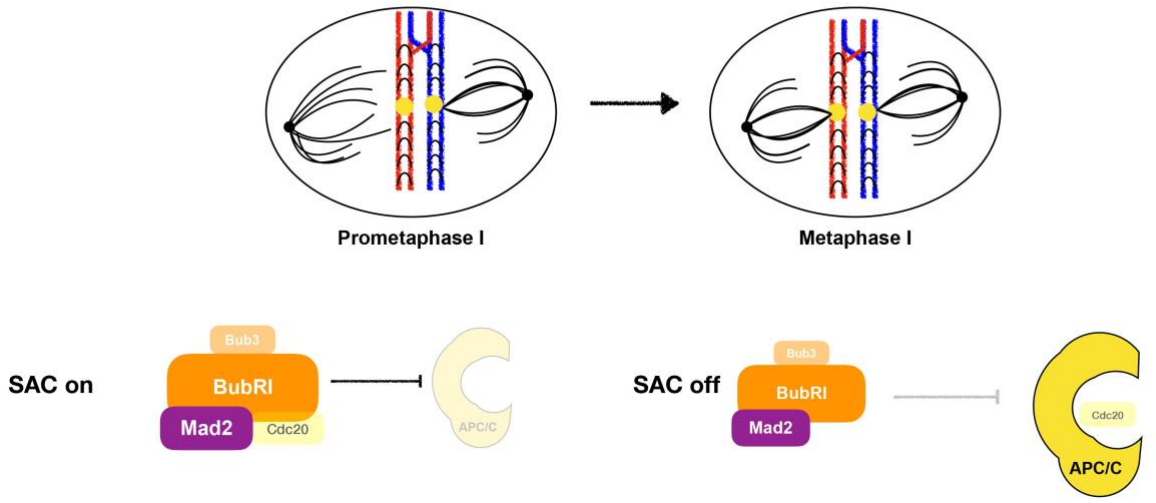

Figure1.5: SAC mediated APC/C inhibition.
In the case of incorrect kinetochore-microtubule attachments, SAC proteins can bind to CDC20 and sequestered it from APC/C binding. Until, the cell makes correct attachments, APC/C activity is inhibited, and chromosome segregation is delayed.

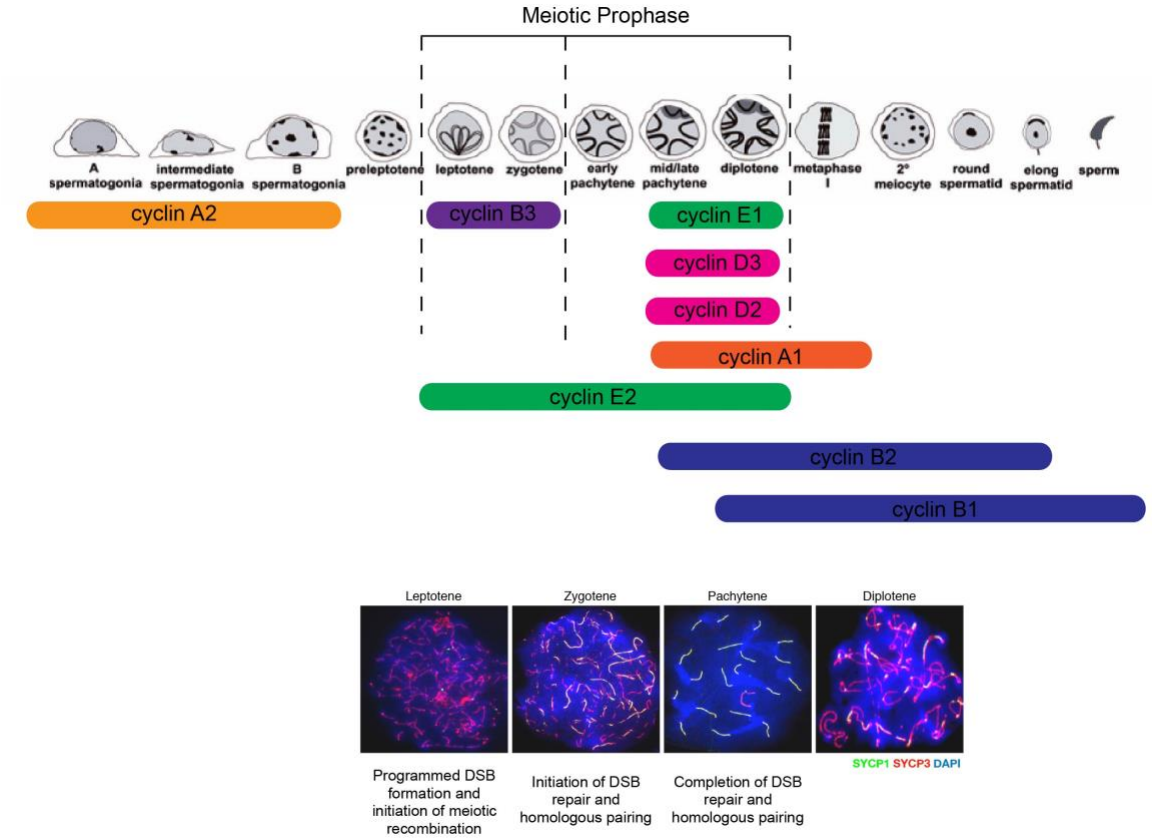

Figure1.6: Cyclin expression during spermatogenesis and meiotic prophase stages.
Expression of individual cyclins during spermatogenesis. *Cyclin B3* (shown with purple bar) expression is confined in the early meiotic prophase. Besides *cyclin B3*, *cyclin A1*, *A2*, *E1*, *E2*, *D3*, *D2*, *B1* and *B2* are also highlighted on the diagram. (Adapted from (Wolgemuth et al., 2013)). Bottom side shows the representative micrographs stained with SYCP1 and SYCP3 from leptotene to diplotene stage. Important meiotic recombination events are noted below each micrograph.

SCOPE OF THE THESIS:

The central focus of my thesis is the role of *Ccnb3* in mammalian meiosis. The story begins with the generation of antibodies against cyclin B3 and of *Ccnb3* knock out animals by utilizing CRISPR-Cas9 mediated genome targeting. By breeding founder mice, I generated *Ccnb3* knock out males and females, which were viable. Since *Ccnb3* was thought to have a role in spermatogenesis, I expected the males to be sterile. However, *Ccnb3* knock out males were fully fertile, had normal testis sizes, and displayed no detectable meiotic abnormalities (i.e., meiotic progression, recombination, and divisions appeared completely normal). Using monoclonal antibodies generated against cyclin B3, I found that full-length protein was absent from mutant testes and, importantly, no truncated form of the protein could be observed. Thus, the frame shift alleles appear to be null or near-null for *Ccnb3* expression. Therefore, *Ccnb3* appears to be dispensable for normal male meiosis.

Remarkably however, *Ccnb3* knock out females were sterile. Importantly, *Ccnb3* knock out ovaries and follicular oocytes appeared structurally normal, and oocyte numbers were normal. Thus, meiotic prophase and development of oocytes up to entry into meiosis I are normal in *Ccnb3* knock out females. However, *Ccnb3* knock out oocytes do not complete MI properly under *in vitro* culture conditions. Specifically, *Ccnb3* knock out oocytes do not extrude polar bodies, which suggests a failure to progress through the metaphase-to-anaphase transition. By

western blot analysis, I showed that arrested knock out oocytes do not degrade securin and cyclin B1 efficiently compared to WT oocytes during MI division. Moreover, *Ccnb3* knock out phenotype can be rescued by injection of wild type and D-box deleted *Ccnb3* mRNAs, but not with MRAIL-mutant *Ccnb3* mRNA. Furthermore, *Ccnb3* knock out phenotype can be rescued by the injection of *X. laevis* and *D. rerio* and *D. melanogaster Ccnb3* mRNA, indicating an evolutionarily conserved role for *Ccnb3*.

CHAPTER II: THE ROLE OF CYCLIN B3 IN SPERMATOGENESIS:

Summary:

To analyze the *in vivo* role of *Ccnb3*, I generated a *Ccnb3* mutant allele (*Ccnb3*^{em1}) by employing a CRISPR-Cas9 mediated gene targeting, which deleted 14 bp and caused an out-of-frame mutation in the coding sequence of *Ccnb3*. *Ccnb3* knock out mice (both male and females) were viable and did not show any somatic phenotypes during their development. Contrary to my hypothesis, male mice lacking *Ccnb3* were fertile and displayed no meiotic abnormalities, indicating that *Ccnb3* is dispensable for spermatogenesis. I generated monoclonal antibodies against cyclin B3 and detected the presence of the endogenous mammalian cyclin B3 signal for the first time. Cyclin B3 signal was absent in knock out animals and the levels of *Ccnb3* mRNA were greatly reduced too, indicating that the *Ccnb3*^{em1} allele represents a null allele of *Ccnb3*.

Background:

As described in the introduction, in budding yeast, cyclin-CDK complexes play an essential role during meiosis. In mammalian meiosis, *Ccnb3* mRNA is germ-line specific and it is expressed in both spermatocytes and oocytes during the

leptotene and zygotene stages of meiotic prophase I when most DSBs are formed (Nguyen et al., 2002). I would like to test the hypothesis that *Ccnb3* regulates events during early meiosis, such as initiation of meiotic recombination. In this chapter, I addressed the role of *Ccnb3* during spermatogenesis.

RESULTS:

CCNB3 antibody generation and CCNB3 expression pattern.

The *Ccnb3* locus, which spans 62 kb on the X chromosome (coordinates chrX:6,556,778–6,618,745, mm10 genome assembly), gives rise to a 4.1-kb mRNA that comprises 14 exons and encodes a protein of 157.9 kDa (Figure 2.1). Until now, although *Ccnb3* mRNA could be detected in mammalian germ cells, endogenous cyclin B3 could not be detected due to lack of appropriate antibody (Nguyen et al., 2002). To overcome this, I generated monoclonal antibodies against CCNB3 with Abmart Inc (Shanghai, China). A total of 23 monoclonal antibodies were raised against 8 different peptides (see the positions of the peptides in Figure 2.1B).

To detect endogenous cyclin B3, I sought to enrich the cyclin B3 signal by immunoprecipitation (IP) prior to detection by western blotting. Out of 23 monoclonal antibodies, I found that two antibodies (N-term anti-CCNB3 (peptide #18) and C-term anti-CCNB3 (peptide #5) behaved well in the IP-western blot experiments. By using C-term anti-CCNB3 for IP and probing with N-term anti-

CCNB3 for western blotting, I was able to detect endogenous cyclin B3 from wild type testes extract but not spleen tissue extract (Figure 2.2A). The protein migrated as a doublet above 150 kDa. The slower-migrating band may present post-translational modification states of cyclin B3.

To gain further insights into *Ccnb3* expression during the first wave of meiosis, I collected testes from wild type males at 6, 10, 12 and 16 days postpartum (dpp) and analyzed mRNA expression levels by quantitative reverse transcription polymerase chain reaction (RT-qPCR). I found that *Ccnb3* expression is at minimal or background level at 6 dpp, where seminiferous tubules contain only somatic and spermatogonia cells. At 10 dpp, *Ccnb3* signal was elevated and peaked at 12 dpp where seminiferous tubules are mostly populated with leptotene and zygotene cells (Figure 2.2B). This is in agreement with published RNA-seq results (Margolin et al., 2014) and a previous cyclin B3 study (Nguyen et al., 2002).

To evaluate whether protein levels mirrored the mRNA levels, I also performed IP- western blot experiments with extracts from 6, 10, 12 and 16 dpp testes. Although the best way is to analyze RNA and protein levels from the same samples or animals, the material obtained from juvenile animals does not suffice for both experiments. Thus, I had to collect samples from two different cohorts of animals, which will be relevant to the interpretation of the results below. I repeated the IP-western blot experiment three times and each repeat showed a

slightly different result. In my first experiment (Figure 2.2C, left western blot), I detected cyclin B3 protein in 16 dpp samples only. In the second experiment (Figure 2.2C, middle western blot), I detected cyclin B3 protein in 12 dpp and 16 dpp samples, with highest levels at 12 dpp. In the last experiment (Figure 2.2C, right western blot), I also found cyclin B3 signal in both 12 and 16 dpp samples, but the highest levels were detected in the 16 dpp sample. This variability could be due to technical variability, or different developmental clock for juvenile animals, or both. However, it is clear that cyclin B3 could be detected starting from 12 dpp, where the tubules are populated with early meiotic cells. Further experiments would be required to determine more precisely the dynamics of cyclin B3 expression during the first wave of spermatogenesis. The RT-qPCR experiments above showed that *Ccnb3* expression is detectable at 10 dpp, but the protein was not detected at 10 dpp. This observation could be attributed to the lower sensitivity of the IP-western blot assay. It is also possible that a post-transcriptional control mechanism delays cyclin B3 translation during spermatogenesis. Overall, these experiments confirmed the presence of CCNB3 in early meiotic cells, which is consistent with a previous study (Nguyen et al., 2002).

Ccnb3 knock out design and knock out confirmation.

To determine the function of mouse *Ccnb3*, we generated an endonuclease mediated (*em*) mutation by CRISPR-Cas9-mediated genome editing. We used a guide RNA to target the 3' end of the 2.7-kb long exon 7. Among the founder

animals, I identified several out-of-frame alleles (Figure 2.3A). For this study, I focused on the *Ccnb3*^{em1} allele (hereafter *Ccnb3*$^{-}$), which has a 14-bp deletion causing a frameshift and premature stop codon upstream of the cyclin box, which is encoded in exons 9–13.

I used IP-western blot analysis to address whether cyclin B3 was present in the *Ccnb3*$^{-/Y}$ testis samples. To detect a possible truncated protein (predicted to be 1090 amino acids long, ~123 kDa), IP-western blot experiments were performed with N-term anti-CCNB3 antibodies for both IP and blotting. Whole cell extracts from *Ccnb3*$^{-/Y}$ mutant testes failed to yield signal for either full-length cyclin B3 or at the expected position of the truncation product (Figure 2.3B). However, I cannot rule out the possibility that a C-term portion of mutant protein is expressed since I don't have an antibody to detect the predicted fragment (the C-term portion of the protein). Overall, IP-western blot results suggested that the truncated form of the protein is unstable, if it is made at all.

I also tested whether the steady state mRNA transcript level of *Ccnb3* is decreased in *Ccnb3*$^{-/Y}$ testis samples. Analysis of mRNA expression levels by RT-qPCR showed ~10-fold decrease in mRNA transcripts of *Ccnb3* in *Ccnb3*$^{-/Y}$ compared to wild-type littermates, which is probably caused by non-sense mediated decay (NMD) and provides further support that *em1* allele is a *bona fide Ccnb3* knock out (Figure 2.3C).

Ccnb3$^{-/Y}$ males do not show any gross defect in spermatogenesis or meiotic prophase progression.

Ccnb3 has been thought to have a role in the meiotic prophase I due to its expression pattern and disrupted spermatogenesis caused by the prolonged expression of *Ccnb3* during meiotic prophase I (Nguyen et al., 2002; Refik-Rogers et al., 2006). I therefore addressed whether *Ccnb3*$^{-/Y}$ males have a defect in meiosis. Problems during spermatogenesis typically lead to reduced fertility or sterility, reduced testis size and/or seminiferous tubule abnormalities (de Rooij and de Boer, 2003). *Ccnb3*$^{-/Y}$ males and their wild-type littermates were placed in cages with wild-type females for 2 months. Both *Ccnb3*$^{-/Y}$ males and their wild-type littermates were able to copulate with wild type females and produced progeny (30 and 27 pups sired respectively). Next, I dissected adult *Ccnb3*$^{-/Y}$ males and their wild-type littermates and found no difference in their testis weights (Figure 2.4A). Moreover, in histological analyses of the tubule sections, I did not observe any gross differences between *Ccnb3*$^{-/Y}$ males and their wild-type littermates (Figure 2.4B). Seminiferous tubules from *Ccnb3*$^{-/Y}$ contained the full array of spermatogenic cells including spermatogonia, spermatocytes, round and elongated spermatids. These results suggest that in the absence of *Ccnb3,* spermatogenesis is not grossly impaired.

To further analyze the phenotype of *Ccnb3*$^{-/Y}$ mice, I immunostained meiotic chromosome spreads with established meiotic markers to address whether meiotic progression in *Ccnb3*$^{-/Y}$ mice differs from the wild-type pattern. In meiotic

prophase, cells can be classified into four different cytological stages; leptotene, zygotene, pachytene and diplotene. Transition between each stage can be followed by the changes in the staining pattern of components of the synaptonemal complex (SC) (de Vries et al., 2005). SYCP3, an axial element of the SC, appears as dots or short patches in the leptotene stage. Later during zygotene stage SYCP3 elongates along the axis and SYCP1, which forms the transverse filaments of the SC, starts to appear. During pachytene, the SC is assembled between homologs along their entire length, before the SC disassembles in diplotene. I followed meiotic progression in terms of SC formation and disassembly in *Ccnb3*$^{em1/Y}$ males and their wild type littermates by staining the chromosome spreads with SYCP3/SYCP1 antibodies. I did not observe any aberrant SC formation or disassembly defects, suggesting normal meiotic prophase I progression (Figure 2.5A).

Next, I used cytological markers to evaluate the formation and repair of meiotic DSBs. To visualize the response to DSBs, I used an antibody against γH2AX, a phosphorylated form of the histone variant H2AX. In wild-type mice, γH2AX signal appears at the leptotene/zygotene stage, then disappears from the autosomes as the breaks are repaired, leaving γH2AX signal only in the sex body, a heterochromatic domain containing the sex chromosomes, which is visible during pachytene and diplotene (Barchi et al., 2005; Mahadevaiah et al., 2001). The pattern of γH2AX signal appearing and disappearing was similar in *Ccnb3*$^{em1/Y}$ males and their wild-type littermates. (Figure 2.5B)

Moreover, by using γH2AX signal and SYCP3 axis information, I also counted the number of cells in different stages of meiotic prophase in *Ccnb3*$^{em1/Y}$ males and their wild-type littermates (Figure 2.5B, right panel). The distribution of the cells at different stages was similar between *Ccnb3*$^{-/Y}$ males and their wild-type littermates, suggesting no transition problems during meiotic prophase I.

To follow the formation and repair of DSBs, I counted the number of foci observed with the recombinase DMC1 at different stages of meiotic prophase I (Moens et al., 2002). DMC1 foci numbers peak at the early-mid zygotene stage and then decrease as the breaks are repaired via homologous recombination. *Ccnb3*$^{-/Y}$ males displayed similar numbers and temporal progression of DMC1 foci as their wild-type littermates (Figure 2.6A), suggesting that DSB repair occurs efficiently in the mutant. Lastly, I counted MLH1 foci, which mark nascent crossover sites from mid-late pachytene cells (Gray and Cohen, 2016). The *Ccnb3*$^{-/Y}$ males showed a slight increase in MLH1 foci formation compared to their wild-type littermates (means of 26 foci *Ccnb3*$^{-/Y}$ vs. 25 foci in wild type) (Figure 2.6B). Though statistically significant (p value < 0.05, Student t-test) the biological significance of this finding should be confirmed. Regardless, the difference in MLH1 foci number does not grossly affect spermatogenesis and meiotic chromosome segregation. Overall, these data suggest *Ccnb3* is dispensable for meiotic recombination and spermatogenesis.

Cyclin mRNA levels do not change in *Ccnb3*$^{-/Y}$ testes.

During spermatogenesis, around thirty cyclins and cyclin related genes are present in different cell populations (Malumbres and Barbacid, 2005; Malumbres et al., 2009; Margolin et al., 2014). Therefore, I speculated that there may be some redundancy between *Ccnb3* and other cyclins. Redundancy between cyclins is well-documented in several cases. For example, in meiosis, deletion of *Ccne2* causes the upregulation of *Ccne1* levels in terms of mRNA and protein levels, which compensates for the absence of *Ccne2* (Martinerie et al., 2014). Conversely, *Ccne2* is upregulated in a *Ccne1* mutant, which compensates for the absence of *Ccne1* (Martinerie et al., 2014). Therefore, I quantified mRNA levels of a panel of cyclins by RT-qPCR in *Ccnb3*$^{-/Y}$ adult testis samples. I found no drastic change in cyclin mRNA expression between *Ccnb3*$^{-/Y}$ and wild type samples (Figure 2.7). However, this does not rule out the possibility that one of these cyclins exerts a redundant role with *Ccnb3*.

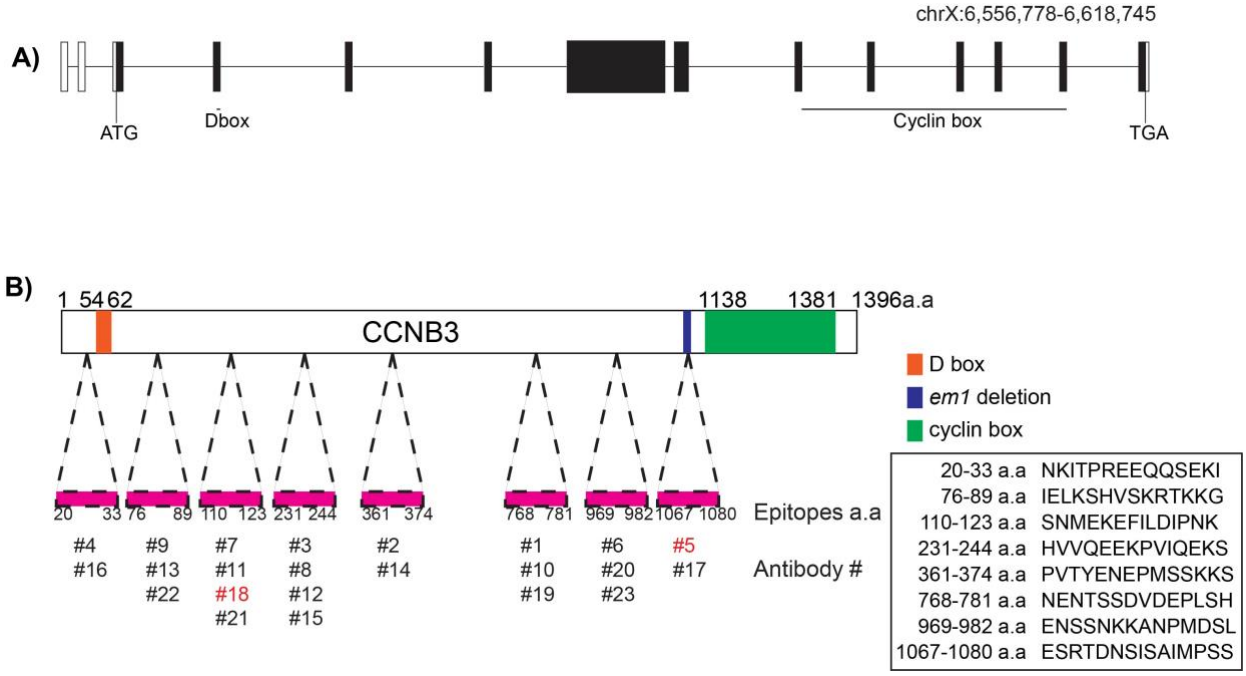

Figure 2.1: *Ccnb3* Gene Diagram and CCNB3 Protein Diagram.
A) Diagram of *Ccnb3* locus. Coding exons are shown as filled black boxes and 5′ and 3′ UTR exons are shown as empty boxes.
B) Protein diagram shows the cyclin box domain of CCNB3 (green filled box) and the destruction box of CCNB3 (orange filled box). Magenta labeled peptide fragments were used to raise antibodies. The peptide sequences are shown on the lower right part.

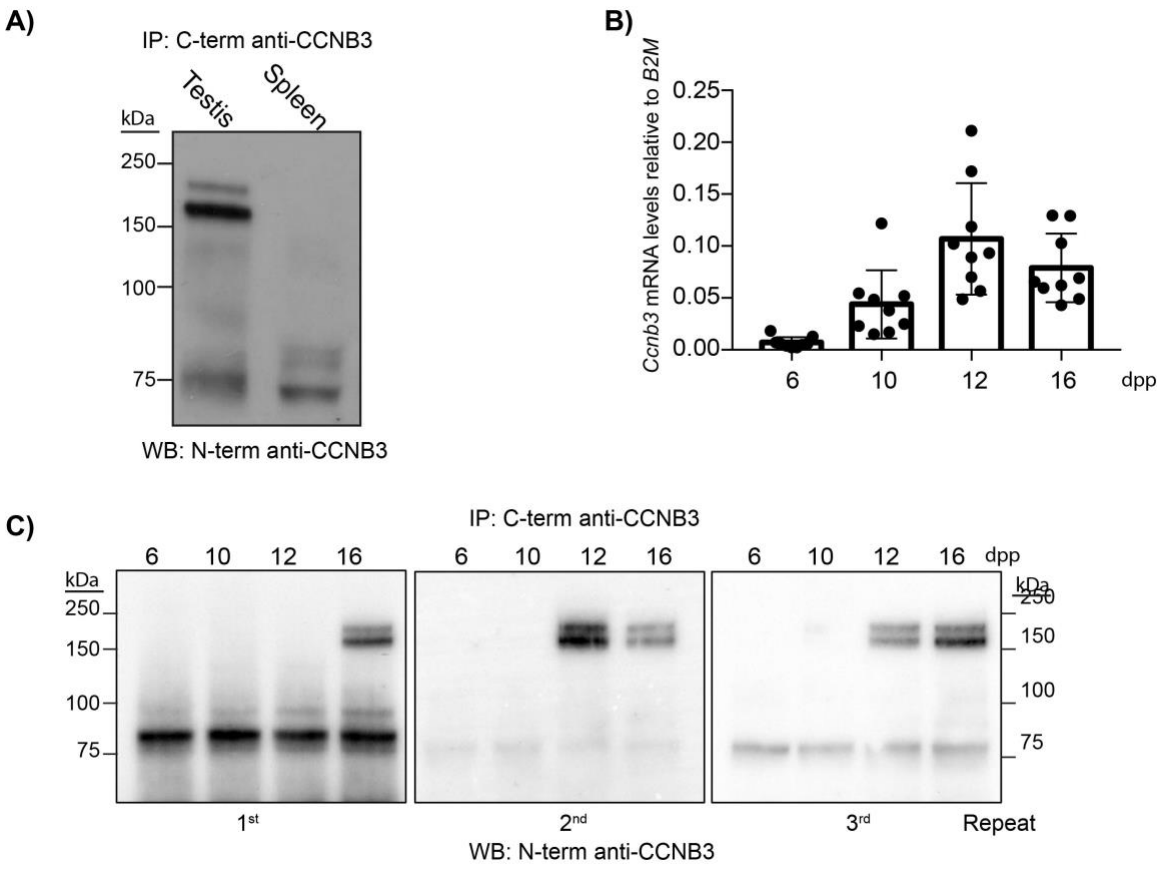

Figure 2.2: Endogenous CCNB3 detection and *Ccnb3* expression pattern during the first wave of spermatogenesis.
A) IP-western blot experiments for endogenous CCNB3 on the testis and spleen extracts from adult mice.
B) Quantative RT-PCR analysis of whole testis RNA extracted from 6, 10, 12, 16 dpp juvenile animals. Three different primers used to amplify *Ccnb3*. The plotted values are the expression levels of *Ccnb3* normalized to *B2M* and the graph includes three independent qPCR experiments. Three different sets of mice.
C) Three biological replicates of the IP-Western blot experiments for CCNB3 using protein extracts from 6, 10, 12, 16 dpp juvenile testis.

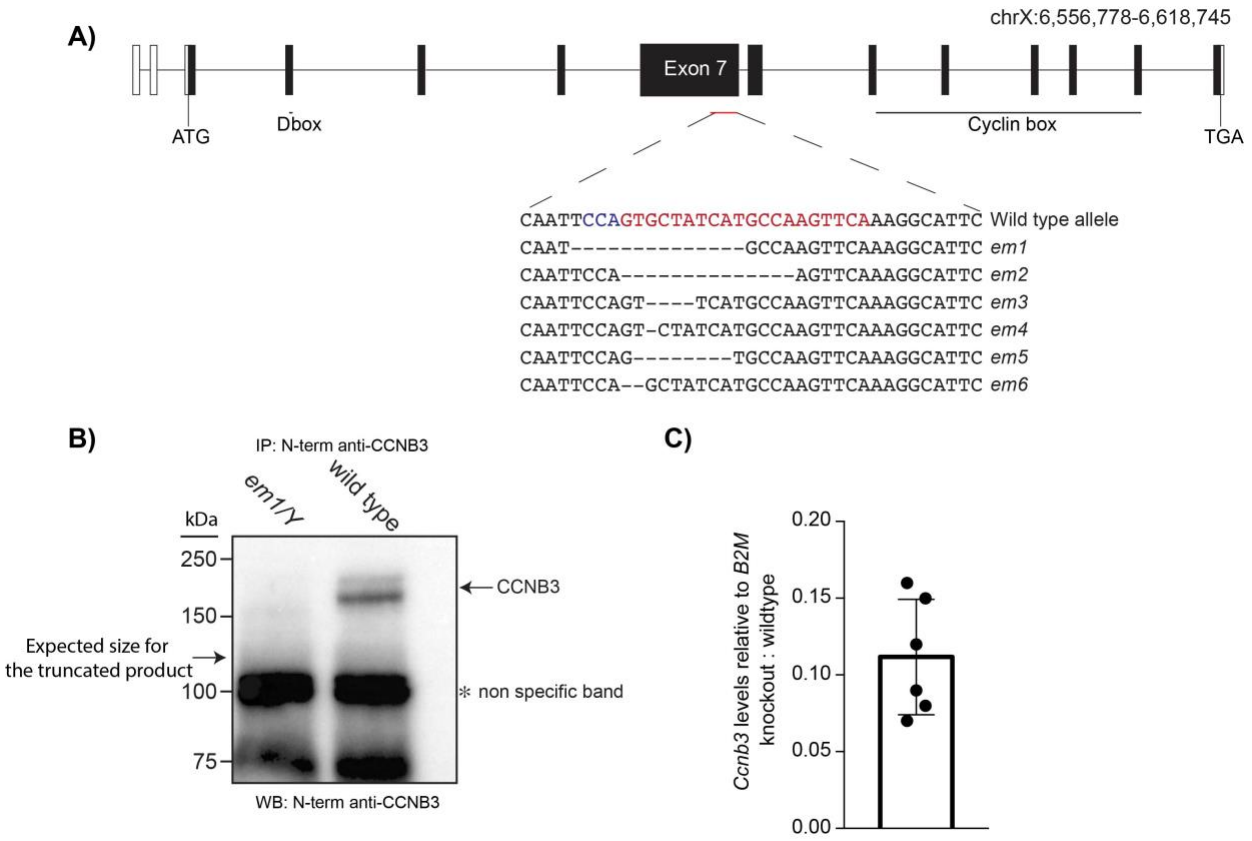

Figure 2.3: *Ccnb3 em1* allele generation and confirmation:
A) *Ccnb3* gene diagram: open black boxes show 5' and 3' UTR and black filled boxes show the coding exons. Position of the targeted locus indicated with the red bar.
B) IP-Western Blot experiments performed on *Ccnb3*$^{em1/Y}$ and wild type sample with N-term anti-CCNB3 antibody.
C) Quantative RT-PCR analysis of whole testis RNA extracted from adult *Ccnb3*$^{em1/Y}$ and wild type testes for *Ccnb3* levels normalized to *B2M*. The plotted values represent *Ccnb3* fold difference between *Ccnb3*$^{em1/Y}$ and wild type for three different pairs of *Ccnb3* primers. The graph includes two independent RT-qPCR experiments.

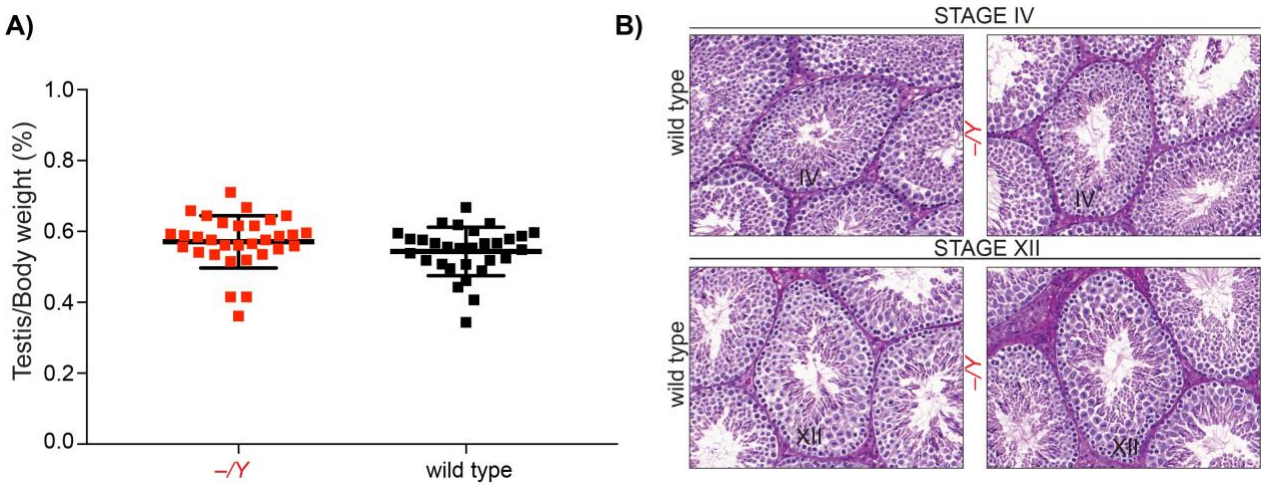

Figure 2.4: Ablation of *Ccnb3* did not affect the testis size and seminiferous tubule structure.
A) The graph represents the percent of the testis weight (mg) to body weight (g) from *–/Y* and wild type adult animals.
B) Representative PAS stained testis sections from adult mice from stage IV and stage XII.

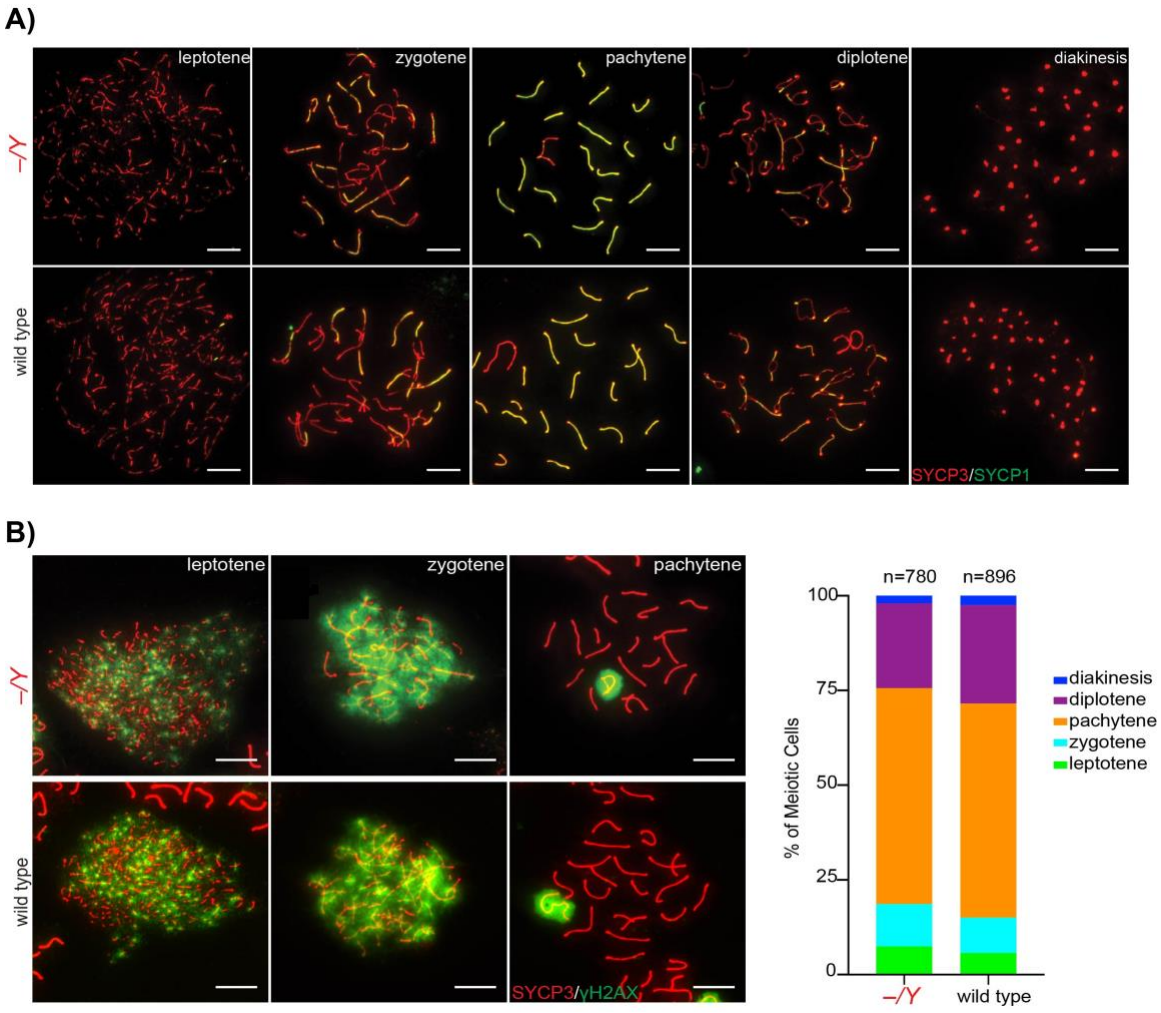

Figure 2.5: Meiotic Progression is normal in *Ccnb3*$^{-/Y}$ males.
A) Representative images of meiotic prophase stages. Meiotic spreads from wild type and *–/Y* males stained with SYCP3 and SYCP1 antibodies.
B) Representative images of meiotic spreads stained with SYCP3 and γH2AX antibodies from indicated genotypes. The graph shows the distribution of meiotic prophase stages from leptotene to diakinesis.

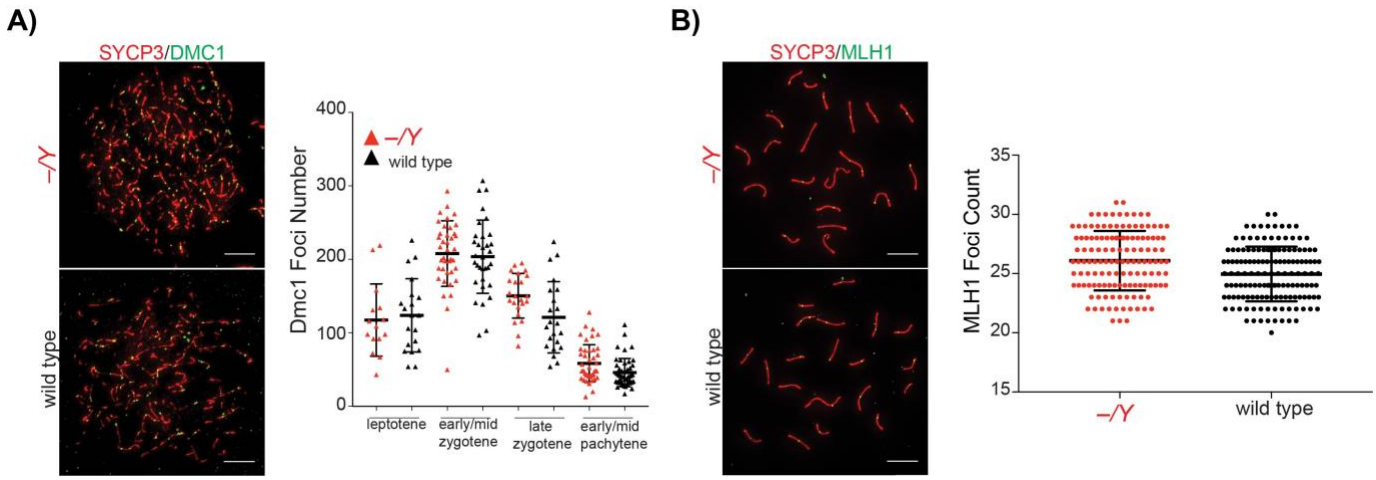

Figure 2.6: DMC1 foci and MLH1 foci numbers are not affected in *Ccnb3*$^{-/Y}$ males.
A) Representative images of meiotic spreads stained with DMC1 and SYCP3 antibodies The graph shows the quantification of DMC1 foci from different stages of meiotic prophase.
B) Representative images of meiotic spreads stained with MLH1 and SYCP3 antibodies. The graph shows the quantification of MLH1 foci from *–/Y* and wild type males.

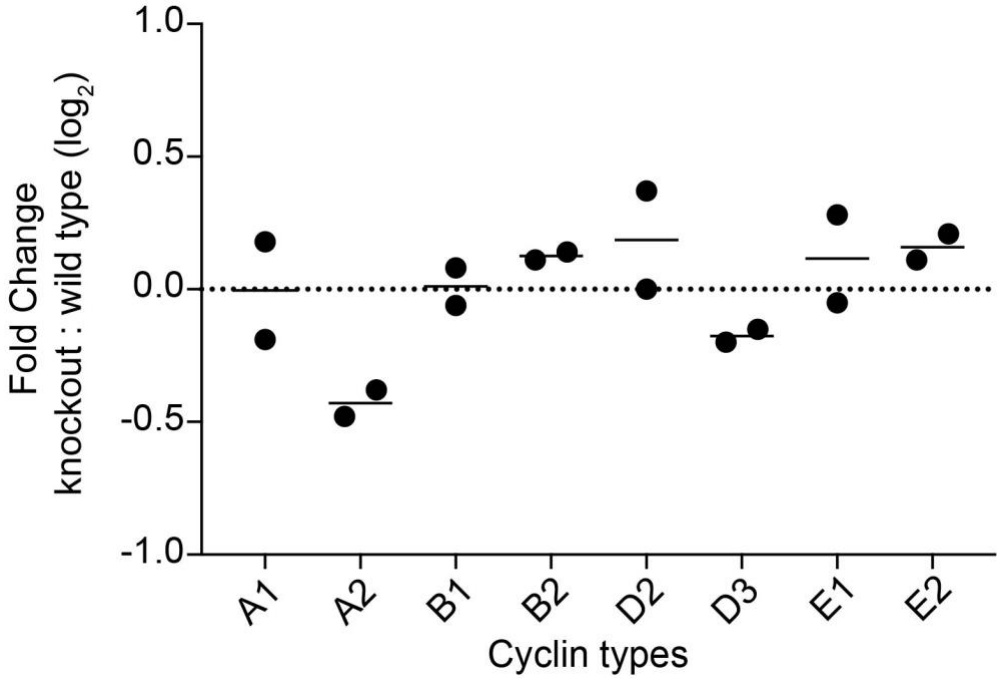

Figure 2.7: Cyclin levels are not changed in testis of *Ccnb3*$^{-/Y}$ males.
Quantative RT-PCR analysis of whole testis RNA extracted from adult *–/Y* and wild type testes for the indicated cyclin levels normalized to *B2M*. The graph includes two independent RT-qPCR experiments. Black lines represent the mean.

Discussion:

Surprisingly, despite prominent, regulated expression during spermatogenesis, *Ccnb3*-deficient males are fully fertile, with no detectable meiotic abnormalities. Generation of monoclonal antibodies allowed us to show that CCNB3 was no longer detectably expressed in the testis samples in knock out males. Moreover, RT-qPCR results showed that *Ccnb3* mRNA levels dropped ~10 fold in the *Ccnb3* knock out males. Both results support the notion that the CRISPR-Cas9 mediated allele of *Ccnb3* is a null or severe loss-of-function mutant of *Ccnb3*.

Cyclin B3 is dispensable for spermatogenesis and meiotic prophase.

According to our hypothesis, we were expecting *Ccnb3*$^{-/Y}$ males to have problems in meiotic recombination events, such as meiotic DSB formation. In that case, we would have expected a similar phenotype to mice that lack essential DSB proteins, including the *Spo11*, *Mei4*, *Mei1*, *Iho1*, *Top6bl* knock out animals (Baudat et al., 2000; Kumar et al., 2010; Libby et al., 2002; Robert et al., 2016; Stanzione et al., 2016). Another possibility would have been that *Ccnb3* contributes to later events, in which case we would have expected phenotypes similar to *Ccne1* or *Cdk2* knock out animals (Geng et al., 2003; Martinerie et al., 2014). However, *Ccnb3*$^{-/Y}$ mice did not show any problems associated with spermatogenesis. The same observation was also made by three other groups

(Jale Refik Roger, 2006 Ph.D Thesis)(Tang et al., 2018; Yufei Li et al., 2018). All these data indicate that in mice *Ccnb3* is dispensable during spermatogenesis. Interestingly, earlier studies from flies indicated that null *Ccnb3* mutations did not affect male fertility (Jacobs et al., 1998). Nevertheless, differences in the meiotic progression in the flies, such as lack of meiotic recombination between homologs, suggests that the situation could have been different in mice.

Does another cyclin take the role of cyclin B3 during the spermatogenesis?

The lack of a phenotype in *Ccnb3*$^{-/Y}$ males triggers a generic question in the field of cyclins: whether the role of *Ccnb3* is obscured by compensation by another cyclin. I have already mentioned several examples of the redundant roles between cyclins. I attempted to test this idea by measuring mRNA levels of other major cyclins in adult testis, based on the hypothesis that this compensation mechanism might result in increased expression of another cyclin. Only *Ccna2* levels showed a slight decrease but no other cyclin expression was elevated. It is also possible that the translation of a compensatory cyclin may be increased in the *Ccnb3* knock out animals without changes in mRNA levels, or that a compensatory mechanism is operational without changes in protein levels.

Given the recent data on *cyclin E* expression during spermatogenesis mentioned above (Martinerie et al., 2014), it is plausible that E-type cyclins can take over the role of *Ccnb3* since both cyclins are present in meiotic prophase. In particular,

Ccne2 expression overlaps with the expression window of *Ccnb3*. Thus, I started to generate double knock out animals for *Ccne1*, *Ccnb3* and *Ccne2*, *Ccnb3* to characterize their phenotype. It is known that the testis size is reduced in *Ccne2* knock out (Geng et al., 2003; Martinerie et al., 2014). *Ccne2*, *Ccnb3* double knock out also resulted in small testis size (within the range of reported testis size for *Ccne2* knock out), and preliminary meiotic spread analysis showed similar results as observed in *Ccne2* knock out (not shown). *Ccne1*, *Ccnb3* double knock out animals are in production and their phenotype will be analyzed soon.

Was cyclin B3 expression pattern during spermatogenesis a red herring?

It is quite intriguing to find that a gene which is specifically expressed in testis and whose temporal expression is confined to meiotic prophase (in male mice) did not contribute to meiosis or spermatogenesis in any detectable manner. However, the studies indicated there are ~2300 genes in mouse genomes expressed predominantly in the testis (Schultz and K., 2003). In a heroic effort, a recent study reported the generation of 54 knock out alleles of testes-specific genes, all of which yielded fertile mice (Miyata et al., 2016). This shows that the negative results presented in this chapter are far from unusual.

Nevertheless, it should be noted that all these experiments are done with laboratory mice that are not under stress or reproductive competition. These

experiments may therefore fail to capture biological functions that would manifest in more natural conditions. For example, one of 54 genes presented in the study by Miyata and colleagues was the polycystin (PKD) family receptor for egg jelly (*Pkdrej*). *Pkdrej* knock out males were fertile as their wildtype littermates in unrestricting mating trials. However, they performed poorly when competing with wild type males in sequential mating trials and in artificial insemination of mixed-sperm populations, indicating that *Pkdrej* is important in postcopulatory reproductive selection (Sutton et al., 2008).

A possible way of testing the importance of cyclin-CDK complexes in mammalian spermatogenesis:

A recent study identified the *MER2* homolog in mouse, which is called *Iho1* (*Ccdc36*)(Stanzione et al., 2016). Genetic ablation of *Iho1* resulted in a defect of DSB formation in meiosis, as expected for a *bone fide* DSB protein. Whether cyclin-CDK components phosphorylate IHO1 in mouse, as is the case with Mer2 in yeast, has not yet been addressed. IHO1 carries minimal CDK phosphorylation sites: 2 SP and 1 TP sites are found in the sequence. If the mechanism of Mer2 regulation is conserved, it is tempting to hypothesize that cyclin-CDK complexes can phosphorylate IHO1. This hypothesis can be tested in various ways, some of which are described below. The published paper developed antibodies against IHO1, and they also detected the expression of the protein from testis whole cell extracts. To address if IHO1 has post translational modifications such as phosphorylation, it would be possible to perform IP-mass spectrometry and map

the phosphorylation sites on IHO1. Depending on the results, further genetic experiments can be performed by mutating the phosphorylation sites of IHO1 in the whole animal.

Although IHO1 is a good candidate substrate for cyclin-CDK complexes, a more general approach may be better to find cyclin-CDK substrates. One approach would be to map phospho-peptides by proteomics methods in juvenile animals where the cells start to experience DSB breaks in meiosis. To eliminate the peptides observed from somatic cells, c-Kit mutant animal testis can be used, which contains somatic cells and non-differentiating A type spermatogonia in the testis but no differentiating spermatocytes (Yoshinaga et al., 1991). This approach would yield a broad picture of which proteins might be subjected to phosphorylation by cyclin-CDK complexes. It is possible that cyclin-CDK complexes regulate the initiation of meiotic prophase but target a different substrate. For example, in budding yeast, Sld2 is the CDK target and the phosphorylation of Sld2 and Sld3 by CDK complexes lead to the interaction of these proteins with Dbp11 and the recruitment of Cdc45, Pol ε and GINS to replication origins to activate the MCM helicases (Tanaka et al., 2007; Zegerman and Diffley, 2007). On the other hand, however, in the mammalian system, the Sld2 ortholog RECQL4 was not identified as a CDK substrate (Matsuno et al., 2006; Sangrithi et al., 2005). Instead TRESLIN, a distant Sld3 ortholog, is phosphorylated by CDK and binds TOPBP1, which recruits CDC45 and leads to MCM activation, indicating that different substrates are used by CDK in

mammalian replication than in yeast (Mueller et al., 2011; Sanchez-Pulido et al., 2010). I believe that this type of approach would be fruitful to identify the link between meiotic recombination and cell cycle because redundancy mechanisms are likely to obscure any effects in candidate approaches.

Chapter 3: Cyclin B3 promotes metaphase to anaphase I transition in the mouse oocytes[1].

Summary:

This chapter addresses the role of cyclin B3 during oogenesis. In contrast to males, *Ccnb3*$^{-/-}$ female mice are sterile. *Ccnb3*$^{-/-}$ oocytes proceed through meiotic prophase I, but cannot progress beyond metaphase I. Our data indicate that cyclin B3 fine-tunes the activity of APC/C towards its meiotic substrates in oocytes, at least in part through the catalytic activity of CDK1. In addition, I provide evidence that this function of cyclin B3 is conserved in vertebrates.

Background:

Mus musculus Ccnb3 mRNA has previously been detected in fetal ovaries and maturing oocytes, but the role of cyclin B3 in female meiosis has not been addressed in detail (Nguyen et al., 2002). *Drosophila melanogaster* cyclin B3 is dispensable for mitotic divisions and for male fertility but is essential for female fertility (Jacobs et al., 1998). In flies, cyclin B3 promotes anaphase onset in early embryonic divisions (Yuan and O'Farrell, 2015), and loss of cyclin B3 perturbs exit from meiosis I (Jacobs et al., 1998), which suggests the possible role of cyclin B3 in female meiosis in mammals. Indeed, RNAi-mediated knock-down of

[1] Adapted from Karasu*, Bouftas* et al (2018), Cyclin B3 promotes APC/C activation and anaphase I onset in oocyte meiosis (bioRxiv). * co-first authors. Except figure 6A, all oocyte injection experiments were performed by Nora Bouftas at Paris Univ VI.

cyclin B3 to ~30% of wild-type levels in cultured mouse oocytes perturbed progression through meiosis I, which provides support for this hypothesis (Zhang et al., 2015). In this study, I performed a detailed investigation of the role of cyclin B3 in female meiosis.

Results:

Cyclin B3 is dispensable for meiotic prophase in oocytes.

Similar to cyclin B3-deficient males, heterozygous females also displayed normal fertility and homozygous mutant females were born in Mendelian frequencies from heterozygous parents [(105 +/– (25.7%) : 100 –/– (25.5%) : 102 +/Y (25%) : 101 –/Y (24.8%) offspring from *Ccnb3*$^{+/-}$ females crossed with *Ccnb3*$^{-/Y}$ males)]. *Ccnb3*$^{-/-}$ animals displayed no gross abnormalities in histopathological analysis of major organs and tissues (see Methods), indicating that cyclin B3 is dispensable in most if not all non-meiotic cells.

Strikingly, however, cyclin B3-deficient females were sterile. No pregnancies were observed, and no pups were born from *Ccnb3*$^{-/-}$ females (n=9) bred with wild-type males for two rounds of mating, which indicates that whereas cyclin B3 is dispensable for male meiosis, it is essential for female fertility.

To understand why *Ccnb3*$^{-/-}$ females are sterile, I examined the behavior of mutant oocytes. In mice, as in other mammals, female meiosis initiates during fetal development (El Yakoubi and Wassmann, 2017; Herbert et al., 2015).

Oocytes complete the chromosome pairing and recombination steps of meiotic prophase prior to birth, then enter a prolonged period of arrest (the dictyate stage) and coordinate with surrounding somatic cells during the first few days after birth to form follicles. Primordial follicles are the resting pool of germ cells that will be recruited for further development and ovulation during the reproductive life of the animal. Ovary sections from *Ccnb3*$^{-/-}$ females showed abundant oocytes in primordial and growing follicles at 2–3 months of age, and were quantitatively and morphologically indistinguishable from littermate controls (Figure 3.1A). Follicle formation is highly sensitive to pre-meiotic and meiotic prophase I defects, such that mutations compromising oogonial development, meiotic initiation, or recombination result in drastically reduced or absent follicles within the first few weeks after birth if not earlier (Baltus et al., 2006; Bolcun-Filas et al., 2014; Di Giacomo et al., 2005; Jain et al., 2018; Li et al., 2007). The normal number and appearance of follicles in *Ccnb3*$^{-/-}$ females therefore leads us to infer that cyclin B3 is largely if not completely dispensable for germ cell divisions prior to meiosis and for early events of meiotic prophase I (DNA replication, recombination, and chromosome pairing and synapsis).

Cyclin B3 is required for metaphase to anaphase I transition in oocytes.

I next tested the ability of mutant oocytes to be induced to enter meiosis I and to carry out the meiotic divisions *in vitro*. Germinal vesicle (GV) stage oocytes were collected from ovaries of adult *Ccnb3*$^{-/-}$ mice and age-matched controls from the

same breedings (*Ccnb3*$^{+/-}$) and cultured *in vitro*. Under these conditions, germinal vesicle breakdown (GVBD, corresponding to nuclear envelope breakdown in mitosis) occurred with normal timing (within 90 min) and efficiency in *Ccnb3*$^{-/-}$ oocytes (Figure 3.1B), indicating that cyclin B3 is dispensable for entry into meiosis I. At ~7–10 hours in culture after entry into meiosis I, depending on the mouse strain, oocytes extrude a polar body (PB), indicating execution of the first division and exit from meiosis I (El Yakoubi and Wassmann, 2017; Holt et al., 2013)[6, 28]. Unlike for other aspects of female reproduction described above, *Ccnb3*$^{-/-}$ mice displayed a highly penetrant defect at this stage of meiosis: oocytes failed to extrude a PB in most cyclin B3-deficient mice (65 out of 73 mice) (Figure 3.1B). These findings indicate that cyclin B3 is required for progression through meiosis I, suggesting in turn that meiotic progression failure is the cause of female infertility. Because the penetrance of meiotic arrest was mouse specific, (i.e., most mice yielded only arrested oocytes), subsequent experiments were done on the large majority of mice where no PB extrusion was observed. Possible reasons for the incomplete penetrance are addressed in the Discussion.

To further characterize this meiotic arrest, meiotic progression was followed by live imaging. GV oocytes were injected with mRNA encoding histone H2B fused to RFP and β-tubulin fused to GFP to visualize chromosomes and spindles, respectively. Whereas control oocytes separated their chromosomes and extruded PBs ~8 hours after GVBD, *Ccnb3*$^{-/-}$ oocytes that did not extrude PBs

remained in a metaphase I-like state, with a spindle that had migrated close to the cortex and chromosomes aligned at the spindle midzone (Figure 3.2A)

The previous results led the hypothesis that mutant oocytes were failing to make the transition from metaphase I to anaphase I; this idea predicts that homologous chromosomes will still be conjoined in those oocytes that failed to extrude PBs in the absence of cyclin B3. In chromosome spreads from control oocytes, 20 bivalent chromosomes were observed as expected (homolog pairs connected by chiasmata) prior to the first division (6 hours after GVBD) and pairs of sister chromatids juxtaposed near their centromeres afterwards (metaphase II arrest, 16 hours after GVBD) (Figure 3.2B). In contrast, as predicted, *Ccnb3*$^{-/-}$ oocytes displayed intact bivalents throughout the arrest in culture and no homolog separation was observed, indicating a metaphase I arrest (Figure 3.2B).

Arrest was not due to failure in forming either spindles or stable kinetochore-microtubule interactions, because metaphase I spindles displayed no obvious morphological defects and cold-stable microtubule fibers were observed in *Ccnb3*$^{-/-}$ oocytes comparable to control oocytes in metaphase I (Figure 3.2C). Microtubule fibers attached to kinetochores were clearly visible, indicating that cyclin B3 is not required for kinetochore-microtubule attachments (Figure 3.2C). Importantly, the bipolar spindles in *Ccnb3*$^{-/-}$ oocytes retained the barrel-shaped appearance characteristic of metaphase I even at late time points 16 hours after GVBD, when control oocytes had progressed to metaphase II (Figure 3.2C).

APC/C is not fully active in *Ccnb3*$^{-/-}$ oocytes.

Next, the molecular basis of the failure in chromosome segregation is investigated in *Ccnb3*$^{-/-}$oocytes. Separase is a cysteine protease that cleaves the kleisin subunit of cohesin complexes to dissolve sister chromatid cohesion at anaphase onset in mitosis and meiosis (Stemmann et al., 2006). Prior to anaphase, separase activity is restrained in part by binding to its inhibitory chaperone, securin, and by high cyclin B-CDK activity (Stemmann et al., 2006). In oocytes, the APC/C-dependent degradation of securin and cyclin B1 leads to activation of separase, which then cleaves the meiotic kleisin REC8, allowing the separation of homologous chromosomes (Herbert et al., 2003; Kudo et al., 2006; Terret et al., 2003). To follow separase activity in live oocytes, a separase activity sensor was expressed, recently developed in the Wassmann laboratory (Nikalayevich et al., 2018), similar to one described in mitotic tissue culture cells (Shindo et al., 2012). The sensor harbors two fluorescent tags separated by the mitotic cohesin subunit RAD21 as a separase cleavage substrate; this ensemble is fused to histone H2B to allow it to localize to chromosomes. Upon cleavage by separase, colocalization of the fluorophores is lost, leaving only the H2B-attached fluorophore on chromosomes (Figure 3.3A). Sensor cleavage occurs only under conditions when endogenous REC8 is removed from chromosome arms (Nikalayevich et al., 2018). When control oocytes in culture were injected with mRNA encoding the sensor, the fluorescent signal on chromosomes changed abruptly from yellow to red upon anaphase onset (Figure 3.3A, top row,

compare 6:20 to 6:40 time points). In contrast, both fluorophores of the sensor remained chromatin-associated throughout the arrest in *Ccnb3*$^{-/-}$ oocytes (Figure 3.3A, bottom row), indicating that separase cannot be activated in meiosis I in the absence of cyclin B3, explaining in turn why the mutant oocytes cannot separate homologous chromosomes and extrude PBs.

The failure to activate separase was potentially due to a failure to degrade cyclin B1 and securin, the two inhibitors of separase. To test this, I analyzed levels of each protein by western blotting (Figure 3.3B). In control oocytes, the levels of both proteins decreased precipitously at metaphase-to-anaphase onset (compare 8:30 to 3:30 after GVBD). In *Ccnb3*$^{-/-}$ oocytes in contrast, cyclin B1 levels did not decrease at any point during culturing, even at late time points. In fact, cyclin B1 levels were consistently higher during arrest (8:30 and later) as compared to prometaphase (3:30). Securin levels decreased between 3:30 and 8:30 after GVBD, but remained at much higher levels than in the controls. Thus, although securin levels drop partially, both proteins are inappropriately stabilized in cyclin B3-deficient cells at the time wild-type cells would normally carry out the meiosis I division.

The next question was whether stabilization of cyclin B1 in *Ccnb3*$^{-/-}$ oocytes correlated with elevated kinase activity of MPF (M-phase promoting factor), a heterodimer of CDK1 and either cyclin B1 or B2 (usually called simply "cyclin B") (Kubiak et al., 1992; Malumbres and Barbacid, 2009; Morgan, 1997). For this, *in*

vitro kinase assays were performed by using oocyte extracts at the indicated time points to assess MPF activity (Kubiak et al., 1992) (Figure 3.3C). As previously shown, control oocytes showed high MPF activity in metaphase I (6:00 after GVBD), and a drop in kinase activity when they extrude PBs (8:00 after GVBD) (Ledan et al., 2001). *Ccnb3*$^{-/-}$ oocytes similarly showed high MPF activity in metaphase I (6:00 after GVBD), but no drop in kinase activity was observed at the time when normal cells extruded PBs (8:00 after GVBD) (Figure 3.3C).

Because endogenous securin levels decreased slightly in *Ccnb3*$^{-/-}$ oocytes (Figure 3.3B), whereas cyclin B1 levels and MPF activity did not at a time when control oocytes extrude PBs, I asked whether inhibiting MPF activity at the normal time of anaphase I onset would be sufficient for *Ccnb3*$^{-/-}$ oocytes to undergo the metaphase I-to-anaphase I transition and PB extrusion. Indeed, addition of the CDK inhibitor roscovitine (De Azevedo et al., 1997; Meijer et al., 1997) rescued PB extrusion and chromosome segregation in *Ccnb3*$^{-/-}$ oocytes, suggesting that the failure to undergo anaphase I without cyclin B3 is mainly attributable to persistently elevated MPF activity (Figure 3D).

Collectively, the results thus far pointed out that *Ccnb3*$^{-/-}$ oocytes that do not extrude PBs are arrested in metaphase I with aligned homologous chromosome pairs, bipolar metaphase I spindles, high securin and cyclin B1 protein levels, and little or no separase activity. In oocytes, degradation of cyclin B1 and securin depends on their ubiquitination by the APC/C (Herbert et al., 2003; Terret et al.,

2003). Hence, without cyclin B3, the APC/C is not sufficiently activated on time to properly target endogenous cyclin B1 and securin. Because endogenous securin levels did decrease slightly in the mutant, however, I suspected that the APC/C might be partially active. To test this, I asked whether exogenously expressed securin and cyclin B1 were also stabilized in *Ccnb3*$^{-/-}$ oocytes that were arrested in metaphase I. mRNAs coding for either protein fused to fluorescent tags were injected into GV oocytes and followed by live imaging (Gui and Homer, 2012; Herbert et al., 2003; Kudo et al., 2006; Lane et al., 2012; Niault et al., 2007; Rattani et al., 2014). Surprisingly, cyclin B1-GFP and securin-YFP were both efficiently degraded in *Ccnb3*$^{-/-}$ oocytes (Figure 3.4). Securin-YFP was degraded with kinetics and final extent similar to the controls, whereas cyclin B1-GFP appeared to be degraded slightly more slowly and was higher in *Ccnb3*$^{-/-}$ than in control cells specifically at the time the controls underwent PB extrusion (Figure 3.4). Thus, even though both exogenous substrates were more efficiently degraded than their endogenous counterparts, the differences between the two substrates were similar in both contexts (i.e., securin was degraded to a greater extent than cyclin B1 in the absence of cyclin B3). These results indicate that the APC/C does indeed become partially active in the mutants, but the data further suggest that cyclin B3 in some manner specifically promotes the degradation of endogenous APC/C substrates. This may be by modulating APC/C specificity per se, or by regulating the substrates or their localization to affect their ability to be ubiquitylated. This role of cyclin B3 appears to be largely dispensable in the case of exogenously expressed, tagged substrates.

SAC is not over activated in *Ccnb3*$^{-/-}$ oocytes.

Timely APC/C activation depends on satisfaction of the SAC (Holt et al., 2013; Touati and Wassmann, 2016). It would be possible that inappropriate SAC activity was the reason for arrest in *Ccnb3*$^{-/-}$ oocytes. Kinetochore recruitment of SAC components, such as MAD2, is a readout for SAC activation (Lischetti and Nilsson, 2015). MAD2 was recruited to unattached kinetochores early in meiosis I (Gui and Homer, 2012; Wassmann et al., 2003) in both control and *Ccnb3*$^{-/-}$ oocytes, and that neither control nor *Ccnb3*$^{-/-}$ oocytes retained MAD2 at kinetochores in metaphase I (Figure 3.5A). This result shows that *Ccnb3*$^{-/-}$ oocytes have a functional SAC (i.e., it can recognize unattached kinetochores in early meiosis I) that is appropriately satisfied upon kinetochore-microtubule attachment at metaphase I. To further test involvement of the SAC, *Ccnb3*$^{-/-}$ oocytes were treated with reversine, which inhibits the essential SAC kinase MPS1 (Santaguida et al., 2010). The SAC was induced in control oocytes by nocodazole treatment, and as previously shown (Touati et al., 2015), reversine treatment was sufficient to overcome arrest (Figure 3.5B). Crucially, reversine treatment of metaphase I arrested *Ccnb3*$^{-/-}$ oocytes did not rescue the metaphase-to-anaphase transition or PB extrusion (Figure 3.5B).

Cyclin B3 is a later APC/C substrate.

Like other M-phase cyclins, cyclin B3 harbors a conserved destruction box (D-box) (Nguyen et al., 2002), a motif typically targeted for APC/C-dependent

ubiquitination (Yuan and O'Farrell, 2015) (shown in chapter 2). In mitosis, exogenously expressed cyclin B3 was shown to be degraded after cyclin B1 (Nguyen et al., 2002). I therefore asked whether cyclin B3 protein stability is regulated in a cell cycle-dependent manner in oocytes. mRNA encoding cyclin B3 tagged with RFP was injected into wild-type oocytes together with mRNA for either securin-YFP or cyclin A2-GFP, and oocytes were followed by live imaging. Exogenously expressed cyclin B3-RFP accumulated during meiosis I, then was degraded abruptly just before PB extrusion. Importantly, cyclin B3 degradation occurred after degradation of both cyclin A2 and securin (Figure 3.6A and B), showing temporally ordered degradation of APC/C substrates in oocyte meiosis I. No re-accumulation of cyclin B3-RFP was observed as oocytes progressed into meiosis II. Deleting the D-box stabilized cyclin B3-RFP (Figure 3.5C) (the protein has no obvious KEN-box or ABBA motif (Davey and Morgan, 2016). These findings support the conclusion that cyclin B3 is an APC/C substrate in oocyte meiosis.

Cyclin B3 can form a complex with CDK1 and cyclin B3 associated kinase activity is required for the progression of meiosis I.

To determine whether mouse cyclin B3 can support CDK1-dependent kinase activity (as for the *C. elegans*, *Drosophila*, and chicken proteins (Gallant and Nigg, 1994; Jacobs et al., 1998; van der Voet et al., 2009)), I co-expressed and purified recombinant murine protein complexes from insect cells. I expressed cyclin B3 that was N-terminally tagged with maltose binding protein (MBP) and

hexahistidine (^{MBPHis}cyclin B3) and untagged CDK1 or a hemagglutinin (HA) tagged version of CDK1 that runs slightly slower than untagged on SDS-PAGE. Both CDK1 and CDK1-HA could be co-purified with ^{MBPHis}cyclin B3 upon affinity purification on amylose resin (Figure 3.7A, left, lanes 2-3), and both types of cyclin B3-CDK1 complex displayed kinase activity towards histone H1 *in vitro* (Figure 3.7A, right, lanes 2-3).

To further investigate this kinase activity, I mutated the MRAIL motif on cyclin B3, which is conserved among different cyclins and is located on the hydrophobic patch formed by the cyclin fold (Jeffrey et al., 1995; Schulman et al., 1998). MRAIL mutations were previously shown to prevent binding of cyclin-CDK complexes to potential substrates without affecting cyclin-CDK interactions (Schulman et al., 1998), although other studies also reported loss of cyclin-CDK interaction (Bendris et al., 2011). Mutating the methionine, arginine, and leucine residues of the MRAIL motif to alanine (cyclin B3-MRL mutant) did not affect the ability to co-purify CDK1 or CDK1-HA (Figure 3.7A, left, lanes 5-6), but the affinity-purified ^{MBPHis}cyclin B3 MRL-CDK complexes were not active in the histone H1 kinase assay (Figure 3.7A, right, lanes 5-6). Furthermore, affinity purification of wild-type cyclin B3 without co-expressed CDK1 yielded detectable H1 kinase activity, presumably attributable to cyclin B3 association with an endogenous insect cell CDK(s), but the MRL mutant gave no such baseline activity (Figure 3.7A, right, lanes 1 and 4). I conclude that cyclin B3 can form an active kinase complex with CDK1, suggesting in turn that CDK1 may be a

physiological partner of cyclin B3 *in vivo*. I also conclude that the MRL mutant permits CDK1 binding but abolishes associated kinase activity.

I further tested whether oocyte division requires cyclin B3-associated kinase activity. To this end, I first performed live imaging on *Ccnb3*$^{-/-}$ oocytes injected with mRNA encoding wild-type cyclin B3 or protein with the D-box deleted (ΔD-box). Both constructs efficiently rescued PB extrusion in the mutant (Figure 3.7B). Chromosome spreads demonstrated that separation of homologous chromosomes was also rescued upon cyclin B3 expression (Figure 3.7C). This finding confirmed that meiotic arrest is attributable to absence of cyclin B3 per se and established feasibility of structure/function experiments based on complementation of *Ccnb3*$^{-/-}$ oocyte arrest. In striking contrast to wild-type cyclin B3, injection of mRNA encoding the MRL mutant was unable to rescue meiosis I division, PB extrusion, or chromosome segregation (Figure 3.6B and C), indicating that cyclin B3-CDK complexes (likely CDK1) bring about anaphase I onset through their kinase activity towards yet unknown substrates. Note that, unlike cyclin B3, expression of exogenous cyclin B1 was unable to rescue PB extrusion (Figure 3.4E) or homolog disjunction (Figure 3.7C). The data indicates that cyclin B3-CDK1 substrates are likely distinct from cyclin B1-CDK1 substrates, perhaps due to distinct substrate specificity or accessibility.

Functional conservation of vertebrate cyclin B3 in meiosis I.

It was previously reported that *X. laevis* oocytes contain cyclin B3 mRNA but not detectable levels of the protein, from which it was inferred that cyclin B3 plays no role in Xenopus oocyte meiosis (Hochegger et al., 2001). Furthermore, mammalian cyclin B3 is much larger than cyclin B3 from non-mammalian vertebrates due to the presence of the extended exon 7 (Lozano et al., 2012), suggesting that the protein might be functionally distinct in mammals. To explore this possibility, inter-species cross-complementation was tested by injecting mRNAs encoding cyclin B3 from either *X. laevis* or zebrafish (*Danio rerio*) into mouse *Ccnb3*$^{-/-}$ oocytes. Remarkably, heterologous expression of cyclin B3 from either species efficiently rescued PB extrusion (Figure 3.8A**)**. Live imaging of oocytes stained with SiR-DNA to visualize chromosomes showed no obvious defect in chromosome alignment or anaphase I onset in oocytes rescued with *X. laevis* cyclin B3 (Figure 3.8B). These findings demonstrate that the extended exon 7 in mouse cyclin B3 is dispensable to promote anaphase I onset. Moreover, these findings suggest that biochemical functions of cyclin B3 protein are conserved across vertebrates, in turn raising the possibility that cyclin B3 promotes the oocyte meiosis I division throughout the vertebrate lineage. Even more remarkably, Drosophila cyclin B3 was also able to rescue the mouse mutant oocytes (Figure 3.7A), suggesting conservation of biochemical properties throughout metazoa.

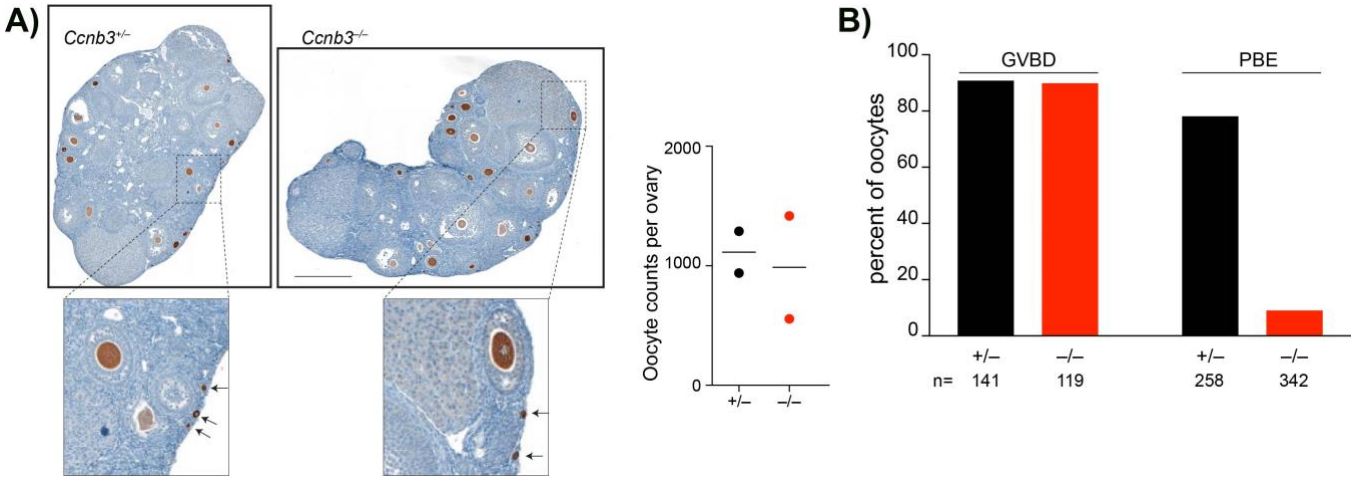

Figure 3.1: *Cyclin B3* is dispensable for meiotic prophase I but required for meiotic maturation.

A) Apparently normal folliculogenesis and oocyte reserves in *Ccnb3*-deficient females. (Left) PFA-fixed, anti-MVH stained ovary sections from three-month-old animals. Zoomed images show presence of primary/primordial follicles indicated by black arrows. Scale bar represents 500 µm. (Right) Oocyte counts from two three-month-old females of each genotype. PFA-fixed ovaries were sectioned completely and stained with anti-MVH. Stained oocytes were counted in every fifth ovary section and summed. Each point is the count for one ovary of one animal.

B) The scheme on the left illustrates progression through the meiotic divisions until metaphase II arrest in oocytes of the mouse strain used for generating *Ccnb3*-deficient females. On the right, percentages of mature oocytes of the indicated genotypes (which were not maintained arrested in GV stage) that underwent GVBD (germinal vesicle breakdown) within 90 min in culture, and oocytes that extruded polar bodies (PB) (n: number of oocytes).

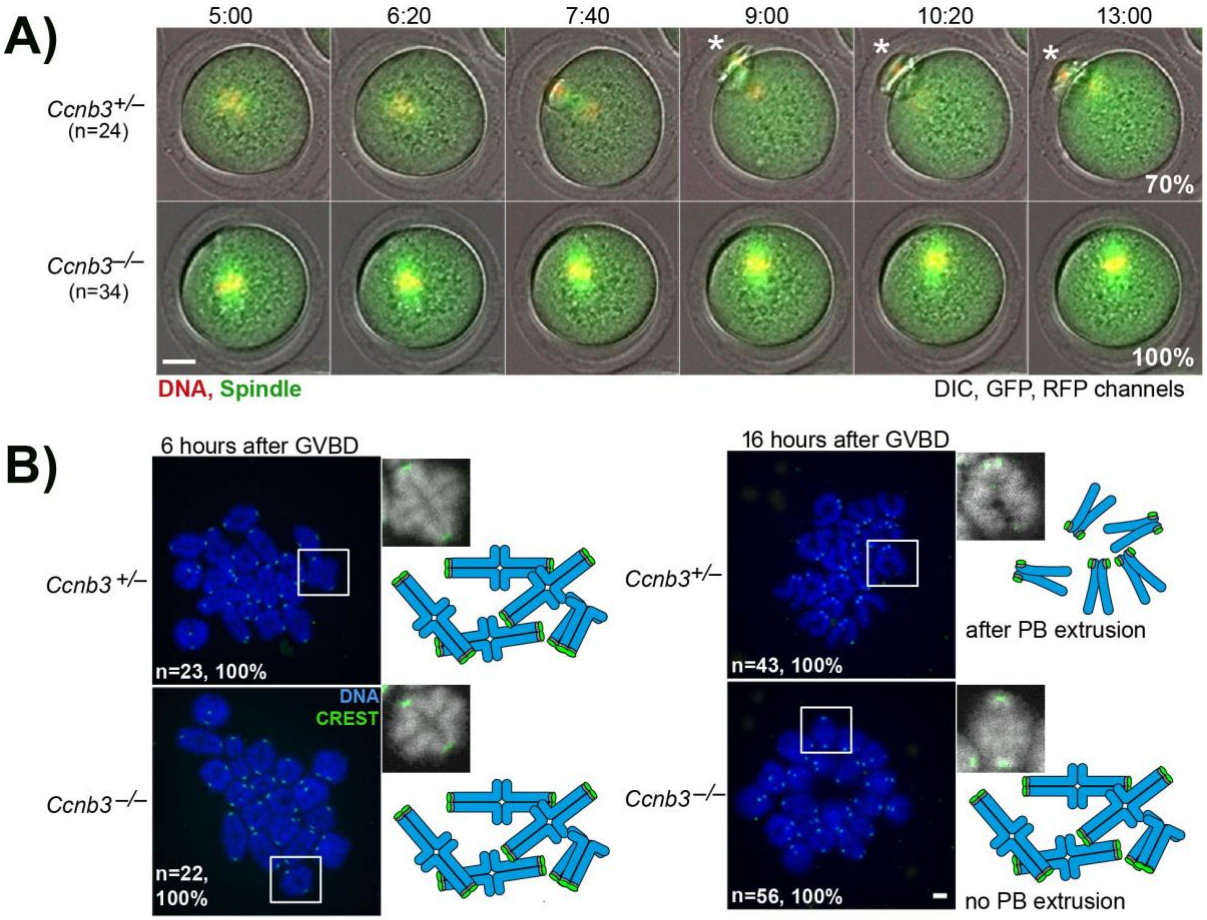
A)
5:00
6:20
7:40
9:00
10:20
13:00
Ccnb3+/–
(n=24)
Ccnb3–/–
(n=34)
70%
100%
DNA, Spindle
DIC, GFP, RFP channels
B)
6 hours after GVBD
16 hours after GVBD
Ccnb3 +/–
Ccnb3–/–
n=23, 100%
DNA
CREST
n=22,
100%
Ccnb3+/–
Ccnb3–/–
n=43, 100%
after PB extrusion
n=56, 100%
no PB extrusion
C)
6 hours after GVBD
16 hours after GVBD
Ccnb3+/–
Ccnb3–/–
n=19, 100%
after PB extrusion
n=13, 100%
DNA
CREST
Spindle
n=12, 100%
no PB extrusion
n=28, 100%

Figure 3.2: Cyclin B3 is dispensable for meiotic prophase in oocytes.
A) Live-cell imaging of meiotic maturation. -tubulin-GFP and H2B-RFP mRNA to visualize the spindle and chromosomes, respectively, were injected into GV-stage oocytes, which were then induced to enter meiosis I. Selected time frames are shown with an overlay of DIC, GFP and RFP channels from representative movies. Time after GVBD is indicated as hours : minutes. Percentage of oocytes of the observed phenotype is indicated. Scale bar represents 20 µm, white asterisks indicate PBs. Related to supplemental movie 1 and 2.
B) Chromosome spreads 6 hours (corresponding to metaphase I) and 16 hours (corresponding to metaphase II in controls) after GVBD. Kinetochores were stained with CREST (green) and chromosomes with Hoechst (blue). Insets show typical chromosome figures observed, for better visualization chromosomes are shown in grey scale. Scale bar represents 5 µm.
C) Whole-mount immunofluorescence staining of cold-treated spindles. Microtubules were stained with anti-tubulin antibody (green), kinetochores with CREST (red), and chromosomes with Hoechst (blue). Spindle poles typical of metaphase I and metaphase II are indicated with an arrowhead, in controls. Scale bar represents 5 µm.

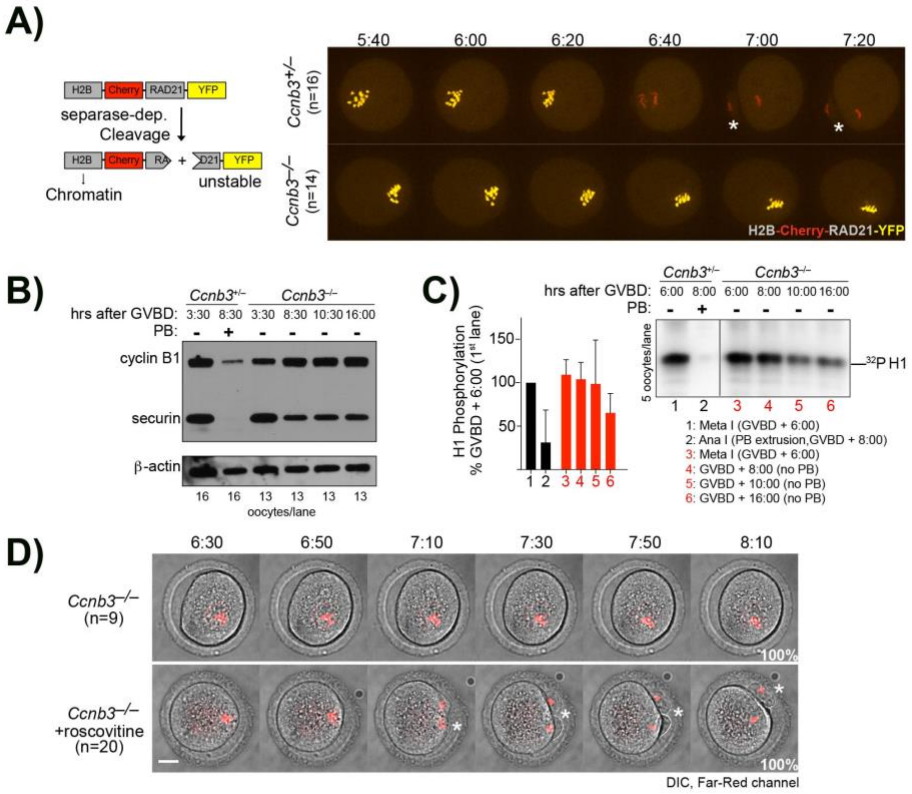

Figure 3.3: Cell cycle arrest in *Ccnb3* $^{-/-}$ oocytes is due to incomplete APC/C activation.

A) Schematic of the separase activity sensor. See text for details.

B) Failure to activate separase in the absence of cyclin B3. Separase activity sensor mRNA was injected into GV oocytes, which were released into meiosis I and visualized by spinning disk confocal microscopy. Selected time frames of collapsed z-sections (11 section, 3-µm steps) from a representative movie are shown. Time points after GVBD are indicated as hours : minutes. Scale bar represents 20 µm; white asterisks indicate PBs.

C) Western blot analysis of cyclin B1 and securin during oocyte maturation, at the time points indicated as hours : minutes after GVBD. β-actin serves as loading control. The number of oocytes used and the presence or absence of a PB are indicated.

D) Total cyclin B-CDK1 activity during oocyte maturation, at the time points indicated as hours : minutes after GVBD. Histone H1 was used as a substrate. Five oocytes were used per kinase reaction, and the presence or absence of a PB is indicated. The graph on the side shows the quantification of phosphate incorporation from 3 independent experiments and error bars indicate standard deviation.

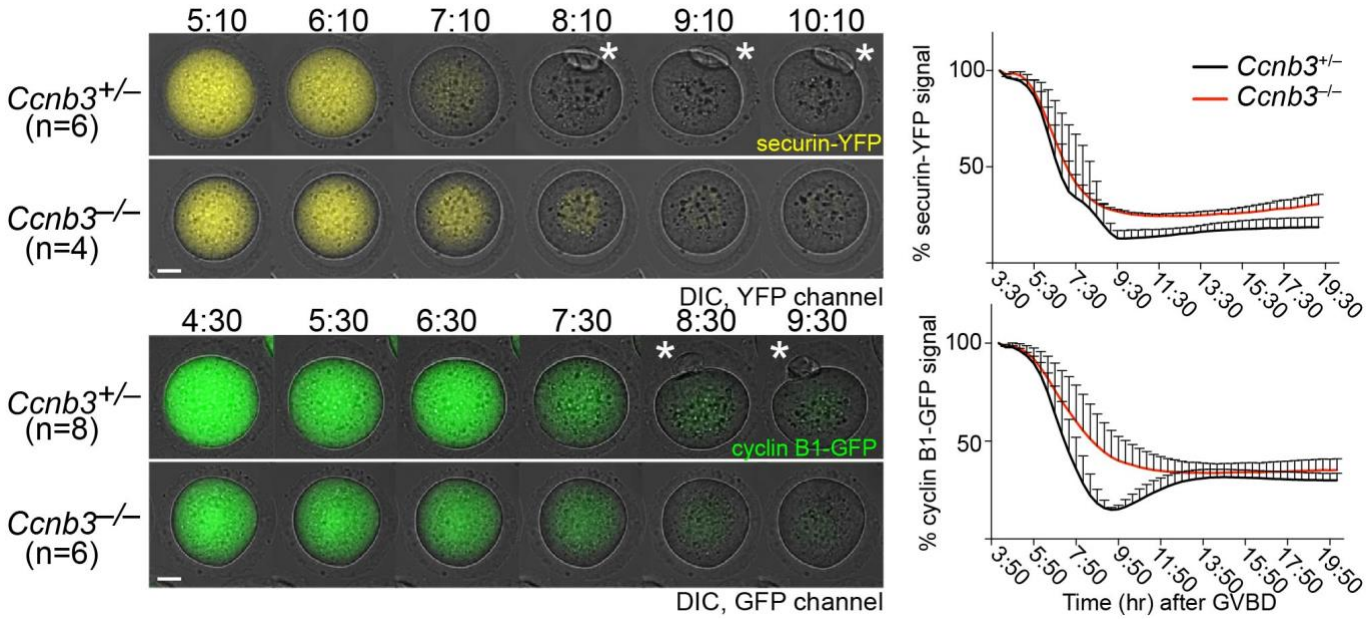

Figure 3.4: Degradation of exogenous APC/C substrates.
Securin-YFP (above) or cyclin B1-GFP (below) mRNA was injected into GV oocytes. Stills from representative movies are shown. Time points after GVBD are indicated as hours: minutes. Scale bar represents 20 μm (n: number of oocytes) and white asterisk indicates polar body extrusion (PBE). Quantification of fluorescence intensities is shown on the right (mean ± s.d. from the indicated number of oocytes imaged).

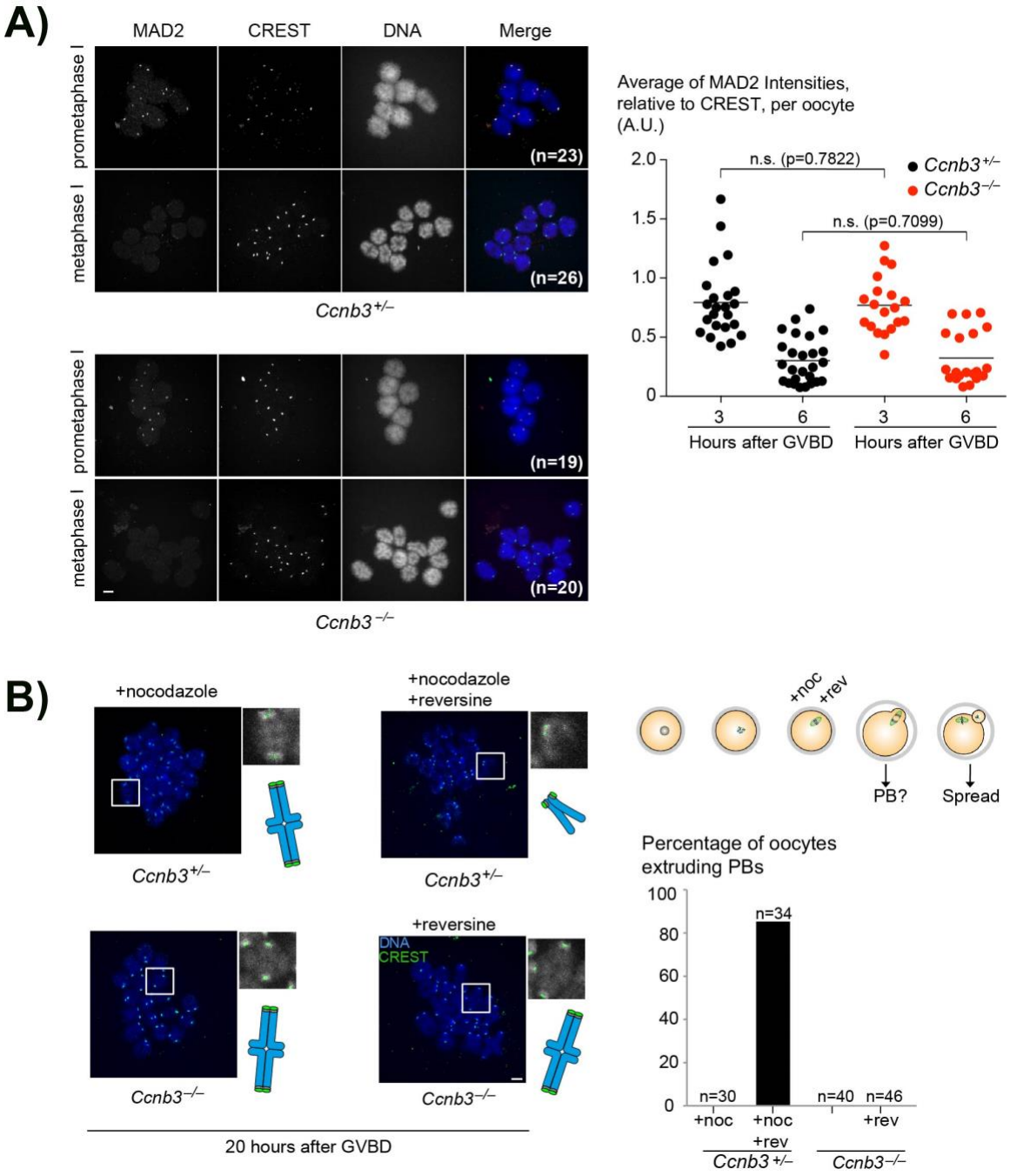
A)
MAD2
CREST
DNA
Merge
prometaphase I
metaphase I
(n=23)
(n=26)
Ccnb3+/–
(n=19)
(n=20)
Ccnb3 –/–
Average of MAD2 Intensities, relative to CREST, per oocyte (A.U.)
n.s. (p=0.7822)
n.s. (p=0.7099)
Ccnb3+/–
Ccnb3–/–
2.0
1.5
1.0
0.5
0
3
6
3
6
Hours after GVBD
Hours after GVBD
B)
+nocodazole
+nocodazole
+reversine
Ccnb3+/–
Ccnb3+/–
+reversine
DNA
CREST
Ccnb3–/–
Ccnb3–/–
20 hours after GVBD
+noc
+rev
PB?
Spread
Percentage of oocytes extruding PBs
100
80
60
40
20
0
n=34
n=30
n=40
n=46
+noc
+noc
+rev
+rev
Ccnb3 +/–
Ccnb3–/–

Figure 3.5: SAC activation is not the cause of metaphase I arrest in *Ccnb3*$^{-/-}$ oocytes.

A) Top: Chromosome spreads were prepared 3 hours (early prometaphase I) and 6 hours (metaphase I) after GVBD, then stained with Hoechst (blue), CREST (green), and anti-MAD2 (red). Scale bar represents 5 µm. Bottom: Quantification of MAD2 signal intensity relative to CREST; each point is the mean relative intensity averaged across centromeres in an oocyte. P values are from t tests (n.s., not significant).

B) Oocytes were treated with reversine to override a potential SAC arrest. Control oocytes were treated with nocodazole from 6 hours after GVBD onwards, whereas *Ccnb3*$^{-/-}$ oocytes were left untreated. 6 hours 40 min after GVBD, reversine was added to control and *Ccnb3*$^{-/-}$ oocytes. PB extrusion was scored visually (graph on the left), and oocytes were spread 20 hours after GVBD. Kinetochores were stained with CREST (green) and chromosomes with Hoechst (blue). Insets show typical chromosome figures observed, for better visualization chromosomes are shown in grey scale. Scale bar represents 5 µm.

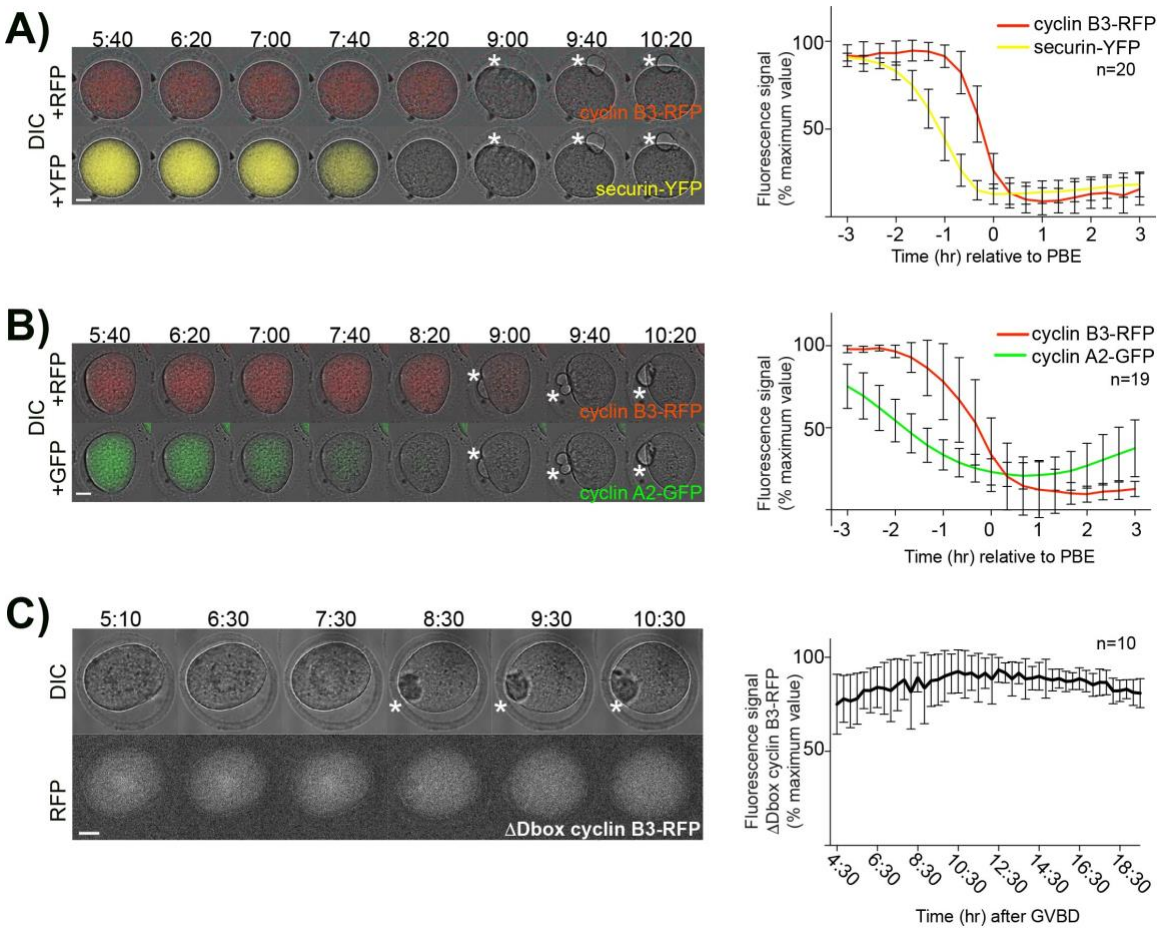

Figure 3.6: Ordered degradation of APC/C substrates in oocyte meiosis I.
A,B) Cyclin B3 is degraded after securin or cyclin A2. mRNA encoding cyclin B3-RFP and either securin-YFP (panel A) or cyclin A2-GFP (panel B) were co-injected into GV oocytes of CD-1 mice. Each panel shows selected frames from a movie of a representative oocyte, with an overlay of DIC and RFP channels in the top rows, and DIC and YFP or GFP channels in the bottom rows.
C) The D box of cyclin B3 is required for degradation. CD-1 GV oocytes were injected with mRNA encoding cyclin B3-RFP with the D box deleted (ΔDbox). Frames from a representative movie are shown, with the DIC channel on top and RFP at the bottom. All panels: Time points after GVBD (BD) are indicated as hours : minutes. Scale bar represents 20 μm and white asterisks indicate PBs. Quantification of fluorescence intensities is shown on the right (mean ± s.d. of the indicated number of oocytes).

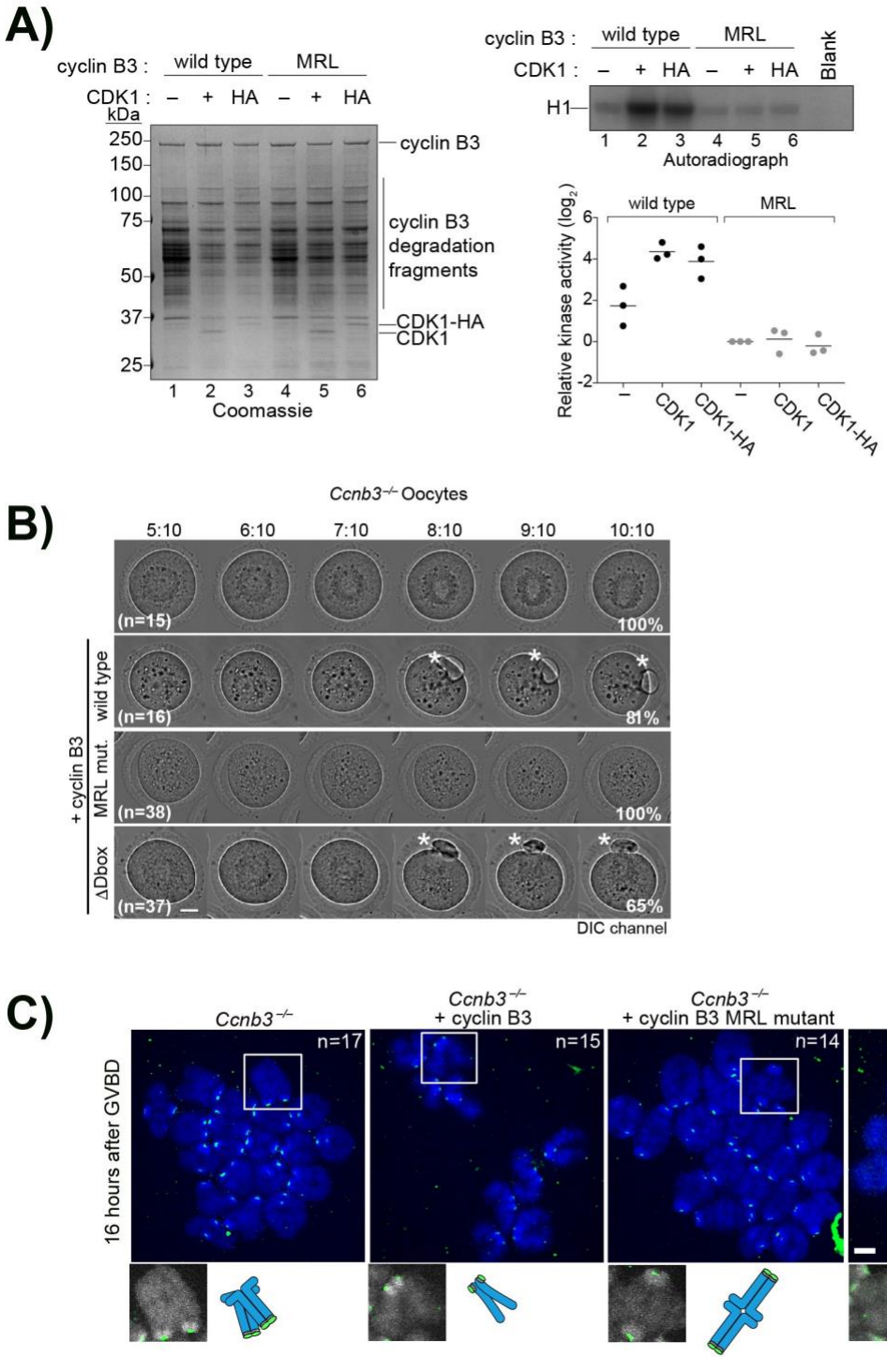
A)
cyclin B3 : wild type MRL
CDK1 : – + HA – + HA
kDa
250
150
100
75
50
37
25
cyclin B3
cyclin B3 degradation fragments
CDK1-HA
CDK1
1 2 3 4 5 6
Coomassie
cyclin B3 : wild type MRL Blank
CDK1 : – + HA – + HA
H1
1 2 3 4 5 6
Autoradiograph
wild type
MRL
Relative kinase activity (log2)
6
4
2
0
-2
–
CDK1
CDK1-HA
CDK1
CDK1-HA
B)
Ccnb3−/− Oocytes
5:10
6:10
7:10
8:10
9:10
10:10
(n=15)
100%
+ cyclin B3
wild type
(n=16)
81%
MRL mut.
(n=38)
100%
ΔDbox
(n=37)
65%
DIC channel
C)
Ccnb3−/−
Ccnb3−/− + cyclin B3
Ccnb3−/− + cyclin B3 MRL mutant
Ccnb3−/− + cyclin B1
16 hours after GVBD
n=17
n=15
n=14
DNA
CREST

Figure 3.7: Only cyclin B3 that can support *in vitro* kinase activity can rescue *Ccnb3*$^{-/-}$ oocytes.

A) Affinity purification of cyclin B3-CDK1 complexes. ^{MBPHis}cyclin B3 or ^{MBPHis}cyclin B3 MRL mutant were expressed in insect cells alone or co-expressed with either untagged or HA-tagged CDK1. (Left) The eluates from purification on amylose resin were separated on SDS-PAGE and stained with Coomasssie. (Right) Representative autoradiograph (top) and quantification (bottom) from histone H1 kinase assays. In the graph, values in each experiment (n = 3) were normalized to the signal from the ^{MBPHis}cyclin B3 MRL sample (lane 4 in the autoradiograph).

B) MRL-mutant cyclin B3 fails to rescue *Ccnb3*$^{-/-}$ oocytes. *Ccnb3*$^{-/-}$ oocytes were sham-injected or injected with the indicated cyclin mRNA, then released into meiosis I. Frames of representative movies are shown in panel B. Times after GVBD are indicated as hours : minutes and percentages of oocytes of the shown phenotypes are indicated. Scale bar represents 20 µm and white asterisks indicate PBs. Panel C shows representative chromosome spreads 16 hours after GVBD. In the case of oocytes injected with the wild type cyclin B3 construct, only oocytes that had extruded PBs were analyzed.

C) Chromosomes were stained with Hoechst (blue) and kinetochores with CREST (green). Insets show typical chromosome figures observed, for better visualization chromosomes are shown in grey scale. Schemes show corresponding chromosome figures. Scale bar represents 5 µm.

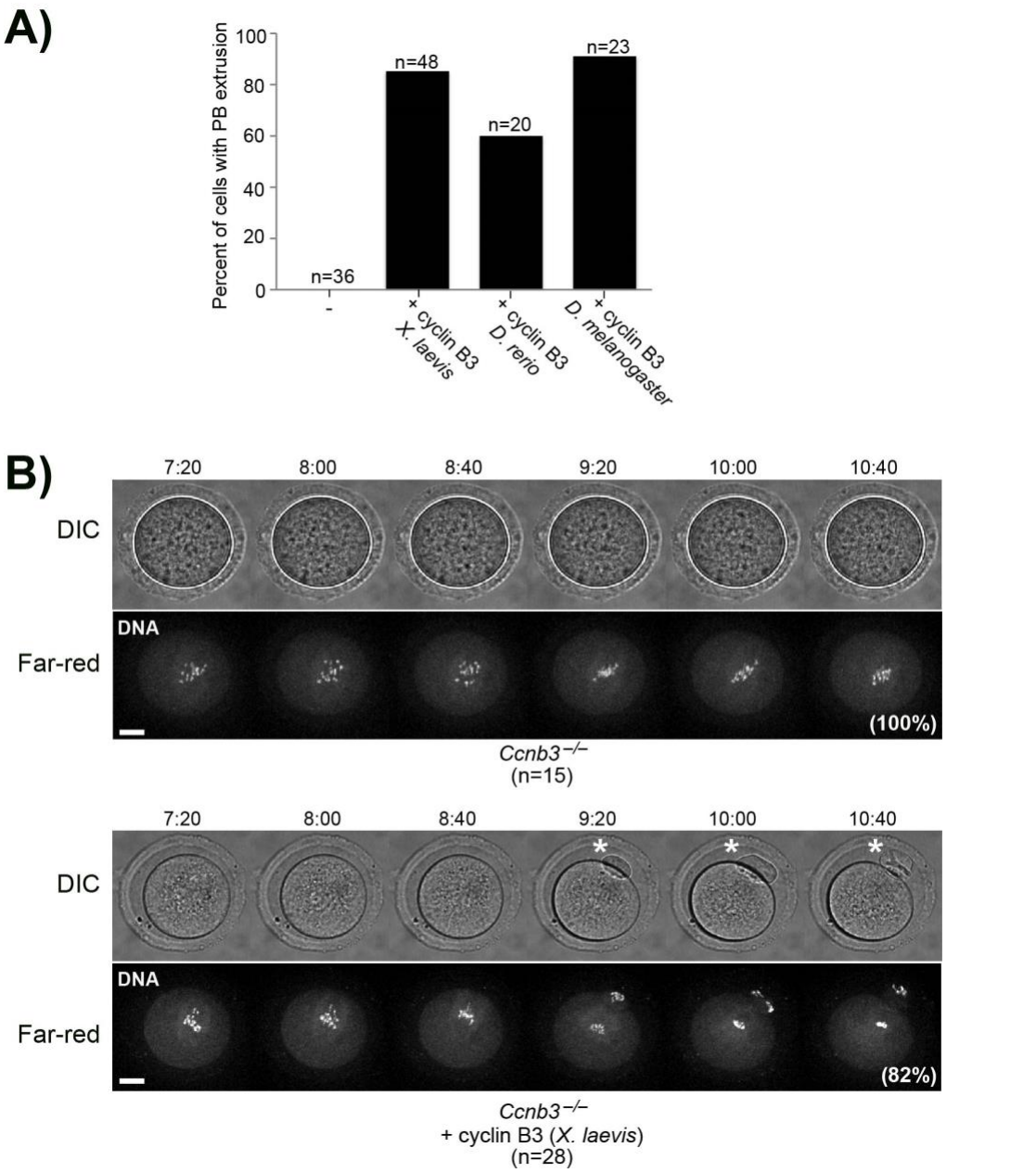

Figure 3.8: Inter-species cross-complementation of *Ccnb3* $^{-/-}$ oocytes.
A) *Ccnb3*$^{-/-}$ oocytes were injected with the indicated mRNA, induced to enter meiosis I, and scored for PB extrusion.
B) Selected time frames of collapsed z-sections (12 sections, 3-µm steps) from a representative spinning disk confocal movie of *Ccnb3*$^{-/-}$ sham-injected oocytes, and *Ccnb3*$^{-/-}$ oocytes injected with *X. laevis* cyclin B3 mRNA. Prior to live imaging oocytes were incubated with SiR-DNA. Top panel shows the DIC channel and bottom panel shows SiR-DNA staining in far-red. Time points after GVBD are indicated as hours : minutes. Scale bar represents 20 µm and white asterisks indicate PBs.

Discussion:

The aim of this study was to determine whether cyclin B3 is specifically required for meiosis, using a knock-out strategy to create mice devoid of the protein. Whereas loss of cyclin B3 has no effect on male fertility (chapter II), mutant females are sterile because cyclin B3 promotes APC/C activation and thus anaphase onset in the first meiotic division in oocytes. Similar findings were obtained independently with a different targeted mutation in *Ccnb3* (Yufei Li et al., 2018). Our findings definitively establish a crucial role for mouse cyclin B3 in the female germline.

Cyclin B3 is essential for metaphase I to anaphase I transition.

The requirement anaphase I onset in mouse is similar to *Drosophila* oocytes (Deyter et al., 2010; Yuan and O'Farrell, 2015). It has been proposed that cyclin B3 regulates APC/C activity during the rapid mitotic cycles of the early *Drosophila* embryo (Yuan and O'Farrell, 2015). The data presented in here is in accordance with a similar role in mouse oocyte meiosis I. Interestingly, however, cyclin B3-deficient oocytes show a distinct partial APC/C activation phenotype in which exogenous APC/C targets are degraded efficiently but endogenous substrates are not. This is the first time that such a discrepancy has been observed in mouse oocytes. It is not yet clear what distinguishes exogenous from endogenous substrates. One possibility is that expression timing (i.e., starting upon mRNA injection into GV oocytes) places the exogenous proteins at a disadvantage relative to endogenous proteins for binding to essential partners,

e.g., of securin to separase and cyclin B1 to CDK. It is also possible that the fluorescent protein tags interfere slightly with this binding. It is noteworthy in this context that free securin is degraded earlier than separase-bound securin, which is stabilized by maintenance in a non-phosphorylated state through association with phosphatase PP2A (Hellmuth et al., 2014). Securin phosphorylation enhances its affinity for the APC/C (Hellmuth et al., 2014; Holt et al., 2008). Regardless of the source of the distinction, our data clearly demonstrate that APC/C becomes partially active on time, but not sufficiently active to robustly provoke degradation of all of its intended targets and to trigger anaphase I.

Why is fine tuning of APC/C activity by cyclin B3 important in oocyte meiosis?

APC/C in association with CDH1 is required to maintain oocyte arrest in prophase I by destabilizing cyclin B1 and Cdc25 (Holt et al., 2010; Rattani et al., 2014). At meiosis I entry, CDH1 is only gradually shut off, leading to a slow increase of MPF (cyclin B1-CDK1) kinase activity (Polanski et al., 1998; Reis et al., 2006), and not the sharp rise observed in mitotic cells. Once MPF activity is high enough, CDH1 is inactivated. At this time in prometaphase I, SAC control keeps APC/C-CDC20 in check to prevent precocious securin and cyclin B degradation (Hached et al., 2011; Rattani et al., 2014; Reis et al., 2006). In mice, the slow handover from APC/C-CDH1-dependent to APC/C-CDC20-dependent ubiquitination is specific to oocytes. Furthermore, unlike in mitosis, SAC control is leaky in oocyte meiosis I, and onset of APC/C-dependent degradation occurs

before full kinetochore attachment status has been achieved (Touati and Wassmann, 2016). Because of these specificities, cyclin B3 may be required in oocytes, and only in oocytes, to ensure the sudden and full activation of separase by mediating rapid and efficient degradation of the pool of securin and cyclin B1 that is inhibiting separase after the degradation of free securin and cyclin B1 in the cytoplasm.

Cyclin B3 promotes full APC/C activity.

The results presented above suggest that cyclin B3 is required to tip the balance towards synchronized, full APC/C activity and progression into anaphase. Without cyclin B3 the APC/C is active, but endogenous cyclin B1 is not at all, and securin not efficiently, targeted for degradation. Consistent with this view, the rescue of *Ccnb3*$^{-/-}$ oocytes by artificially downregulating MPF activity with roscovitine indicates that sufficient separase has been liberated from its inhibitory interaction with securin in the mutant. Cyclin B3 in mammalian oocytes appears dispensable for turning off the SAC, unlike in *C. elegans* (Deyter et al., 2010), so it is possible that cyclin B3-CDK1 complexes promote full APC/C activity directly by specifically modifying APC/C substrates, APC/C subunits, APC/C activators (CDC20 and CDH1), or some combination (Alfieri et al., 2017). Nevertheless, cyclin B3 is not strictly essential, in that a small proportion of mice harbored oocytes that were able to progress through meiosis I. The reason for this incomplete penetrance is not yet clear, but may reflect subtle variation (perhaps from strain background) in either the degree of APC/C activation or the threshold

of APC/C activity needed for progression. Put in another way, cyclin B3-deficient oocytes occasionally achieve just enough APC/C activity during a critical time window to cross a threshold needed for the switch-like transition into anaphase I.

Chapter 4: Concluding discussion:

Possible role for cyclin B3 in metaphase to anaphase I transition in spermatogenesis:

The experiments in chapter 2 suggested that cyclin B3 is dispensable for spermatogenesis and detailed analysis indicated there is no abnormal behavior for recombination-related events (such as DSB formation and repair and homologous pairing) during prophase I. Similarly, meiotic prophase for cyclin B3 deficient oocytes was also not affected. Although I did not perform a detailed analysis of chromosome spreads from *Ccnb3*$^{-/-}$ oocytes, as I showed for spermatocytes in chapter 2, I counted the number of growing and developed follicles in the adult ovaries. Defects during meiotic prophase affect oocyte follicle development and leads to a depletion of oocyte pool (Baltus et al., 2006; Bolcun-Filas et al., 2014; Di Giacomo et al., 2005; Jain et al., 2018; Li et al., 2007) . Since oocyte numbers were normal in the mutant, I conclude that cyclin B3 is indeed dispensable for the meiotic prophase, both in males and females.

This is an interesting result, considering that all the previous studies suggested a role of cyclin in meiotic prophase (Nguyen et al., 2002; Refik-Rogers et al., 2006), based on in its expression pattern. Although the assays I used here cannot reveal minor effects, any possible changes did not affect meiotic progression through prophase. Redundancy between cyclins is one possible caveat that might have obscured a possible role of cyclin B3 in prophase I, as I

discussed in detail in chapter 2. Either way, cyclin B3 is not essential for meiotic prophase I in mammals.

However, I found that cyclin B3 is essential for metaphase I to anaphase I transition in oocyte maturation. This observation raises the question of whether cyclin B3 is also involved in metaphase I to anaphase I transition during spermatogenesis. Experiments in chapter 3 indicated that APC/C activity is compromised in *Ccnb3*$^{-/-}$ oocytes, which leads to inefficient degradation of APC/C substrates and inhibition of separase activation. APC/C activity is regulated during oocyte prometaphase and needs to reach a certain threshold to ubiquitinate its substrates efficiently. Our data suggest that cyclin B3, possibly as a complex with CDK1, positively contributes to the activity of APC/C in oocytes. One possibility would be that the absence of cyclin B3 also leads to reduced APC/C activity during spermatogenesis, but that this effect is not sufficient to cause a metaphase arrest. This is a hypothesis that would be worth testing.

Does cyclin B3 affect APC/C activity during spermatogenesis, similar to oocyte transition? Unfortunately, there is no available reporter system to measure APC/C activity in spermatogenesis. However, there are indirect ways of approaching that question: If *Ccnb3* spermatocytes experience lower APC/C activity than the wild type, one might expect a slower metaphase to anaphase transition, which might lead to an increased population of spermatocytes in that cell stage. To estimate cells in metaphase I, I plan to count the stage XII tubules

that contain cells going through MI and MII transition. If there is any delay in the transition, I might be able to detect an increase in stage XII tubules and in MI and MII cells within *Ccnb3*$^{-/Y}$ tubules, compared to the wild type.

In another experimental design, I would follow the degradation kinetics of APC/C substrates such as cyclin B1 and securin in spermatocytes. By staining seminiferous tubules sections with antibodies against APC/C substrates, I may be able to quantify APC/C activity during spermatogenesis. Again, if *Ccnb3*$^{-/Y}$ mice have decreased APC/C activity, the prediction would be that MI cells would retain higher levels of APC/C substrates.

Assuming that cyclin B3 actually has a role in MI transition in males, why would this role be essential in females and not in males? Perhaps, the reason lies in the fact that the MI and MII division are faster in males than in females. Thus, it is possible that the wiring between molecular players is different in MI and MII transitions in males. Specifically, the required level of APC/C activity to degrade its substrates could be lower in spermatocytes, in which case APC/C activity would be sufficient to drive MI transition even in the absence of cyclin B3. Further research will shed light on possible importance of cyclin B3 in metaphase I to anaphase I transition in spermatogenesis.

How does cyclin B3 function at the metaphase I to anaphase I transition?

In chapter 3, the data suggest the importance of cyclin B3-CDK1 complexes at the metaphase to anaphase I transition. However, mechanistically it is not known how cyclin B3-CDK1 complexes function in this transition. To investigate this, I intended to take a phospho-proteomics approach to analyze the phosphorylation status of proteins during oocyte maturation. However, the limited amount of material extracted from mouse oocytes did not make proteomics approaches feasible. Thus, I do not have any conclusive way to explain the role of cyclin B3 in metaphase to anaphase transition. Here are few possible scenarios.

The simplest model would be that cyclin B3-CDK1 contributes to APC/C activation directly by phosphorylating the subunits of APC/C or the APC/C activator, CDC20. Recent biochemical studies showed how cyclin B1-CDK phosphorylation activates APC/C *in vitro* with purified components (Fujimitsu et al., 2016; Qiao et al., 2016). Thus, it would be possible to take an *in vitro* approach to investigate if cyclin B3-CDK1 complexes regulate APC/C activity. An alternative possibility would be that some of the key APC/C substrates such as cyclin B1 and securin may not be optimal in the absence of cyclin B3. Perhaps their localization is affected and APC/C does not have efficient access to a subset of the population, or perhaps the substrates carry distinct post-translational modifications that affect their degradation. It would be possible to evaluate the cellular localization of a subsets of key APC/C substrates by

immunofluorescence experiments (but of course this could not directly prove or disprove the hypothesis).

We found that exogenously injected APC/C substrates (cyclin B1 and securin) were degraded with similar kinetics in *Ccnb3*$^{-/-}$ oocytes as in wild type oocytes. This provides evidence in support for the hypothesis that the APC/C substrates are sub-optimal in the *Ccnb3* mutant and that they may perhaps carry different modifications or somehow localize differently to the exogenous substrates. These exogenously expressed substrates might therefore serve as an experimental tool to understand what is different in the endogenous substrates. Using affinity tags, one could pull down two different populations of these proteins from the same oocytes and analyze their PTMs by using proteomics approaches. In addition, immunofluorescence staining of exogenous and endogenous substrates could also help to reveal aberrant substrate localizations within the oocytes.

Although I showed that SAC is not over-activated and is not a reason for the low APC/C activity, there is another pathway to restrict APC/C activity. CSF is mainly responsible to keep APC/C activity under regulation during MII arrest (Masui and Markert, 1971). EMI2 was identified as a key CSF factor that binds to and inhibits APC/C activity (Madgwick et al., 2006; Shoji et al., 2006). EMI2 expression is tightly regulated during MI and MII and EMI2 protein starts to accumulate at the end of MI. It is conceivable that in *Ccnb3*$^{-/-}$ oocytes, EMI2 expression is mis-regulated and starts to express prematurely. In this case, premature inhibition of

APC/C by EMI2 prior to MI transition could prevent APC/C substrate degradation and lead to metaphase I to anaphase I arrest. I tried to address this question by performing western blot experiments to quantify EMI2 expression in oocytes, but the available antibodies did not provide a conclusive result. This hypothesis could be further investigated by raising better antibodies against EMI2 to perform the western blots. Moreover, it should be possible to perform quantitative mass-spectrometry on arrested oocytes and see if EMI2 levels are elevated prematurely. Analysis on these aspects of APC/C and substrate regulation might help one to narrow down the possibilities of how cyclin B3-CDK1 complexes might function in the cell. Whether the role of cyclin B3 on APC/C activity is direct or indirect is the most important outstanding question.

Evolutionarily conserved role for cyclin B3

Since its identification in chicken, *Ccnb3* has also been found in flies, worms, humans and mice. Recently, it has been identified in proto-vertebrates such as *Ciona* and *Oikopleura dioica* (Feng and Cycle, 2018; Treen et al., 2018).

In chapter 3, I showed that injections of frog *Ccnb3* mRNA can rescue the arrest phenotype observed in the absence of *Ccnb3*. The role of *Ccnb3* has also previously been investigated in flies and a similar meiotic arrest phenotype was observed in flies lacking Ccnb3 (Sigrist et al., 1995; Yuan and O'Farrell, 2015). These observations suggest that the role of *Ccnb3* in metaphase to anaphase I transition might be widely conserved. However, the role of Ccnb3 in oogenesis

was not investigated in detail in frogs. A previous study demonstrated the presence of *Ccnb3* mRNA in oocytes, but since the protein was not detectable by western blot, the authors suggested that *Ccnb3* expression may not be important for oocyte maturation (Hochegger et al., 2001). However, my experiments suggest that Xenopus cyclin B3 may have a role, too. It would be interesting to pursue functional studies for cyclin B3 in these organisms such as frogs and zebrafish.

If the depletion of *Ccnb3* in frogs or zebrafish were to result in similar phenotypes as observed in *Ccnb3*$^{-/-}$ mouse oocytes, these experimental systems would provide valuable tools for molecular studies. Frog oocytes are much larger and around 1 mm in diameter, compared to mouse oocytes that are about 80 μm in diameter. Thus, the extracts of even a few frog oocytes are sufficient to perform several biochemistry experiments. In this respect, the experiments discussed above can be easily done with the frog oocyte extracts, which might shed light on the function of cyclin B3-CDK1 complexes in oocytes. For sure, any finding(s) from frog oocytes must be tested in the mouse oocyte system to see if the mechanism for cyclin B3-CDK1 complexes is conserved.

The data in chapter 3 indicate that *Ccnb3*$^{-/-}$ embryos develop normally since *Ccnb3*$^{-/-}$ embryos were born at the expected Mendelian frequency. However, the recent study from *Ciona* embryos investigated the genes that are important for maternal to zygotic transition and zygotic genome activation, which happens

during embryo development (Treen et al., 2018). They reported that in the absence of cyclin B3, precocious zygotic genome activation (ZGA) was observed, indicating that cyclin B3 contributes to proper timing of ZGA in this organism. Therefore, this result suggests a role for cyclin B3 in embryo development after oocyte maturation. In the system I used, it is possible that maternal *Ccnb3* mRNA stock from *Ccnb3*$^{+/-}$ would be enough to support the early steps of embryo development. Therefore, it is possible that cyclin B3 could be important for the oocyte maturation and embryo development. Further research will shed light the importance of cyclin B3 in early embryo development.

Chapter 5: Materials and Methods:

Animals:

Mice in the SK lab were maintained and sacrificed for the experiments under regulatory standards approved by the Memorial Sloan Kettering Cancer Center (MSKCC) Institutional Animal Care and Use Committee.

Generation of *Ccnb3* knock-out mouse strain, husbandry and genotyping:

Endonuclease mediated (*em*) allele was generated by the MSKCC Mouse Genetics Core Facility. Exon 7 was targeted by guide RNA (C40-TGAACTTGGCATGATAGCAC). Guide RNA was cloned into pDR274 vector for *in vitro* transcription. *In vitro* transcribed guide RNA (10 ng/μl) and Cas9 (20 ng/μl) were microinjected into pronuclei of CBA/J × C57BL/6J F2 hybrid zygotes using conventional techniques.

Genomic DNA from founder animals were subjected to PCR by using following primers, CCN3B-A GAGTATTAGCACTGAGTCAGGGAC and CCN3B-B GGAATACCTCAGTTTCTTTTGCAC and under the following conditions: 3 minutes at 94°C, then 35 cycles of 15 seconds at 94°C, 90 seconds at 68°C, followed by a final extension 3 minutes at 68°C and T7 endonuclease I digestion was performed to identify the animals carrying indels. Since male animals have one copy of the X-linked *Ccnb3* gene, T7 assay on males was performed in the presence of wild type genomic DNA.

To define the molecular nature of indels, genomic DNA from T7-positive animals was amplified using the primers indicated above. Amplified PCR fragments were used for TA Cloning (TA Clonining™ Kit with pCR™ 2.1 vector, Invitrogen). Ten white bacterial colonies were selected, inserts were sequenced, and the mutations were characterized as deletions, insertions or substitutions. The *em1* allele, an out of frame deletion, was chosen to generate the *Ccnb3*^{em1Sky} line. After two rounds of backcrossing to C57BL/6J, animals were interbred to generate homozygous and heterozygous female animals and hemizygous male animals. Primers for genotyping were

GT4-F TGTTGATGAAGAGGAATTTTTCAAATCATTCCT and

GT4-R TTCTTTTGCACCCAGAGTTGACTTAAAG.

The PCR was performed under following conditions: 2 minutes at 94°C, then 35 cycles of 20 seconds at 94°C, 30 seconds at 54°C and 30 seconds at 72°C followed by a final extension 3 minutes at 72°C. Later, the amplified PCR product (202 bp) was subjected to BsrI enzyme digestion (NEB) (two fragments, 103 and 99 bp, respectively). A BsrI site is lost in the *em1* allele. Since *Ccnb3* is X-linked, no *Ccnb3*$^{+/+}$females can be obtained through crosses yielding homozygous *Ccnb3*$^{-/-}$ mice. Therefore, we bred *Ccnb3*$^{-/Y}$ males with *Ccnb3*$^{+/-}$ females to obtain *Ccnb3*$^{-/-}$ and *Ccnb3*$^{+/-}$ females to use as experimental and littermate controls, respectively.

Total mRNA extraction, cDNA library generation and RT-qPCR:

Testes tissue from *Ccnb3*$^{+/Y}$, *Ccnb3*$^{-/Y}$ animals and juvenile animals were dissected and frozen on dry ice. Total mRNA was extracted using RNeasy Plus Mini Kit (QIAGEN, 74134) following the manufacturer's instructions. Superscript™ III First-Strand Synthesis SuperMix (Invitrogen, 18080400) was used with oligo dT primers to generate testis cDNA, which was diluted 1:10 to be used in RT-qPCR carried out using LightCycler 480 SYBR Green I Master (Roche, 4707516001) under following conditions: 10 minutes at 95°C, then 45 cycles of 10 seconds at 95°C, 20 seconds at 55°C and 10 seconds at 72°C. Amplification products were detected on the LightCycler 480 II Real-Time PCR instrument (Roche). LightCycler 480 Software was used to quantify products by absolute quantification analysis using the second derivative maximum method. All reactions were done in triplicate and the mean of crossing point (Cp) value were used for the analysis. Cp values were normalized to the value obtained for *B2M* reactions (ΔCp). Then, the differences between knockout and wild-type samples were calculated for each primer set ($\Delta\Delta$Cp) and the fold change (knockout vs wild type) was calculated as $2^{-\Delta\Delta Cp}$. In the case of the time course with juvenile testis, *Ccnb3* levels were normalized to *B2M* expression. Primers used for RT-qPCR are listed below:

(Primer: Forward 5' to 3'/ Reverse 5' to 3')

Ccnb3-1**:** CCACTACTTACATGATTGCAGCC/ AGGATGCTGCTTTCCAAAGAT

Ccnb3-2: AAAGGCATTCAATCCTGTCG/ GGATCTTGGCCTTCCTTTTC

Ccnb3-3: GCGTAGATATGCTTCGTGCATC/ AGGCTGCAGCTAGCTTTGAA

Ccna1: TGGACAGGTTTCTCTCCTGC/ CGGGCGGATATATCTCTTCA

Ccna2: TTACCCGGAGCAAGAAAACC/ TTCATTAACGTTCACTGGCTTG

Ccnb1: GGCTGACCCAAACCTCTGTA/ TCCAGTCACTTCACGACCCT

Ccnb2: AGCCTCTGTGAAACCAGTGC/ TGCAGAGCAGAGCATCAGAG

Ccne1: GTGGCTCCGACCTTTCAGTC/ CACAGTCTTGTCAATCTTGGCA

Ccne2: AGGAATCAGCCCTTGCATTATC/ CCCAGCTTAAATCTGGCAGAG

Ccnd2: CGCAGACCTTCATCGCTC/ CTGCTGAAGCCCACAGATG

Ccnd3: TGCATCTATACGGACCAGGC/ AATCAAGGCCAGGAAGTCGT

B2M: ACACTGAATTCACCCCCACTGA/ CGATCCCAGTAGACGGTCTTGG

Oocyte harvesting and *in vitro* culture:

GV stage oocytes were collected from ovaries of sacrificed CD-1 mice or *Ccnb3*$^{+/-}$ and *Ccnb3*$^{-/-}$ mice aged 8-16 weeks. Ovaries were transferred to homemade M2 medium at a temperature of 38°C and dissected to obtain oocytes. Oocytes were collected and isolated from follicular cells with mouth pipetting using torn-out Pasteur pipettes. For all microinjection experiments, ovaries and oocytes were incubated in commercial M2 medium (Sigma-Aldrich) and kept at GV stage by the addition of dibutyl cyclic AMP (dbcAMP, Sigma-Aldrich) at 100 µg/ml final concentration. Oocytes undergoing GVBD within at most 90 min after ovary dissection or release from dbcAMP were used for experiments. For experiments using *Ccnb3*$^{-/-}$ mice, 5 oocytes per mouse were left untreated and were released into meiosis I to ascertain that no PB extrusion

occurred. Roscovitine was added 6h20 after GVDB at a final concentration of 0,2 mM.

Histology:

Ovaries from *Ccnb3*$^{+/-}$ and *Ccnb3*$^{-/-}$ adult mice were fixed overnight in 4% paraformaldehyde (PFA) at 4°C. Fixed tissues were washed in water and stored in 70% ethanol at 4°C. Fixed tissues were submitted to the Molecular Cytology Core Facility (MSKCC) for embedding in paraffin and sectioning of the embedded tissue (whole ovary) as 8 µm sections and preparation of slides with ovary sections. The slides were then subjected to immunohistochemistry as follows: The immunohistochemical staining was performed at Molecular Cytology Core Facility (MSKCC) using a Discovery XT processor (Ventana Medical Systems). Ovary sections were de-paraffinized with EZPrep buffer (Ventana Medical Systems), antigen retrieval was performed with CC1 buffer (Ventana Medical Systems). Sections were blocked for 30 minutes with Background Buster solution (Innovex), followed by avidin-biotin blocking for 8 minutes (Ventana Medical Systems). Sections were then incubated with anti-VASA (Abcam, cat#ab13840, 0.17 µg/ml) for 5 hours, followed by 60 minutes incubation with biotinylated goat anti- rabbit (Vector Labs, cat# PK6101) at 1:200 dilution. The detection was performed with DAB detection kit (Ventana Medical Systems) according to manufacturer instruction. Slides were counterstained with hematoxylin and cover slipped with Permount (Fisher Scientific). IHC slides were scanned using Pannoramic Flash 250 with a 20×/0.8 NA air objective. Images were analyzed

using Pannoramic Viewer Software (3DHistech). To count oocytes, every fifth section on the slide was analyzed and the number of oocytes in primordial, primary, secondary and antral follicles were noted and summed.

Histological examination of somatic tissues:

Gross histopathological analysis of major organs and tissues was performed by the MSKCC Laboratory of Comparative Pathology Core Facility for the following male mice: two 2-month old *Ccnb3*$^{-/Y}$ males and one 2-month old *Ccnb3*$^{+/Y}$ male. Histological examination of following tissues was perfomed: diaphragm, skeletal muscle, sciatic nerve, heart/aorta, thymus, lung, kidneys, salivary gland, mesenteric lymph nodes, stomach, duodenum, pancreas, jejunum, ileum, cecum, colon, adrenals, liver, gallbladder, spleen, uterus, ovaries, cervix, urinary bladder, skin of dorsum and subjacent brown fat, skin of ventrum and adjacent mammary gland, thyroid, parathyroid, esophagus, trachea, stifle, sternum, coronal sections of head/brain, vertebrae and spinal cord. Tissues were fixed in 10% neutral buffered formalin and bones were decalcified in formic acid solution using the Surgipath Decalcifier I (Leica Biosystems) for 48 hr. Samples were routinely processed in alcohol and xylene, embedded in paraffin, sectioned (5 µm), and stained with hematoxylin and eosin. Examined tissue and organs were grossly normal in both *Ccnb3*$^{-/Y}$ males and *Ccnb3*$^{+/Y}$ male.

Extract preparation and western blotting:

To analyze endogenous protein levels, oocytes were cultured as described above. Oocytes were harvested at the indicated time points, washed in phosphate buffer saline (PBS) to remove proteins from the medium and then placed on the wall of the Eppendorf tube and snap-frozen in liquid nitrogen. Later, 7.5 µl 1× Laemmli lysis buffer was added to the tube and samples were boiled 5 minutes at 100°C.

For western blotting, samples were separated on 4–12% Bis-Tris NuPAGE precast gels (Life Technologies) at 150 V for 70 minutes. Proteins were transferred to polyvinylidene difluoride (PVDF) membranes by wet transfer method in Tris-Glycine-20% methanol, at 120 V for 40 minutes at 4°C. Membranes were blocked with 5% non-fat milk in PBS-0.1% Tween (PBS-T) for 30 minutes at room temperature on an orbital shaker. Blocked membranes were incubated with primary antibodies 1 hr at room temperature or overnight at 4°C. Membranes were washed with PBS-T for 30 minutes at room temperature, then incubated with HRP-conjugated secondary antibodies for 1 hr at room temperature. Membranes were washed with PBS-T for 15 minutes and the signal was developed by ECL Plus Perkin Elmer or ECL Prime GE Healthcare.

To analyse protein levels from mouse testis extracts, dissected testes were placed in an Eppendorf tube, frozen on dry ice and stored at -80°C. The frozen tissue was resuspended in RIPA buffer (50 mM Tris-HCL pH 7.5, 150 mM NaCl,

0.1% SDS, 0.5% sodium deoxycholate, 1% NP40) supplemented with protease inhibitors (Roche, Mini tablets). The tissue was disrupted with a plastic pestle and incubated by end-over-end rotation for 15 minutes, at 4°C. After brief sonication, samples were centrifuged at 15000 rpm for 15 minutes. The clear lysate was transferred to a new tube, and used for immunoprecipitation. Whole cell extract was pre-cleared with protein G beads by end-over-end rotation for 1 hr, at 4°C. Antibodies were added to pre-cleared lysates and incubated overnight with end-over-end rotation, at 4°C. Protein G beads were added to the tubes and incubate for 1 hr with end-over-end rotation, at 4°C. Beads were washed three times with RIPA buffer, resuspended in 1x NuPAGE LDS sample buffer (Invitrogen) with 50 mM DTT, and boiled 5 minutes to elute immunoprecipitated proteins.

Primary antibodies were used at the following dilutions to detect proteins: mouse anti-securin (ab3305, Abcam, 1:300), mouse anti-cyclin B1 (ab72, Abcam, 1:400), mouse anti-β actin (8H10D10, CST,1:1000), mouse-anti-cyclin B3 (Abmart Inc, 1:500), and rat anti-tubulin alpha (MCA78G, Biorad, 1:1000). Secondary antibodies were used at the following dilutions: goat anti-mouse IgG (H+L)-HRP (1721011, Biorad, 1:10000), and goat anti-rat IgG-HRP (AP136P, Millipore, 1:10000).

Plasmids:

Mouse *Ccnb3* mRNA was amplified by PCR from whole testis cDNA library and cloned into pRN3-RFP vectors using the In-Fusion cloning kit (Clontech, Takara).

X. laevis cyclin B3 cDNA (clone ID: 781186, NCBI ID: 379048) was purchase from Dharmacon and used as a template for PCR amplification. *D. rerio* and *D. melanogaster cyclin B3* (NCBI ID: 767751 and 42971, respectively) were amplified by PCR from cDNA from *D. rerio* embryo or the S2 cell line, respectively. Amplified products for *X. laevis*, *D. rerio* and *D. melanogaster* were cloned into pRN3-GFP vector using the In-Fusion cloning kit (Clontech, Takara). To generate *Ccnb3* MRL mutation, overlapping primers with specific mutation were used to amplify PCR product from the wild-type template pRN3-cyclin B3-RFP, the template was digested by DpnI treatment, and the PCR product was used to transform *E. coli* DH5α competent cells. To generate the ΔD-box mutation, PCR primers that delete the D-box were used to amplify the *Ccnb3* plasmid, and the resulting PCR product was phosphorylated and ligated. Primer list can be found below. Plasmids for in vitro transcription of cyclin B1-GFP, securin-YFP, histone H2B-RFP, cyclin A2-GFP and β-tubulin-GFP have been used (Brunet et al., 1998; Herbert et al., 2003; Terret et al., 2003; Touati et al., 2012; Tsurumi et al., 2004).

(Primer pair: Forward 5' to 3'/ Reverse 5' to 3')

pRN3-eRFP-cyclin B3:

ATCTGAATTCGGATCC GCCACCATGCCACCACCACTACTACCC/

AGGAGGTCATGGATCC GTGGAATAATGCACAATTCAAAAGATTCTC

pRN3-eRFP-cyclin B3 ΔDbox:

CTTTACTGCGCCTTGAGTTGAAG/ GCATCTCATAGTCAATGTGTCCAG

pRN3-eRFP-cyclin B3 MRL:

GAACTCACCAGTG ATGCGGCAGCCATTGCTGTGGACTGGTTGGTG/

CACCAACCAGTCC ACAGCAATGGCTGCCGCATCACTGGTGAGTTC

pRN3-eGFP-*X.laevis* cyclin B3:

CGCGGGCCCGGGATCC ATGATGCCTTCTCTTCGTCCATCTC/

TAGATCCGGTGGATCC TTAGCTCTGAAGGGCCTCTGTAAG

pRN3-eGFP-D*.rerio* cyclin B3

CGCGGGCCCGGGATCC ATGCCGTTTTCAAAAGGAAAAAAGCCC/

TAGATCCGGTGGATCC TCACTTCAAAAGCCCTTCAAGCTTCTC

pRN3-eGFP-D*.melanogaster* cyclin B3

CGCGGGCCCGGGATCC ATGGCGCCCACAAAAGCAACAAC/

TAGATCCGGTGGATCC CTACGACAGATTGCTTTCGTTCAGGTC

pFastBacI-MBP6His-cyclin B3

TACTTCCAATCCAATATTATGCCACCACCACTACTACCC/

TTATCCACTTCCAATATT TCAGTGGAATAATGCACAATTCAAAAG

Expression and purification of recombinant proteins:

Vectors for expression of cyclin B3 (wild type or MRL mutant) N-terminally tagged with maltose-binding protein and 6x histidine were generated by cloning in pFastBac1-MBP6XHis. Wild-type *Ccnb3* was amplified from pRN3-cyclin B3-RFP and the MRL mutant was amplified from pRN3-*cyclin B3 MRL*-RFP. The plasmid was digested with SspI restriction endonucleases. By using In-Fusion cloning kit (Clontech, Takara) the PCR products were cloned into SspI linerazed plasmid. Viruses were produced by a Bac-to-Bac Baculovirus Expression System

(Invitrogen) following the manufacturer's instructions. Baculovirus expressing CDK1 and CDK1-HA were generously supplied by Dr. R. Fisher (Desai et al., 1992).

To express ^{MBPHis}cyclin B3 and ^{MBPHis}cyclin B3 MRL alone, *Spodoptera frugiperda* Sf9 cells were infected with virus at a multiplicity of infection (MOI) of 3. To express ^{MBPHis}cyclin B3-CDK1or CDK1-HA and ^{MBPHis}cyclin B3 MRL-CDK1or CDK1-HA complexes, Sf9 cells were infected with both viruses at a multiplicity of infection (MOI) of 3 and 2, respectively. Cells from two 150 mm plastic dishes per infection (each containing ~ 3×10^7 cells) were harvested 48 hours after infection by centrifugation at 1500 rpm for 5 minutes and then washed with ice-cold PBS. Cell pellets were resuspended in 1.7 ml of ice-cold lysis buffer (25 mM HEPES-NaOH pH 7.5, 150 mM NaCl, 100 μM leupeptin (Sigma-Aldrich, L2884)), 1× Complete protease inhibitor tablet (Roche) and 0.5 mM phenylmethanesulfonyl fluoride (PMSF)). Cells were lysed by sonication and centrifuged at 15000 rpm for 30 minutes, at 4°C. The cleared extract was moved to a 2 ml Eppendorf tube and mixed with 300 µl slurry of amylose resin (NEB, E802L) pre-equilibrated with lysis buffer. After 1 hour at 4°C with end-over-end rotation, the amylose resin was centrifuged at 300 *g*, for 1 minute, at 4°C. Resin was washed briefly with ice-cold lysis buffer before transfer on Bio-Spin chromatography columns (BioRad, 7326008). The resin on the column was washed five times with ice-cold wash buffer (lysis buffer plus 10% glycerol). To elute the proteins from the column, the

resin was incubated with 100–200 μl ice-cold elution buffer (wash buffer plus 10 mM maltose (Sigma, M5885)). All steps during the purification were done at 4°C.

Histone H1 kinase assay with recombinant proteins expressed in Sf9 cells:

Eluates from the amylose affinity purification step were used for histone H1 kinase assays. Reactions were performed in 10 mM HEPES-NaOH pH 7.4, 75 mM NaCl, 1 mM DTT, 10 mM $MgCl_2$, 100 μM ATP (Roche, 11140965001), 1 μCi [γ–^{32}P] ATP and histone H1 (5 μg/μl) (Sigma, 10223549001). 10 μl reaction mix was added to 10 μl eluate from the amylose resin and incubated for 30 minutes at room temperature. To terminate reactions, 5 μl of 4× SDS sample buffer was added to each reaction and samples were boiled for 5 mins before loading on 12% NuPage Bis-Tris NuPAGE precast gels (Life Technologies). Samples were subjected to electrophoresis at 150 V for 60 minutes. The gel was then vacuum dried for 45 minutes, at 80°C. Radiolabelled species were imaged using a Fuji phosphoimager and analyzed by Image Gauge software.

Histone H1 kinase assays using oocyte extracts:

Kinase assays to determine endogenous MPF activity were performed on aliquots of 5 oocytes at the indicated stages of meiotic maturation such as described before [30]. In short, oocytes were lysed in 3 μl of lysis buffer ((50 mM Tris (pH 7.5), 150 mM NaCl, 1% Igepal (Sigma), 10% glycerol, 2 mM EDTA, supplemented with protease inhibitors (Roche, Mini tablets) on ice for 20 minutes before adding 6 μl kinase assay buffer (50mM Tris (pH 7.5), 150 mM NaCl,

10mM $MgCl_2$, 0.5 mM DTT, 2.5 mM EGTA, 150 µM ATP) supplemented with 3 µCi of [γ-^{32}P]ATP (Perkin Elmer) per sample. Histone H1 (Millipore, 0.5 µg per sample) was used as a substrate. Kinase reactions were incubated 30 min at 30°C, denatured, and analyzed by SDS-PAGE. The gel was fixed and dried before being exposed and scanned to detect incorportation of [γ-^{32}P]ATP into the substrate, using a Typhoon FLA9000 phosphorimager (GE Healthcare Life Sciences). Scans were analyzed by ImageJ.

Microinjection and live imaging:

In vitro transcription of all mRNAs was done using the Ambion mMessage Machine kit according to the manufacturer's instructions. mRNAs (1 to 10 pM) were purified on RNeasy purification columns (Qiagen). GV stage oocytes were microinjected with mRNA on an inverted Nikon Eclipse Ti microscope. Microinjection pipettes were made using a magnetic puller (Narishige PN-30). Oocytes were manipulated with a holding pipette (VacuTip from Eppendorf) and injection was done using a FemtoJet Microinjector pump (Eppendorf) with continuous flow. Injection of the oocytes was done on a Tokai Hit temperature controlled glass plate at 38°C. Live imaging of oocytes in Figures 3.3A, 3.3D and 3.8B was carried out on an inverted Zeiss Axiovert 200M microscope coupled to an EMCCD camera (Evolve 512, Photometrics), combined with an MS-2000 automated stage (Applied Scientific Instrumentation), a Yokogawa CSU-X1 spinning disc and a nanopositioner MCL Nano-Drive and using a Plan-APO (40×/1.4 NA) oil objective (Zeiss). Alternatively, a Nikon eclipse TE 2000-E

inverted microscope with motorized stage, equipped with PrecisExite High Power LED Fluorescence (LAM 1: 400/465, LAM 2: 585), a Märzhäuser Scanning Stage, a CoolSNAP HQ2 camera, and a Plan APO (20×/0.75 NA) objective was used. For Figures 3.3A, 3.3D and 3.8B, images of chromosomes were acquired using the inverted microscope Zeiss Axiovert 200M with 11 z-sections of 3 µm. Both microscopes were controlled by Metamorph software.

Chromosome spreads and immunofluorescence:

Oocytes were rinsed in successive drops of Tyrode's acid solution to remove their *zona pellucida.* For chromosome spreads, oocytes were fixed at room temperature using a spread solution (1% paraformaldehyde, 0.15% Triton X-100 and 3 mM DTT, from Sigma-Aldrich), at the time points indicated. For whole-mount immunofluorescence, chambers were coated with concanavaline A (Sigma-Aldrich) in M2 PVP (polyvinylpyrrolidone 0,1mM from Merck-Millipore) medium and oocytes were placed in the chambers and centrifuged at 1400 rpm for 13 min at 38°C. Oocytes were then placed in a cold treatment solution (20 mM HEPES-NaOH, 1 mM $MgCl_2$, pH 7.4) on top of ice (4°C) for 4 min to remove unstable microtubules. Following cold treatment, oocytes were incubated in a formaldehyde fixation solution (BRB80 medium with 0.3% Triton X-100, 1.9% formaldehyde (Sigma-Aldrich)) at 38°C for 30 min. Primary antibodies were used at the indicated concentrations: human CREST serum autoimmune antibody against centromere (Immunovision, HCT-0100, 1:100), rabbit polyclonal anti-MAD2 (1:50)[71], and mouse monoclonal anti-alpha-tubulin (DM1A) coupled

to FITC (Sigma-Aldrich, F2168, 1:100). Secondary antibodies were used at the following concentrations: anti-human Alexa 488 (Life Technologies, A11013, 1:200), anti-human Cy3 (Jackson ImmunoResearch, #709-166-149, 1:200), anti-rabbit Cy3 (Jackson ImmunoResearch, #711-166-152, 1:200). Hoechst 3342 (Invitrogen, H21492) at 50 µg/ml was used to stain chromosomes and AF1 Citifluor mounting medium was used.

Image acquisitions of fixed oocytes:

An inverted Zeiss Axiovert 200M microscope as described above was used to image chromosome spreads and for whole mount immunofluorescence acquisitions, using a 100×/1.4 NA oil objective coupled to an EMCCD camera (Evolve 512, Photometrics). Six z-sections of 0.4 µm were taken for spreads, and 11 z-sections of 1 µm for whole mount oocytes. Stacks were assembled in ImageJ.

Quantification of fluorescent signals:

For the quantification of MAD2 fluorescence signal, the intensity was calculated for each kinetochore using an 8 × 8 pixels square on the kinetochore (where CREST signal is located). The same sized square was used adjacent to the MAD2 fluorescence to measure background, which was subtracted from the MAD2 signal. The MAD2 fluorescence intensity was normalized to the CREST signal of the same kinetochore. For the cyclin B3-RFP, ΔDbox cyclin B3-RFP, cyclin A2-GFP, cyclin B1-GFP, and securin-YFP quantifications, a 150 × 150

pixels circle was placed in the center of each oocyte for the fluorescence intensity signal measurement, and another placed adjacent to the oocyte to measure background. For each oocyte, background-subtracted values were normalized relative to the highest value. All measurements were done using ImageJ software.

Statistical analysis:

For statistical analysis, GraphPad Prism 7 was used. For the comparison of independent samples, unpaired Student's t test was carried out. Error bars indicate means ± standard deviation. Sample size and statistical tests are indicated in the figure and figure legends, respectively. Selection of oocytes for different conditions was at random. No statistical analysis was used to determine sample size. Collection and analysis of the data were not performed blind to the conditions of the experiments, no data from experiments were excluded from analysis.

Appendix: Identification and the role of *Ankrd31* in spermatogenesis[2].

Summary:

In this section, I identified an uncharacterized mouse gene called *Ankrd31*. ANKRD31 interacts with REC114 *in vivo* and *in vitro*. Spermatocytes lacking ANKRD31 lose control of DSB location and fail to target DSBs to X and Y pseudoautosomal regions (PAR). Unrepaired DSBs and pairing failures—stochastic on autosomes, complete on X and Y—cause arrest in prophase or metaphase, inducing male sterility and female premature ovarian failure. *In vivo*, ANKRD31 recruits REC114 to the PAR and elsewhere. Our findings inform a model that ANKRD31 is a scaffold anchoring REC114 and other factors to specific genomic locations, promoting efficient and timely DSB formation but also suppressing formation of clustered DSBs.

Background:

Meiotic DSBs are made by the topoisomerase-like SPO11 protein in conjunction with a suite of accessory proteins ("DSB proteins"), most but not all of which are evolutionarily conserved (Keeney, 2008; Lam and Keeney, 2015; Robert et al., 2016). Spo11 has nine essential partners in budding yeast, where DSB proteins

[2] Adapted from Boekhout*, Karasu*, Wang* et al (2018), REC114 partner ANKRD31 controls number, timing and location of meiotic DNA breaks (bioRxiv). * co-first authors.

are best characterized, including the meiosis-specific Rec114, Mei4, and Mer2. In mice, DSB formation similarly requires REC114, MEI4, and IHO1 (a Mer2 ortholog) (Kumar et al., 2010; Kumar et al., 2018; Stanzione et al., 2016; Tessé et al., 2017). We have a broad-strokes picture of the network of interactions connecting these proteins (e.g., Arora et al., 2004; Li et al., 2006a; Maleki et al., 2007; Miyoshi et al., 2012), but mechanistic detail is lacking. How these proteins localize to chromosomes is also not well defined. Moreover, while many of the DSB proteins are nearly universal in eukaryotes, phylogenetically restricted examples such as vertebrate MEI1 (Libby et al., 2002) raise the possibility that the catalog of relevant proteins may not be complete. In this study, I aimed to find novel DSB protein(s) through a yeast two-hybrid screen.

Results:

Yeast two-hybrid screen for REC114 and MEI4 interacting partners.

To identify proteins involved in meiotic DSB formation, I used mouse REC114 and MEI4 as yeast two-hybrid baits to screen a cDNA library from leptotene/zygotene spermatocytes. REC114 was recovered when MEI4 was the bait, consistent with known interactions in mouse (Kumar et al., 2010) and yeasts (Arora et al., 2004; Miyoshi et al., 2012). When REC114 was the bait, the screen yielded two clones encoding portions of the previously uncharacterized protein ANKRD31 (Figure A.1A), among other hits (see Methods).

These candidates were prioritized by evaluating sequence conservation. Meiotic factors are often rapidly evolving (Keeney, 2008; Swanson and reviews genetics, 2002). For example, the meiotic DNA strand exchange protein DMC1 and the meiotic cohesin subunits REC8, RAD21L, and SMC1β have diverged more than their paralogs that function in all cells (RAD51, RAD21, and SMC1α) (Figure A.1B,C). It is conceivable that proteins displaying this signature might be directly involved in meiotic processes. Therefore, I focused on ANKRD31 because it has relatively high rates of sequence divergence in mammals (Figure A.1C).

Characterization of *Ankrd31* expression during meiotic prophase I in spermatogenesis.

Ankrd31 cDNA (5.9 kb) from testis matched NCBI reference RNA XM_006517797.1, comprising 26 exons and encoding a predicted protein of 206 kDa (Figure A.2A). ANKRD31 has two ankyrin-repeat domains (ARDs) with three ankyrin repeats apiece. Each repeat is a ~33-amino-acid alpha-helical motif and ARDs are often involved in protein-protein interactions (Li et al., 2006b). Orthologs of were identified across the vertebrate subphylum including cartilaginous fish (e.g., ghost shark *Callorhinchus milii*), but not in more distant taxa. Alignments of vertebrate orthologs identified conserved domains (CDs) overlapping each ARD (the first appears to be absent in fish species) plus three CDs in the C-terminal third of the protein (Figure A.2A). CD5 at the C-terminus

interacts directly with REC114 (detailed below); functions of the others remain to be determined.

To further characterize ANKRD31 expression, I raised polyclonal antisera in rabbit and guinea pig. IP- western blot experiments recognized a protein migrating near the expected size from extracts of adult testes, and this protein was absent from homozygotes for an *Ankrd31* frameshift allele described below, confirming specificity (shown below Figure A.3A). *Ankrd31* protein and mRNA were present in adult testis with little or no expression in somatic tissues (Figure A.2B,C), and they accumulated during the first wave of meiosis in testes of juvenile mice (Figure A.2D). *Ankrd31* expression thus appears to be largely meiosis-specific.

To analyze the ANKRD31 expression pattern during meiotic prophase I, I stained meiotic chromosome spreads with ANKRD31 antibodies (Figure A.3). At pre-leptonema, ANKRD31 already formed a few bright foci. At leptonema, ANKRD31 formed numerous foci mostly decorating chromosome axes . Focus numbers then decreased progressively through zygonema, particularly in synapsed regions. Several heavily-stained ANKRD31 blobs were also detected (arrowheads in Figure A.3), which correspond to the PARs of the X and Y chromosomes (see zygotene cells in Figure A.3 and A.4). Both antibodies showed the similar pattern for ANKRD31 staining, confirming the specificity of the antibodies. Little or no background staining was also seen in the *Ankrd31* mutant,

again indicating antibody specificity (Figure A.4A, right side). ANKRD31 colocalized with REC114, both in small foci and in the large blobs, supporting the idea that these proteins interact physically in vivo (Figure A.4A, right side).

To further investigate the interaction between ANKRD31 and REC114, I took a proteomics approach by performing an IP-Mass spectrometry experiment. I pulled down ANKRD31 from 12 dpp old juvenile wild type and *Ankrd31* mutant testis extracts with an antibody raised in rabbits or guinea pigs (Figure A.4C). Extracts from Ankrd31 mutant testes were used as negative control to account for non-specific binding to the beads and antibodies. The mass spec results showed that ANKRD31 is the most abundant protein found in the peptide mixture, as expected (Figure A.4C). ANKRD31 pulled down REC114 and MEI4 from wild type extracts, but not *Ankrd31* mutant extracts, suggesting that ANKRD31 interacts with REC114 *in vivo* as well. This data also suggests that ANKRD31 interacts with MEI4. However, MEI4 is a direct interacting partner of REC114 (Kumar et al., 2010). In addition, yeast two-hybrid experiments did not show any interaction between MEI4 and ANKRD31. It is therefore more likely that MEI4 was pulled down indirectly through REC114.

In vitro expression and purification of ANKRD31$_C$-REC114$_N$ complex.

To delineate how ANKRD31 and REC114 interact, I characterized the interaction biochemically. By yeast two-hybrid assay, the N-terminal two-thirds of REC114

(aa 1–147) and the C-terminal tail of ANKRD31 (aa 1810–1857) were necessary and sufficient for interaction (Figure A.5A,B). I tagged the ANRKD31 fragment with six histidines and the REC114 fragment with Flag sequences, and co-expressed the fragments in *E. coli*. This provided soluble complexes, which I then purified by affinity chromatography (Figure A.5C). A pull-down of ANKRD31 on nickel resin depleted Flag-tagged REC114 from the input (see flow through lane), indicating the formation of a stable complex. Moreover, the eluted fractions showed the presence of both proteins. I subjected the nickel eluates to size exclusion chromatography, which yielded a single peak. The relative intensity of the Coomassie-stained bands, and a comparison of the elution volume with appropriate molecular weight markers, suggest that the complex has a 1:1 stoichiometric ratio (Figure A.5D).

In collaboration with Dr. Juncheng Wang (Patel Lab, MSKCC), a crystal structure of the complex was solved by single-wavelength anomalous diffraction, and refined it at 2.8 Å resolution. $REC114_N$ adopts a β-sandwich fold consisting of two nearly orthogonal antiparallel β-sheets, that is closed at one end by a C-terminal amphipathic α-helix (α1) and remains open at the other end (Figure A.5E). The N-terminal β-sheet is formed by β1 and β4–β6 and the C-terminal sheet comprises β2, β3, and β7–β9. These secondary structure elements form a hydrophobic core that stabilizes the β-sandwich fold. The loop connecting β2 and β3 is invisible in the density map, indicating high flexibility.

ANKRD31$_C$ wraps around the REC114 β-sheets to form an intermolecular sandwich fold, burying ~1800 Å^2 of surface area (Figure A.5E). Almost all ANKRD31$_C$ residues, including the ultimate C terminus, are involved in the interaction with REC114$_N$ (Figure A.5E). and can be well traced in the structure.

CRISPR-Cas9 mediated Ankrd31 knock out alleles.

To determine the function of *Ankrd31*, we used CRISPR-Cas9 to generate endonuclease-mediated (em) mutations in exon 3. Two alleles were recovered with single-nucleotide insertions at the same position (Figure A.6A). Indistinguishable phenotypes were observed for either homozygote where tested, so for simplicity experiments with the *Ankrd31^{em1}* allele (hereafter *Ankrd31$^-$*) are shown unless indicated otherwise. *Ankrd31$^{-/-}$* testes lacked detectable signal in IP/westerns (Figure A.6B), indicating that these are null or severe loss-of-function alleles. Distinct mutations generated by Tóth and colleagues gave similar phenotypes, reinforcing that these alleles abolish ANKRD31 function (Papanikos et al, 2018, BioRxiv).

Ankrd31$^{-/-}$ males are viable and sterile[3].

Ankrd31$^{+/-}$ heterozygotes showed normal fertility and Mendelian transmission of the mutations. Histopathological analysis turned up no obvious somatic defects in homozygous mutants (see Methods), suggesting that ANKRD31 is dispensable

[3] I was mostly involved in preliminary analysis of the *Ankrd31* knock-out mice. The detailed analysis was then conducted by Dr. Michiel Boekhout. Some parts of the figures that I present were provided by Dr. Boekhout.

in non-meiotic cells. However, *Ankrd31*$^{-/-}$ males were sterile: none of the 4 animals tested sired offspring when bred with wild-type females for 16 weeks, and testes were 37% of the size in littermate controls (Figure A.6C).

Male mice unable to initiate or complete meiotic recombination display sterility and hypogonadism because of apoptotic elimination of spermatocytes (de Rooij and de Boer, 2003). To determine when gametogenesis fails in *Ankrd31* mutants, testis sections were examined. Control animals had the full array of spermatogenic cells including spermatocytes and round and elongated spermatids, as expected (Figure A.6D). In contrast, *Ankrd31*$^{-/-}$ tubules contained spermatogonia and primary spermatocytes but were largely if not completely devoid of postmeiotic cells (Figure A.6D). TUNEL staining detected an elevated frequency of apoptosis (Figure A.6E). In a subset of apoptotic tubules, dying cells were pachytene spermatocytes (Figure A.6E), similar to mutants lacking or unable to repair DSBs (e.g., *Spo11*$^{-/-}$ or *Dmc1*$^{-/-}$) (Barchi et al., 2005). However, pachytene arrest was only partially penetrant, as subsets of tubules instead contained apoptotic cells at metaphase I (Figure A.6D).

Sex chromosome pairing and recombination is dependent on *Ankrd31*.

Metaphase I arrest is typical of mutants that can complete DSB repair but that fail to generate crossovers on some or all chromosomes (Kauppi et al., 2011; Libby et al., 2002; Odorisio et al., 1998). Indeed, *Ankrd31*$^{-/-}$ metaphase I

spermatocytes frequently had lagging chromosomes (FigureA.6). To determine if specific chromosomes were primarily responsible, we examined spermatocyte spreads by immunostaining spread spermatocyte chromosomes for SYCP3 and the SC central region component SYCP1 (de Vries et al., 2005). Strikingly, the sex chromosomes were unpaired and asynaptic in majority of otherwise normal-looking pachytene cells (Figure A.7A and B). By comparison, autosomes showed at most only a modest defect: pachytene cells with complete autosome synapsis had a small increase in the number of MLH1 foci (means of 22.4 in wild type and 23.1 in *Ankrd31*$^{-/-}$), which mark most sites where crossovers will form (Gray and Cohen, 2016) (Figure A.7C).

These results indicate that those cells that can progress past pachynema not only successfully navigate pairing and synapsis of autosomes but also efficiently generate autosomal crossovers and chiasmata, thus ensuring proper biorientation on the metaphase I spindle (with perhaps relatively infrequent exceptions). In contrast, the X and Y almost always fail to pair, synapse, and recombine, leading to achiasmate sex chromosomes at metaphase I, which are known to trigger apoptosis (Kauppi et al., 2011; Odorisio et al., 1998). Thus, while ANKRD31 contributes to effective recombination and pairing on autosomes, it is absolutely essential on sex chromosomes in males.

REC114 foci formation is affected in *Ankrd31*$^{-/-}$ spermatocytes.

Because I isolated ANKRD31 as a REC114 interactor and because the variable synaptic defects in *Ankrd31*$^{-/-}$ mutants resemble those in mice with reduced DSB numbers (Kauppi et al., 2013), I hypothesized that ANKRD31 contributes to DSB formation. To test this idea, we examined chromosomal assembly of pre- and post-DSB recombination proteins. *Ankrd31*$^{-/-}$ spermatocytes had fewer and less intense axial foci of REC114 genome-wide throughout prophase I, and REC114 no longer formed blobs on the PAR (Figure A.8) (Acquiaviva et al, unpublished data). This functional dependency strengthens the conclusion that ANKRD31 and REC114 interact *in vivo*.

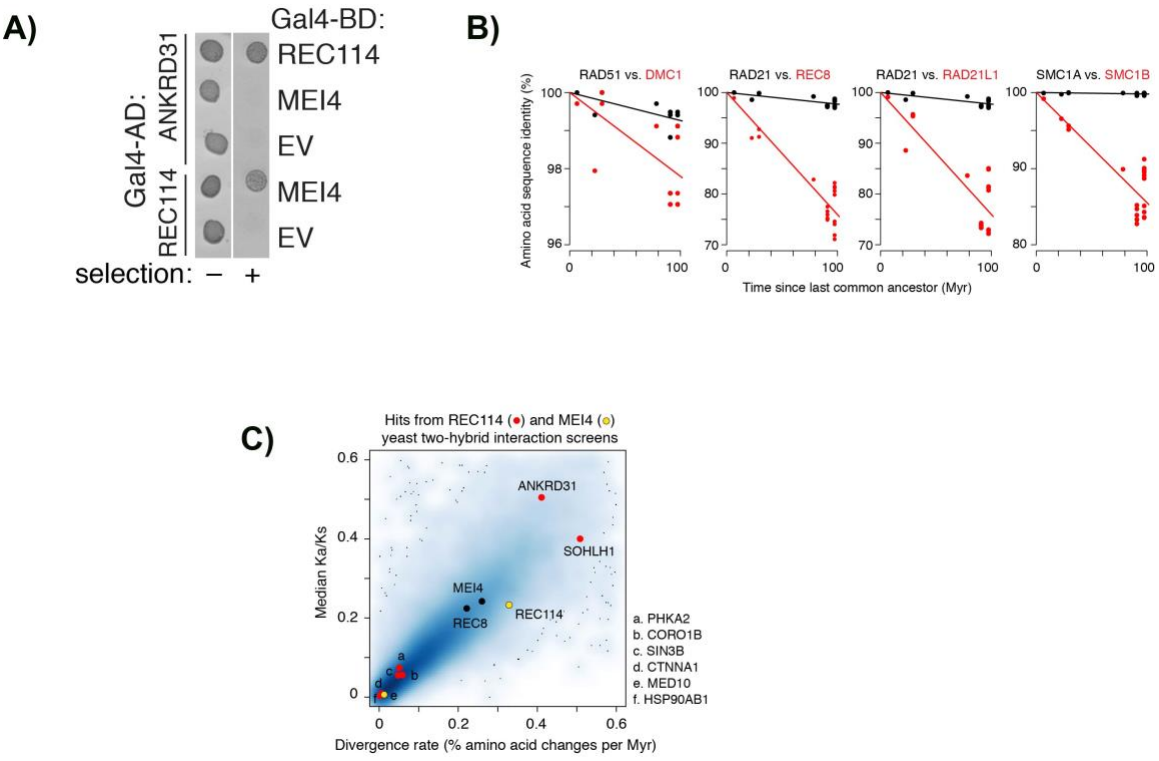

Figure A.1: Identification of ANKRD31 through yeast two hybrid screen.
A) Yeast two-hybrid assay showing REC114 interactions with ANKRD31 and MEI4. Growth of cells expressing the indicated Gal4 activating domain (AD) and binding domain (BD) fusions is shown. EV, empty vector. "Selection" indicates presence of aureobasidin to detect activation of the two-hybrid reporter.
B) Meiosis-specific proteins typically show more rapid sequence divergence than their more ubiquitously expressed paralogs. Graphs show amino acid sequence identity as a function of time since last common ancestor for pairwise comparisons of orthologs in different mammalian species for either a meiosis-specific protein (red) or its ubiquitously expressed paralog (black). Species included: Homo sapiens, Pan troglodytes, Maccaca mulatta, Canis familiaris, Bos taurus, Mus musculus, and Rattus norvegicus. Lines are least squares fits with intercepts set at 100% identity. Note differences in y axes: the trend of more rapid divergence of the meiotic paralog is true regardless of overall rate of sequence divergence for the specific protein type. Even for the relatively highly conserved proteins DMC1 and RAD51, the meiotic version is more rapidly diverging.
C) Plots of Ka/Ks (ratio of the number of nonsynonymous substitutions per non-synonymous site to the number of synonymous substitutions per synonymous site) vs. amino acid sequence divergence rate within mammals (see Methods). Data for all proteins in the NCBI HomoloGene database (Release 68 (April 2014), https://www.ncbi.nlm.nih.gov/homologene) were plotted using the smoothScatter function in R (blue to gray shading), and overlaid with hits from the yeast two-hybrid screens (red and yellow points).

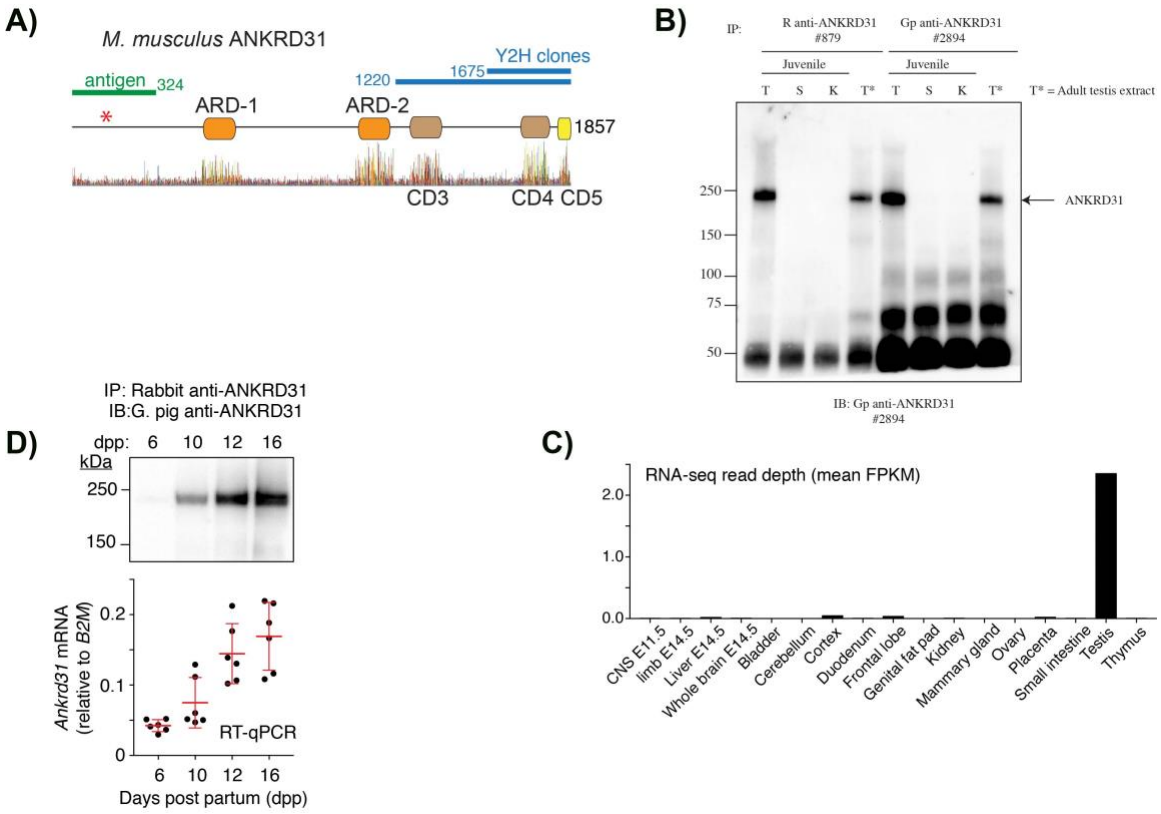

Figure A.2: Characterization of *Ankrd31* expression during spermatogenesis.
A) Domain structure of mouse ANKRD31 (above) and conservation plot for vertebrate homologs (below, (Wheeler et al., 2014)). Positions of frameshift mutation (asterisk), yeast two-hybrid (Y2H) clones, and antigen used for antibody production are indicated. Conserved domains (CD1–CD5) are indicated.
B) Immunoprecipitation (IP) and immunoblotting (IB) of ANKRD31 from extracts of testis (T), spleen (S) or kidney (K) from 17-dpp juveniles or testis from adult, using antisera raised in the indicated species.
C) Ankrd31 RNA-seq read depth in various tissues (FPKM, fragments per kb per million reads).
D) Expression time course of ANKRD31 protein (top, IP/IB) and RNA (below, reverse-transcription quantitative PCR) in testes of juvenile mice. RT-qPCR was normalized to expression of the B2M gene. Red lines, mean ± s.d.

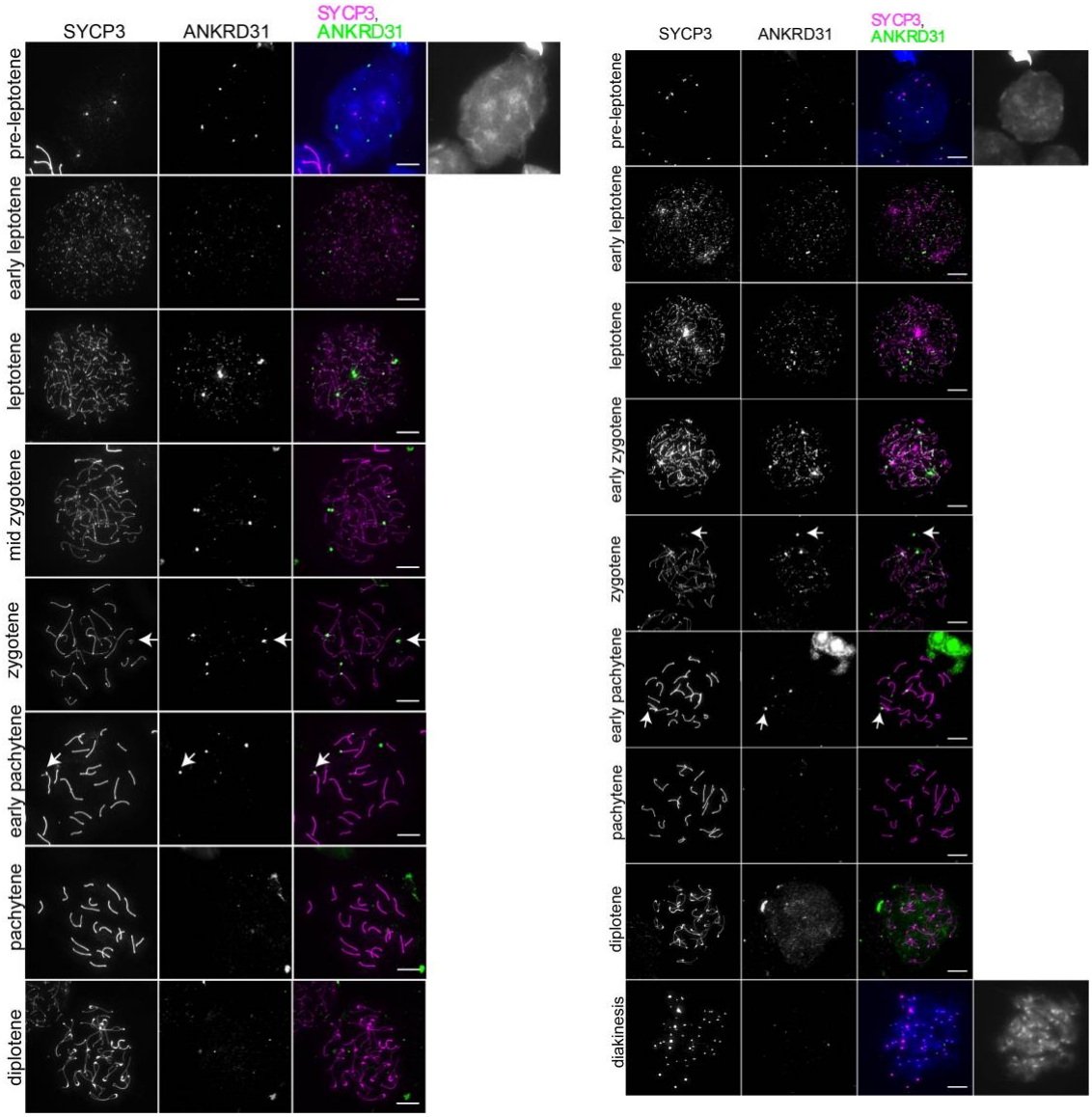

Figure A.3: ANKRD31 localizes to chromatin.
Spread spermatocyte chromosomes during meiotic prophase were stained for SYCP3, ANKRD31 rabbit antiserum on the left, guinea pig antiserum on the right. Arrowheads indicate examples of ANKRD31 localization on the PAR region of the sex chromosomes in zygotene (Y chromosome) and early pachytene. Scale bars are 10 µm.

A)

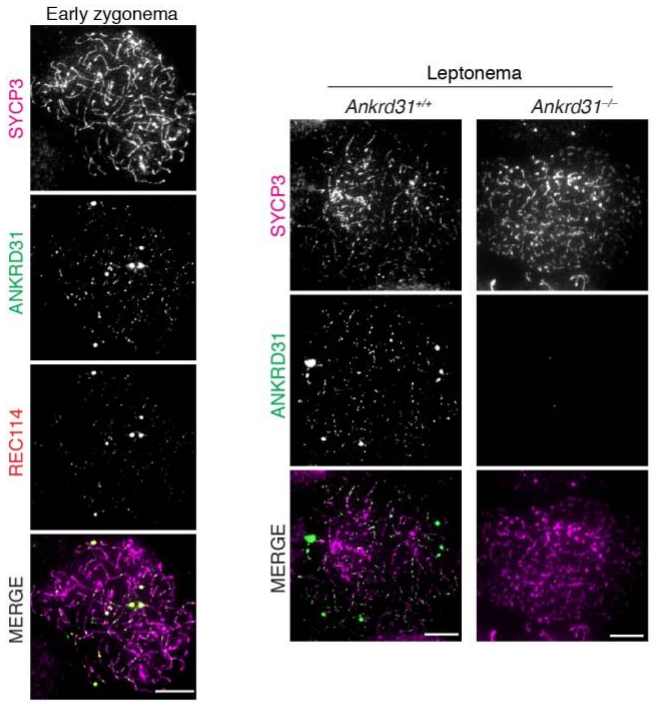

B)

Rabbit anti-ANKRD31 IP-Mass Spec Results

Protein ID	Spectra #
ANKRD31	94
MEI4	12
REC114	9

Guinea Pig anti-ANKRD31 IP-Mass Spec Results

Protein ID	Spectra #
ANKRD31	49
MEI4	16
REC114	7

Figure A.4: ANKRD31 interacts with REC114 *in vivo*.
A). A wild-type spermatocytes at early zygonema on the left.Spread spermatocyte chromosomes were stained for SYCP3, ANKRD31 (guinea pig antiserum), and REC114. It shows ANKRD31 colocalization with REC114, both in small foci and in larger blobs. Scale bars are 10 µm.On the right, Specificity of the guinea pig anti-ANKRD31 antiserum. Representative spreads are shown at equivalent exposures
B) Table summarized the number of total peptide spectra observed in IP-Mass spec experiments by using Rabbit anti-ANKRD31 and Guinea Pig anti-ANKRD31.

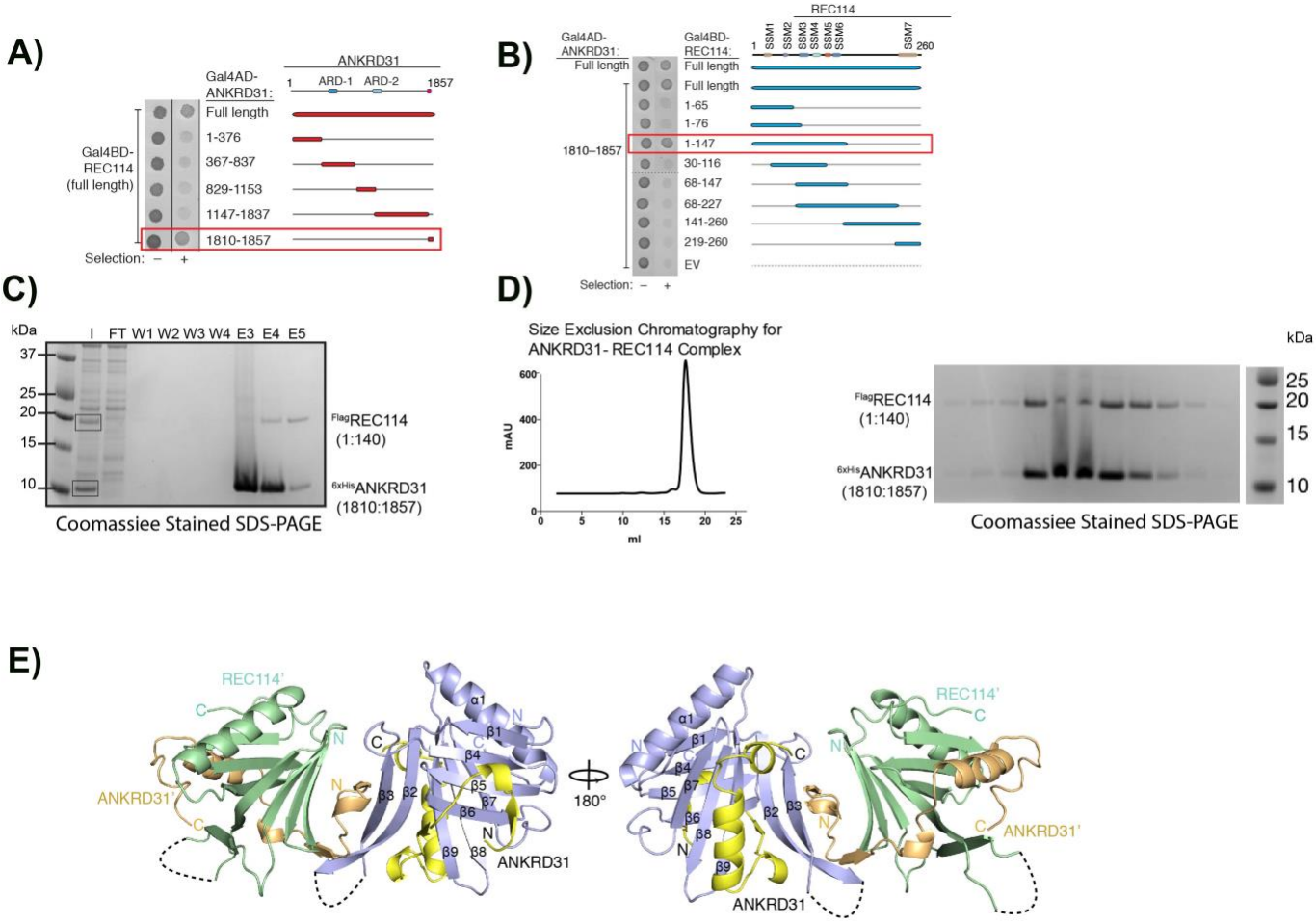
A)
ANKRD31
Gal4AD-
ANKRD31:
1
ARD-1
ARD-2
1857
Full length
1-376
367-837
829-1153
1147-1837
1810-1857
Gal4BD-
REC114
(full length)
Selection: – +
B)
REC114
SSM1
SSM2
SSM3
SSM4
SSM5
SSM6
SSM7
260
Gal4AD-
ANKRD31:
Gal4BD-
REC114:
Full length
Full length
Full length
1-65
1-76
1-147
30-116
68-147
68-227
141-260
219-260
EV
1810–1857
Selection: – +
C)
kDa
I FT W1 W2 W3 W4 E3 E4 E5
37
25
20
15
10
FlagREC114
(1:140)
6xHisANKRD31
(1810:1857)
Coomassiee Stained SDS-PAGE
D)
Size Exclusion Chromatography for
ANKRD31- REC114 Complex
mAU
ml
kDa
FlagREC114
(1:140)
6xHisANKRD31
(1810:1857)
25
20
15
10
Coomassiee Stained SDS-PAGE
E)
REC114'
ANKRD31'
ANKRD31
180°

Figure A.5: Identification of minimal interacting domains between REC114-ANKRD31 and the structure of the minimal interaction domains.
A)The indicated deletion constructs of ANKRD31 fused to Gal4 activating domain (AD) were assayed by yeast two-hybrid for interaction with full-length REC114 fused to Gal4 DNA binding domain (BD). Images show cell growth without (–) and with (+) aureobasidin selection for expression of the two-hybrid reporter. The C-terminal 48 amino acids of ANKRD31 is necessary and sufficient for interaction with REC114 (red box).
B) Similar to panel A, the indicated deletion constructs of REC114 fused to Gal4-BD were assayed by yeast two-hybrid for interaction with ANKRD31 fused to Gal4-AD. The N-terminal 147 amino acids of REC114 is necessary and sufficient for interaction with ANKRD31 (red box).
C) Coomassie stained gel after Ni-NTA column purification. I: input, FT: flow through, W : wash (4 washes in total), E: elution, (5 elution total , last 3 of them shown)
D) The profile of the size exclusion chromatography on the right, the elution fractions were visualized by SDS-PAGE.
E) Front and back views of the overall structure of a pair of REC114N - ANKRD31C heterodimers.

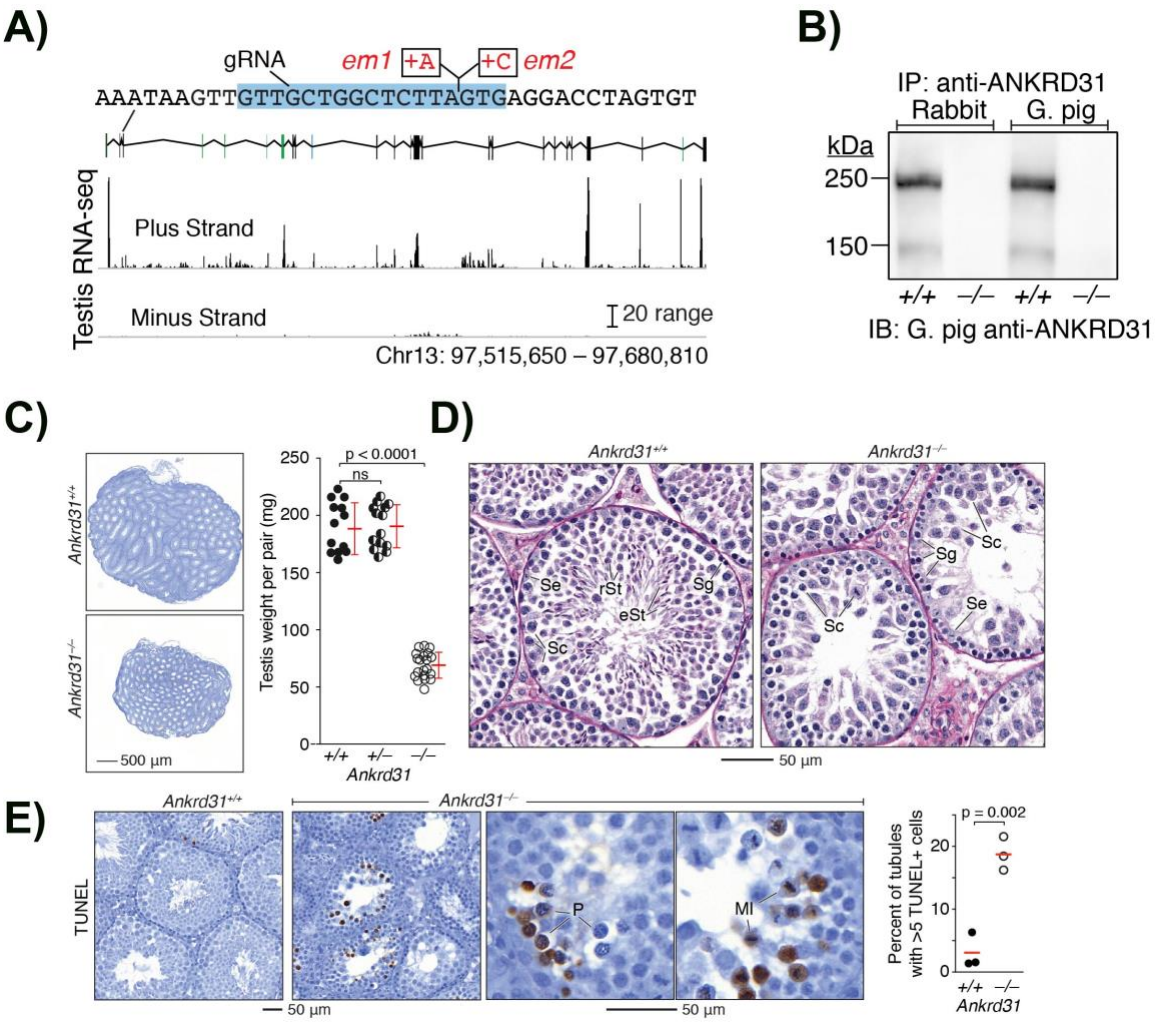

Figure A.6: *Ankrd31* knock out generation and the spermatogenesis phenotype.

A) *Ankrd31* exon map with browser shot showing ENCODE long RNA-sequencing reads from adult testis. Sequence context for the CRISPR-Cas9 guide RNA (gRNA in blue) and frameshift mutations in exon 3 (em1 and em2) is shown.

B) Immunoprecipitation (IP) and immunoblotting (IB) of ANKRD31 from whole-testis extracts using antisera raised in the indicated species.

C) Reduced testis size in *Ankrd31*$^{-/-}$ mutants. Representative sections from adult testes are shown at left (4 mos old); quantification of adult testis weights is at right (red lines, mean ± s.d.).

D) Defective spermatogenesis in *Ankrd31*$^{-/-}$ mutants. Representative Bouin's-fixed and periodic acid Schiff (PAS)-stained seminiferous tubule sections from adult testes are shown (5 mos old). Se, Sertoli cells; Sg, spermatogonia; Sc, spermatocytes; rSt, round spermatids; eSt, elongated spermatids.

E) Increased apoptosis in *Ankrd31*$^{-/-}$ spermatocytes. Lower and higher magnification images (left and right panels, respectively) are shown of adult testis sections stained with TUNEL and counterstained with hematoxylin (4 mos old). Each point on the graph is the measurement from one animal; red line indicates mean.

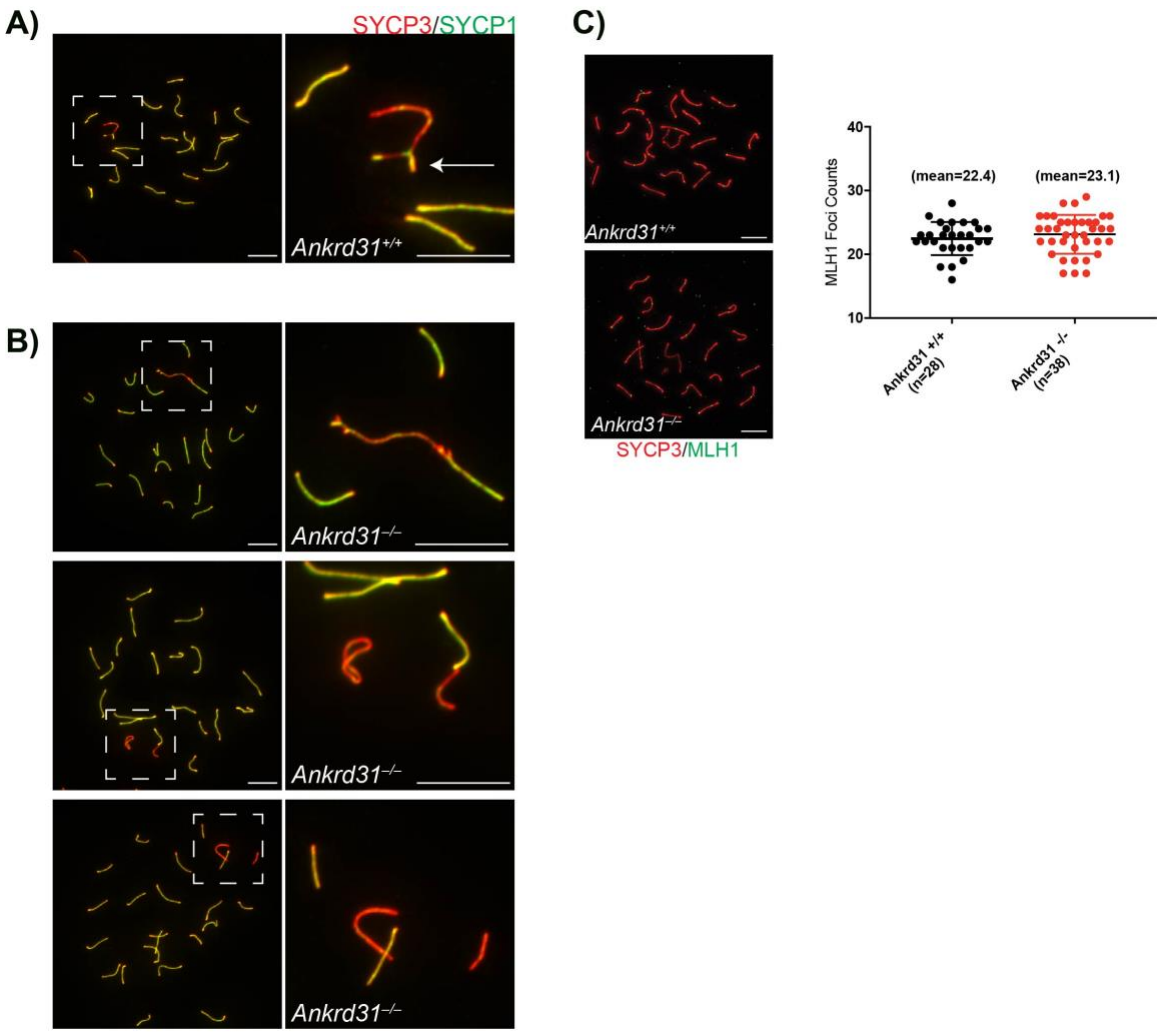

Figure A.7: Sex chromosomes do not pair properly in X and Y frequently fail to pair and synapse in Ankrd31–/– mutant.
A) Representative chromosome spreads stained for SYCP3 and SYCP1. In wild type situation, X-Y chromosomes pair through PAR region (white arrow); below, B) Representative chromosome spreads show the failure of X-Y pairing in different cells. On top, X-Y and an autosome fusion is shown. Middle, X chromosome fuses itself, and bottom shows X-Y are not close in proximity., C) Left, representative pachytene cells stained with SYCP3 and MLH1. Right, quantification of MLH1 focus counts per cell from each genotype (mean focus counts noted on the graph).

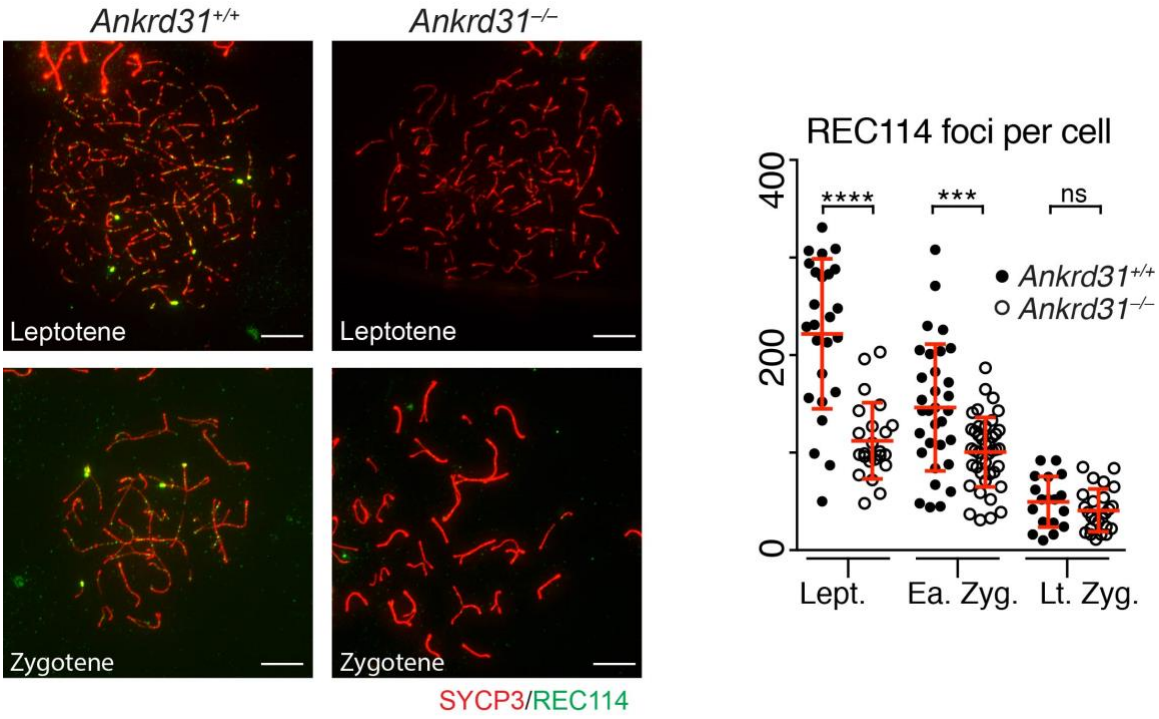

Figure A.8: ANKRD31 is required for normal REC114 localization to chromosomes.
Representative micrographs at matched exposures are shown above. Arrowheads indicate REC114 staining is greatly diminished in *Ankrd31*$^{-/-}$. The quantifications were shown on the right. (red lines indicate mean ± s.d.).

Discussion:

Our search for new components of the mammalian meiotic recombination machinery uncovered mouse ANKRD31 as a direct interaction partner of REC114 and key regulator of multiple aspects of recombination initiation. The principles underlying molecular recognition were elucidated from a crystal structure of the $REC114_N$–$ANKRD31_C$ complex, with observed intermolecular contacts validated from mutational analysis of interfacial residues from both components. ANKRD31 is required for normal assembly of REC114 complexes on chromosomes and for normal location, timing and number of DSBs genome wide and especially in the PAR. Presumably as a consequence of defects in these critical functions, absence of ANKRD31 causes catastrophic failure of spermatogenesis and greatly diminished oogenesis. Studies of this possibly vertebrate-specific factor expand the catalog of essential mammalian meiotic proteins and elucidate how cells control SPO11-generated DSBs.

How does *Ankrd31* carry out its function during spermatogenesis?

Overall, our data suggest that ANKRD31 exerts a dual role of mediating protein-protein interactions with DSB proteins and targeting DSBs to specific parts of the genome, notably the PAR. I have shown that the C-terminus of ANKRD31 is essential for its interaction with REC114 *in vitro*, and that ANKRD31 mediates the formation and/or stabilization of REC114 foci *in vivo*. In addition to the C-terminal domain (CD5), ANKRD31 has four other conserved sites, including the ARD

domains. Thus, it is likely that these conserved domains participate in ANKRD31 function through further protein-protein and/or protein/DNA interactions. Meiotic chromosome spreads indicate that ANKRD31 is associated with chromatin, suggesting that ANKRD31 binds DNA directly or indirectly. A plausible hypothesis is that ANKRD31 associates with chromatin by binding histone tails. Indeed, the ARD domains of TONSL bind unmethylated histone H4 (Saredi et al., 2016). Histone arrays could be a useful tool to identify modified or unmodified histones that may be recognized by ANKRD31. This hypothesis could also be addressed through a proteomics approaches, by immuno-precipitation of ANKRD31 from crosslinked testes extracts.

Materials and Methods:

Animal Handling and *Ankrd31* knock out generation:

Mice were maintained and sacrificed under U.S.A. federal regulatory standards and experiments were approved by the Memorial Sloan Kettering Cancer Center (MSKCC) Institutional Animal Care and Use Committee. Animals were fed regular rodent chow with ad libitum access to food and water.

Endonuclease mediated alleles (*em1, em2*) were generated by the MSKCC Mouse Genetics core facility by targeting exon 3. Guide RNA with sequence (5′-GTTGTTGCTGGCTCTTAGTG) was cloned into pU6T7 vector (Romanienko et al., 2016). In vitro-transcribed guide RNA (100 ng/μl) and Cas9 (50 ng/μl) were microinjected using conventional techniques (Romanienko et al., 2016) into pronuclei of CBA/J × C57BL/6J F2 hybrid zygotes generated by crossing CBAB6F1/J hybrid females with C57BL/6J males. Genomic DNA from founder animals was amplified (PCR conditions: 3 minutes at 94°C, then 35 cycles of 15 seconds at 94°C, 90 seconds at 68°C, followed by a final extension 3 minutes at 68°C) with primers

ANKRD31-A: CTTCTGAATATAGAATTATAAAATTCTGAGAAG and

ANKRD31-B: CTTGTAATTAGTAATTTGCCACAG

and digested with T7 endonuclease I to identify potential indel-carrying animals.

To determine the spectrum of mutant alleles in T7-positive *Ankrd31*^{em} founder mice, the targeted region was amplified by PCR of tail-tip DNA (ANKRD31-A and ANKRD31-B primers) and sequenced on the Illumina MiSeq platform (Illumina

Inc, San Diego, California) at the MSKCC Integrated Genomics Operation. Reads were aligned to mouse genome assembly GRCm37/mm9 and variants were identified using Genome Analysis Toolkit version 2.8-1-g932cd3a (McKenna et al., 2010; DePristo et al., 2011; Van der Auwera et al., 2013). Variants with a minimum variant frequency of 0.01 were annotated using VarScan v2.3.7 software (Koboldt et al., 2012).

Founder mice were crossed to C57BL/J6 mice purchased from Jackson laboratories to obtain germline transmission, then heterozygous animals were backcrossed to C57BL/J6 a further ≥3 generations. Experimental animals were generated by crossing *Ankrd31*$^{+/-}$ heterozygous males with either *Ankrd31*$^{+/-}$ heterozygous or *Ankr31*$^{-/-}$ homozygous females. Genotyping was performed by PCR on genomic DNA with primers
16G008: ACCCAGGTTTCATATATGCTAATGGTACCC
16G011: TGCCACAGATAGCAGTTCCATCTTTTG, under following conditions: 2 minutes at 94°C, then 35 cycles of 20 seconds at 94°C, 30 seconds at 54°C and 1 minutes at 72°C followed by a final extension 3 minutes at 72°C. Then the PCR product was digested with digestion by AflII (NEB) which recognizes *em1* (+A) allele or with HrpChIV (NEB), which recognizes *em*2 (+C) allele. The PCR product is 339 bp and restriction digestion products are 264 and 75 bp. The systematic names of the alleles generated in this study are *Ankrd31*^{em1Sky} and *Ankrd31*^{em2Sky}.

Yeast two-hybrid screen:

Mouse *Mei4* and *Rec114* cDNA were amplified by PCR and cloned into pGBKT7 vector (Clontech). Briefly, PCR products were amplified from testis cDNA library and digested by EcoRI (NEB) and NdeI (NEB) and then cloned into linearized pGBKT7. pGBKT7-*Mei4* or pGBKT7-*Rec114* plasmids were transformed into Y2HGold yeast two-hybrid strain following manufacturer's instructions (Clontech, 630439). Single colonies were picked to verify protein expression by western blotting and to ensure that neither pGBKT7-*Mei4* nor pGBKT7-*Rec114* auto-activated Gal4-driven reporters promoters or were toxic to yeast.

The yeast two-hybrid library was prepared from cDNA generated from whole-testis extracts of 12-dpp males using the Make Your Own "Mate & Plate" Library System according to the manufacturer's instructions (Clontech, 630490). We estimated that the library contained ~10^6 independent clones.

The yeast-two hybrid screen was performed using Matchmaker Gold Yeast Two-Hybrid System according to the manufacturer's instructions (Clontech, 630489). Briefly, individual clones of Y2H bait strains containing pGBKT7-*Mei4* or pGBKT7-*Rec114* were inoculated in liquid synthetic dextrose medium lacking tryptophan (SD-Trp) and grown to OD_{600} of ~0.8, then cells were pelleted and resuspended in SD-Trp at 10^8 cells/ml. Bait strains were mixed with aliquots of the library strain and incubated in 2× YPDA medium with 50 μg/ml kanamycin for 20–24 hours at 30°C, shaking at 40 rpm. Cultures were checked for the presence of zygotes by light microscopy, and then cells were plated on 50 plates (150 mm × 15 mm) of SD lacking tryptophan and leucine and containing X-α-galactose

and aureobasidin A (SD-Trp/Leu/X-α-gal/AbA), and incubated for 5 days at 30°C. Approximately 10^6 zygotes were screened for each bait. Those that formed a blue colony were re-streaked on fresh SD-Trp/Leu/X-α-gal/AbA plates. If also positive in this second growth test, they were subjected to PCR amplification as instructed in Matchmaker Insert Check PCR Mix 2 (Clontech, 630497).
The plasmids were then recovered from yeast and transformed into *E. coli* and sequenced, using Easy Yeast Plasmid Isolation Kit (Clontech, 630467). The screen with pGBKT7-*Mei4* as bait yielded clones containing sequences from *Rec114* and *Med10*. The screen with pGBKT7-*Rec114* yielded *Ankrd31*, *Sohlh1*, *Coro1b*, *Phka2*, *Rps20*, *Sin3b*, *Ctnna1*, and *Hsp90ab*.

Targeted yeast two-hybrid assays:

Genes were amplified from cDNA generated from testes of 12-dpp C57Bl/6J mice as described above. Genes of interest were amplified and cloned into either pGADT7 or pGBKT7. Mating of bait- and prey-containing strains (Y187 and Y2HGold yeast strains) and selection on SD-Trp/Leu/X-α-gal/AbA plates were performed following manufacturer's instructions as described above (Clontech).

Analysis of sequence conservation:

Amino acid sequence divergence (fraction of residues changed) and Ka and Ks values were downloaded from HomoloGene Release 68 (April 2014), https://www.ncbi.nlm.nih.gov/homologene. Estimated times to last common

ancestor were obtained from http://www.timetree.org/ (Hedges et al., 2015) (accessed July 26, 2015).

For each HomoloGene entry with mammalian orthologs (n = 19,498) we generated a least-squares linear regression line fitting amino acid sequence divergence as a function of time since last common ancestor, forcing an intercept of zero. The slope of this line (multiplied by 100) is the divergence rate (percent amino acid changes per Myr) plotted. We also calculated the Ka/Ks ratio for each pairwise comparison between mammalian species within a HomoloGene entry, and took the median value among these as the representative value for that HomoloGene entry. This is the median Ka/Ks ratio plotted.

Likely ANKRD31 orthologs were identified by BLAST searches using full-length human ANKRD31 as the query, or using just the C-terminal 70 amino acids. From a collection of over 150 homologs including representatives from mammals, reptiles, and birds, we generated a multiple sequence alignment of the C-terminal 70 amino acids using MUSCLE (Edgar, 2004) in MegAlign Pro (Lasergene v 14.1.0), then used this alignment as input for a HHMER3 search (http://hmmer.org/). This search again identified ANKRD31 homologs in vertebrates, including one in *Gasterosteus aculeatus* (three-spined stickleback; UniProt G3N8J6), but failed to find any significant hits in fungi. When the stickleback protein was used as a BLAST query, we identified additional homologs from fish that had not turned up in the earlier searches. Interestingly,

the fish homologs all have only one ARD, which by multiple sequence alignment appeared to be a better match for ARD-2 in the mammalian proteins.

Antibody generation:

To raise polyclonal antibodies against ANKRD31, a fragment of *Ankrd31* coding sequence (corresponding to a.a. 1–324) was cloned into pETDuet™-1 (Millipore) using the In-Fusion cloning kit (Clontech, Takara). This expression vector was used to produce 6×His-ANKRD31$_{1–134}$. Briefly, *E. coli* strain BL21 was transformed with the vector and a single colony was picked to inoculate LB overnight at 37°C. The overnight culture was diluted to ~0.04 (OD_{600}) and once OD_{600} had reached ~0.6, the protein expression was induced by addition of 1 mM Isopropyl β-D-1-thiogalactopyranoside (IPTG) for 2 hrs at 37°C. Cells were pelleted by centrifugation at 6000 g, 15 min. Pellets were resuspended in lysis buffer (50 mM HEPES-NaOH pH 8.0, 300 mM NaCl, 0.1 mM dithiothreitol (DTT), 10% glycerol and 20 mM imidazole) and stored at –80°C. To purify the ANKRD31 fragment, the pellet was thawed at room temperature and placed on ice and all further steps were executed at 4°C. The sample was sonicated 8 times 15 seconds on-off, 20% duty cycle. The solution was cleared by centrifugation at 19,000 rpm, 1 hr. Equilibrated Ni-NTA Agarose (QIAGEN, 30230) was added to the cleared protein lysate and incubated for 1 hr, then the lysate-resin slurry was transferred into Poly-prep chromatography columns (BioRad, 731-1550) and washed with lysis buffer several times. The protein was eluted with elution buffer (lysis buffer + 500 mM imidazole) and fractions

containing the ANKRD31 fragment were combined and subjected to size-exclusion chromatography. Sample was loaded on a Superdex 200 column equilibrated with 50 mM HEPES-NaOH pH 8.0, 300 mM NaCl, 1 mM DTT, 10% glycerol and 5 mM EDTA and the fractions under the main peak were collected and analyzed on SDS-PAGE. Purified protein fractions were combined and concentrated (Millipore), then frozen in liquid nitrogen and stored at –80°C. Purified protein fragment was used to immunize two rabbits and two guinea pigs by Pocono Rabbit Farm & Laboratory. Polyclonal anti-ANKRD31 antibodies were enriched from serum using NAb™ Protein A Plus Spin Columns (Thermoscientific, 89952). Polyclonal antibody specificity was tested by immunofluorescent staining of meiotic chromosome spreads and immunoprecipitation followed by western blotting.

Total mRNA extraction, cDNA library generation and RT-qPCR:

Testes tissue from *Ankrd31*$^{+/+}$ and *Ankrd31*$^{-/-}$ animals were dissected and frozen on dry ice. Total mRNA was extracted using RNeasy Plus Mini Kit (QIAGEN, 74134) following the manufacturer's instructions. Superscript™ III First-Strand Synthesis SuperMix (Invitrogen, 18080400) was used with oligo dT primers to generate testis cDNA, which was diluted 1:10 to be used in RT-qPCR carried out using LightCycler 480 SYBR Green I Master (Roche, 4707516001) under following conditions: 10 minutes at 95°C, then 45 cycles of 10 seconds at 95°C, 20 seconds at 55°C and 10 seconds at 72°C. Amplification products were detected on the LightCycler 480 II Real-Time PCR instrument (Roche).

LightCycler 480 Software was used to quantify products by absolute quantification analysis using the second derivative maximum method. All reactions were done in triplicate and the mean of crossing point (Cp) value were used for the analysis. Cp values were normalized to the value obtained for *B2M* reactions (ΔCp). Then, the differences between knockout and wild-type samples were calculated for each primer set ($\Delta\Delta$Cp) and the fold change (knockout vs wild type) was calculated as $2^{-\Delta\Delta Cp}$. Primers used for RT-qPCR are listed below (Primer:Forward 5' to 3'/ Reverse 5' to 3')

Ankrd31-1**:** ATAATGCAGGTTGGACTCCCC/ CCGCAGAAGCACCATGTAAAG

Ankrd31-2: AGCCAAGTTACGATGGGTGG/ CGCATCATGCAGGGGAGTAATC

B2M: ACACTGAATTCACCCCCACTGA/ CGATCCCAGTAGACGGTCTTGG

Immunoprecipitation and western blot analysis of ANKRD31:

Dissected testes were placed in an Eppendorf tube and snap frozen on liquid nitrogen and stored at -–80°C. The frozen tissue was resuspended in RIPA buffer (50 mM Tris-HCl pH 7.5, 150 mM NaCl, 0.1% SDS, 0.5% sodium deoxycholate, 1% NP40) supplemented with protease inhibitors (Roche Mini tablets). The tissue was disrupted with a plastic pestle. The homogenized extract was supplemented with 10 mM $MgCl_2$ and Benzonase nuclease (EMD Millipore (70664-3), 28 unit/μl) and incubated with end-over-end rotation for 1 hr at 4°C. The samples were centrifuged at 15,000 rpm for 20 min. The clear lysate was transferred to a new tube and used for the immunoprecipitation. Whole-cell extract was pre-cleared with protein A/G Dynabeads (Thermofisher, 1004D, 1001D) by end-over-

end rotation for 1 hr at 4°C. Antibodies (home-made, rabbit anti-ANKRD31 or guinea pig anti-ANKRD31, 1–2 μg) were added to pre-cleared lysates and incubated overnight with end-over-end rotation at 4°C. Protein A/G Dynabeads were added to the tubes and incubated for 1 hr with end-over-end rotation, at 4°C. Beads were washed three times with RIPA buffer, resuspended in 1× NuPAGE LDS sample buffer (Invitrogen) with 50 mM DTT, and incubated 10 min at 70°C to elute immunoprecipitated proteins.

For western blotting, samples were separated on 3–8% Tris-Acetate NuPAGE precast gels (Life Technologies) at 150 V for 70 min. Proteins were transferred to polyvinylidene difluoride (PVDF) membranes by wet transfer method in Tris-Glycine-20% methanol, at 120 V for 40 min at 4°C. Membranes were blocked with 5% non-fat milk in 1× phosphate buffered saline (PBS)-0.1% Tween (PBS-T) for 30 min at room temperature on an orbital shaker. Blocked membranes were incubated with primary antibodies (guinea pig anti-ANKRD31, 1:4000) 1 hr at room temperature or overnight at 4°C. Membranes were washed with PBS-T for 30 min at room temperature, then incubated with HRP-conjugated secondary antibodies (rabbit anti-guinea pig IgG (Abcam), 1:10,000) for 1 hr at room temperature. Membranes were washed with PBS-T for 15 min and the signal was developed by ECL Prime (GE Healthcare).

Spermatocyte chromosome spreads:

Testes were dissected and deposited after removal of the tunica albuginea in 50 ml Falcon tubes containing 2 ml TIM buffer (104 mM NaCl, 45 mM KCl, 1.2 mM $MgSO_4$, 0.6 mM KH_2PO_4, 6.0 mM sodium lactate, 1.0 mM sodium pyruvate, 0.1% glucose). 200 μl collagenase (20 mg/ml in TIM buffer) was added, and left shaking at 550 rpm for 55 min at 32°C. Every 15 min, tissue was checked and carefully pulled further apart to enhance digestion. After incubation, TIM buffer was added to a final volume of 15 ml, followed by centrifugation for 1 min at 600 rpm at room temperature. Supernatant was decanted and this wash and centrifuge procedure was repeated 3 times. Separated tubules were resuspended in 2 ml TIM, with 200 μl trypsin (7 mg/ml in TIM) and 20 μl DNase I (400 μg/ml in TIM buffer) and incubated for 15 min. at 32°C at 550 rpm in a thermomixer. 500 μl trypsin inhibitor (20 mg/ml in TIM) and 50 μl DNase I solution were added and mixed. A wide mouthed plastic Pasteur pipette was used to disperse the tissue further by pipetting up and down for 2 min. The Pasteur pipette was first used to pipet a 2% BSA solution in PBS to coat the plastic and minimize cell loss. Cells were passed through a 70-μm cell strainer into a new 50 ml Falcon tube. TIM was added to a final volume of 15 ml and mixed. Cells were centrifuged for 5 min at 1200 rpm. Supernatant was decanted, 15 μl DNase I solution was added and gently mixed, followed by 15 ml TIM. Washing with TIM and resuspension in presence of DNase I was repeated 3 times. Single-cell suspension was pelleted and resuspended in TIM according to original weight (~200 mg in 400 μl). 10 μl of cell suspension was added to 90 μl of 75 mM

sucrose solution, flicked three times and incubated for 8 min at room temperature. Superfrost glass slides were divided in two squares by use of Immedge pen, each square received 100 μl 1% paraformaldehyde (PFA) (freshly dissolved in presence of NaOH at 65°C, 0.15% Triton, pH 9.3, cleared through 0.22 μm filter) and 45 μl of cell suspension was added per square, swirled three times, and dried in a closed slide box for 3 hr, followed by drying with half-open lid 1.5 hr at room temperature. Slides were washed in a Coplin jar 2 × 3 min in milli-Q water on a shaker, 1 × 5 min with 0.4% PhotoFlow, air dried and stored in aluminum foil in –80°C.

LC-MS:

Immunoprecipitated samples were washed as previously described and digested overnight with trypsin, peptides desalted using C18 zip tips, and then dried by vacuum centrifugation. Each sample was reconstituted in 10 µL 0.1% (vol/vol) formic acid and 4 µL analyzed by microcapillary liquid chromatography with tandem mass spectrometry using the NanoAcquity (Waters) with a 100-µ minner-diameter Å~ 10-cm- length C18 column (1.7 um BEH130, Waters) configured with a 180-µ m Å~ 2-cm trap column coupled to a Q-Exactive Plus mass spectrometer (Thermo Fisher Scientifi c). Peptides were eluted with a linear gradient of 0– 35% acetonitrile (0.1% formic acid) in water (0.1% formic acid) over 150 mins with a fl ow rate of 300 nL/min. The QE Plus was operated in automatic, data dependent MS/MS acquisition mode with one MS full scan (380–1800 m/z) at 70,000 mass resolution and up to ten concurrent MS/MS scans for

the ten most intense peaks selected from each survey scan. Survey scans were acquired in profi le mode and MS/MS scans were acquired in centroid mode at 17,500 resolution and isolation window of 1.5 amu and normalized collision energy of 27. AGC was set to 1 Å~ 10 for MS1 and 5 Å~ 10 and 100 ms IT for MS2. Charge exclusion of unassigned and greater than 6 enabled with dynamic exclusion of 15 s. All MS/MS samples were analyzed using MaxQuant (Max Planck Institute of Biochemistry, Martinsried, Germany; version 1.5.3.3) at default settings with a few modifications.

REFERENCES:

Ajimura, M., S.H. Leem, and H. Ogawa. 1993. Identification of new genes required for meiotic recombination in Saccharomyces cerevisiae. *Genetics*. 133:51-66.

Alani, E., R. Padmore, and N. Kleckner. 1990. Analysis of wild-type and rad50 mutants of yeast suggests an intimate relationship between meiotic chromosome synapsis and recombination. *Cell*. 61:419-436.

Alfieri, C., L. Chang, Z. Zhang, J. Yang, and S. Maslen. 2016. Molecular basis of APC/C regulation by the spindle assembly checkpoint. *Nature*.

Alfieri, C., S. Zhang, and D. Barford. 2017. Visualizing the complex functions and mechanisms of the anaphase promoting complex/cyclosome (APC/C). *Open biology*. 7.

Arora, C., K. Kee, S. Maleki, and S. Keeney. 2004. Antiviral protein Ski8 is a direct partner of Spo11 in meiotic DNA break formation, independent of its cytoplasmic role in RNA metabolism. *Molecular cell*. 13:549-559.

Baker, S.M., A.W. Plug, T.A. Prolla, C.E. Bronner, A.C. Harris, X. Yao, D.M. Christie, C. Monell, N. Arnheim, A. Bradley, T. Ashley, and R.M. Liskay. 1996. Involvement of mouse Mlh1 in DNA mismatch repair and meiotic crossing over. *Nature genetics*. 13:336-342.

Baltus, A.E., D.B. Menke, Y.-C.C. Hu, M.L. Goodheart, A.E. Carpenter, D.G. de Rooij, and D.C. Page. 2006. In germ cells of mouse embryonic ovaries, the decision to enter meiosis precedes premeiotic DNA replication. *Nature genetics*. 38:1430-1434.

Barchi, M., S. Mahadevaiah, M. Di Giacomo, F. Baudat, D.G. de Rooij, P.S. Burgoyne, M. Jasin, and S. Keeney. 2005. Surveillance of different recombination defects in mouse spermatocytes yields distinct responses despite elimination at an identical developmental stage. *Molecular and cellular biology*. 25:7203-7215.

Barford, D. 2015. Understanding the structural basis for controlling chromosome division. *Phil. Trans. R. Soc. A*.

Baudat, F., K. Manova, J.P. Yuen, M. Jasin, and S. Keeney. 2000. Chromosome synapsis defects and sexually dimorphic meiotic progression in mice lacking Spo11. *Molecular cell*. 6:989-998.

Bendris, N., B. Lemmers, J.-M.M. Blanchard, and N. Arsic. 2011. Cyclin A2 mutagenesis analysis: a new insight into CDK activation and cellular localization requirements. *PloS one*. 6.

Benjamin, K.R., C. Zhang, K.M. Shokat, and I. Herskowitz. 2003. Control of landmark events in meiosis by the CDK Cdc28 and the meiosis-specific kinase Ime2. *Genes & development*. 17:1524-1539.

Bergerat, A., B. de Massy, D. Gadelle, P.C. Varoutas, A. Nicolas, and P. Forterre. 1997. An atypical topoisomerase II from Archaea with implications for meiotic recombination. *Nature*. 386:414-417.

Berthet, C., E. Aleem, V. Coppola, L. Tessarollo, and P. Kaldis. 2003. Cdk2 knockout mice are viable. *Current biology : CB*. 13:1775-1785.

Beumer, T.L., H.L. Roepers-Gajadien, I.S. Gademan, H.B. Kal, and D.G. de Rooij. 2000. Involvement of the D-type cyclins in germ cell proliferation and differentiation in the mouse. *Biology of reproduction*. 63:1893-1898.

Bloom, J., and F.R. Cross. 2007. Multiple levels of cyclin specificity in cell-cycle control. *Nature reviews Molecular cell biology*. 8:149.

Bolcun-Filas, E., V.D. Rinaldi, M.E. White, and J.C. Schimenti. 2014. Reversal of female infertility by Chk2 ablation reveals the oocyte DNA damage checkpoint pathway. *Science (New York, N.Y.)*. 343:533-536.

Brandeis, M., and T. Hunt. 1996. The proteolysis of mitotic cyclins in mammalian cells persists from the end of mitosis until the onset of S phase. *The EMBO journal*. 15:5280-5289.

Brandeis, M., I. Rosewell, M. Carrington, T. Crompton, M.A. Jacobs, J. Kirk, J. Gannon, and T. Hunt. 1998. Cyclin B2-null mice develop normally and are fertile whereas cyclin B1-null mice die in utero. *Proceedings of the National Academy of Sciences of the United States of America*. 95:4344-4349.

Brunet, S., Z. Polanski, M.H. Verlhac, J.Z. Kubiak, and M.-B. Biology. 1998. Bipolar meiotic spindle formation without chromatin. *Current Biology*.

Burton, J.L., and M.J. Solomon. 2001. D box and KEN box motifs in budding yeast Hsl1p are required for APC-mediated degradation and direct binding to Cdc20p and Cdh1p. *Genes & development*.

Burton, J.L., Y. Xiong, and M.J. Solomon. 2011. Mechanisms of pseudosubstrate inhibition of the anaphase promoting complex by Acm1. *The EMBO journal*.

Bury, L., P.A. Coelho, and D.M. Glover. 2016. From Meiosis to Mitosis: The Astonishing Flexibility of Cell Division Mechanisms in Early Mammalian Development. *Current topics in developmental biology*. 120:125-171.

Cardozo, T., and M. Pagano. 2004. The SCF ubiquitin ligase: insights into a molecular machine. *Nature reviews. Molecular cell biology*. 5:739-751.

Carlile, T.M., and A. Amon. 2008. Meiosis I is established through division-specific translational control of a cyclin. *Cell*. 133:280-291.

Chesnel, F., and J.J. Eppig. 1995. Synthesis and accumulation of p34cdc2 and cyclin B in mouse oocytes during acquisition of competence to resume meiosis. *Molecular reproduction and development*. 40:503-508.

Clermont, Y. 1972. Kinetics of spermatogenesis in mammals: seminiferous epithelium cycle and spermatogonial renewal. *Physiological reviews*. 52:198-236.

Cobrinik, D. 2005. Pocket proteins and cell cycle control. *Oncogene*. 24:2796-2809.

Cole, F., L. Kauppi, J. Lange, I. Roig, R. Wang, S. Keeney, and M. Jasin. 2012. Homeostatic control of recombination is implemented progressively in mouse meiosis. *Nature cell biology*. 14:424-430.

Cool, M., and R.E. Malone. 1992. Molecular and genetic analysis of the yeast early meiotic recombination genes REC102 and REC107/MER2. *Molecular and cellular biology*. 12:1248-1256.

Costa, Y., R. Speed, R. Ollinger, M. Alsheimer, C.A. Semple, P. Gautier, K. Maratou, I. Novak, C. Höög, R. Benavente, and H.J. Cooke. 2005. Two novel proteins recruited by synaptonemal complex protein 1 (SYCP1) are at the centre of meiosis. *Journal of cell science*. 118:2755-2762.

Davey, N.E., and D.O. Morgan. 2016. Building a Regulatory Network with Short Linear Sequence Motifs: Lessons from the Degrons of the Anaphase-Promoting Complex. *Molecular cell*. 64:12-23.

De Azevedo, W.F., S. Leclerc, L. Meijer, L. Havlicek, M. Strnad, and S.H. Kim. 1997. Inhibition of cyclin-dependent kinases by purine analogues: crystal structure of human cdk2 complexed with roscovitine. *European journal of biochemistry*. 243:518-526.

de Boer, E. 2007. Synaptonemal complexes, transverse filaments and intereference in mouse meiotic recombination; an immunocytological study.

de Rooij, D.G., and P. de Boer. 2003. Specific arrests of spermatogenesis in genetically modified and mutant mice. *Cytogenetic and genome research*. 103:267-276.

de Vries, F.A., E. de Boer, M. van den Bosch, W.M. Baarends, M. Ooms, L. Yuan, J.-G.G. Liu, A.A. van Zeeland, C. Heyting, and A. Pastink. 2005. Mouse Sycp1 functions in synaptonemal complex assembly, meiotic recombination, and XY body formation. *Genes & development*. 19:1376-1389.

Desai, D., Y. Gu, and D.O. Morgan. 1992. Activation of human cyclin-dependent kinases in vitro. *Molecular biology of the cell*. 3:571-582.

Deyter, G.M., T. Furuta, Y. Kurasawa, and J.M. Schumacher. 2010. Caenorhabditis elegans cyclin B3 is required for multiple mitotic processes including alleviation of a spindle checkpoint-dependent block in anaphase chromosome segregation. *PLoS genetics*. 6.

Di Fiore, B., N.E. Davey, A. Hagting, D. Izawa, J. Mansfeld, T.J. Gibson, and J. Pines. 2015. The ABBA motif binds APC/C activators and is shared by APC/C substrates and regulators. *Developmental cell*. 32:358-372.

Di Giacomo, M., M. Barchi, F. Baudat, W. Edelmann, S. Keeney, and M. Jasin. 2005. Distinct DNA-damage-dependent and -independent responses drive the loss of oocytes in recombination-defective mouse mutants. *Proceedings of the National Academy of Sciences of the United States of America*. 102:737-742.

Diaz-Martinez, L.A., W. Tian, B. Li, and R. Warrington. 2015. The Cdc20-binding Phe box of the spindle checkpoint protein BubR1 maintains the mitotic checkpoint complex during mitosis. *Journal of Biological …*.

Dix, D.J., J.W. Allen, B.W. Collins, C. Mori, N. Nakamura, P. Poorman-Allen, E.H. Goulding, and E.M. Eddy. 1996. Targeted gene disruption of Hsp70-2 results in failed meiosis, germ cell apoptosis, and male infertility. *Proceedings of the National Academy of Sciences of the United States of America*. 93:3264-3268.

Dix, D.J., J.W. Allen, B.W. Collins, P. Poorman-Allen, C. Mori, D.R. Blizard, P.R. Brown, E.H. Goulding, B.D. Strong, and E.M. Eddy. 1997. HSP70-2 is

required for desynapsis of synaptonemal complexes during meiotic prophase in juvenile and adult mouse spermatocytes. *Development (Cambridge, England)*. 124:4595-4603.
Edgar, R.C. 2004. MUSCLE: multiple sequence alignment with high accuracy and high throughput. *Nucleic acids research*.
El Yakoubi, W., and K. Wassmann. 2017. Meiotic Divisions: No Place for Gender Equality. *Advances in experimental medicine and biology*. 1002:1-17.
Evans, T., E.T. Rosenthal, J. Youngblom, D. Distel, and T. Hunt. 1983. Cyclin: a protein specified by maternal mRNA in sea urchin eggs that is destroyed at each cleavage division. *Cell*. 33:389-396.
Ezhevsky, S.A., H. Nagahara, A.M. Vocero-Akbani, D.R. Gius, M.C. Wei, and S.F. Dowdy. 1997. Hypo-phosphorylation of the retinoblastoma protein (pRb) by cyclin D:Cdk4/6 complexes results in active pRb. *Proceedings of the National Academy of Sciences of the United States of America*. 94:10699-10704.
Feng, C.-W.W., J. Bowles, and P. Koopman. 2014. Control of mammalian germ cell entry into meiosis. *Molecular and cellular endocrinology*. 382:488-497.
Feng, H., and T.-E.M. Cycle. 2018. Specialization of CDK1 and cyclin B paralog functions in a coenocystic mode of oogenic meiosis. *Cell Cycle*.
Fraune, J., S. Schramm, M. Alsheimer, and R. Benavente. 2012. The mammalian synaptonemal complex: protein components, assembly and role in meiotic recombination. *Experimental cell research*. 318:1340-1346.
Froenicke, L., L.K. Anderson, J. Wienberg, and T. Ashley. 2002. Male mouse recombination maps for each autosome identified by chromosome painting. *American journal of human genetics*. 71:1353-1368.
Fujimitsu, K., M. Grimaldi, and H. Yamano. 2016. Cyclin-dependent kinase 1-dependent activation of APC/C ubiquitin ligase. *Science (New York, N.Y.)*. 352:1121-1124.
Gallant, P., and E.A. Nigg. 1994. Identification of a novel vertebrate cyclin: cyclin B3 shares properties with both A- and B-type cyclins. *The EMBO journal*. 13:595-605.
Gardiner, J.M., S.A. Bullard, C. Chrome, and R.E. Malone. 1997. Molecular and genetic analysis of REC103, an early meiotic recombination gene in yeast. *Genetics*. 146:1265-1274.
Geng, Y., Y.-M.M. Lee, M. Welcker, J. Swanger, A. Zagozdzon, J.D. Winer, J.M. Roberts, P. Kaldis, B.E. Clurman, and P. Sicinski. 2007. Kinase-independent function of cyclin E. *Molecular cell*. 25:127-139.
Geng, Y., Q. Yu, E. Sicinska, M. Das, J.E. Schneider, S. Bhattacharya, W.M. Rideout, R.T. Bronson, H. Gardner, and P. Sicinski. 2003. Cyclin E ablation in the mouse. *Cell*. 114:431-443.
Gerhart, J., M. Wu, and K.-M. of cell biology. 1984. Cell cycle dynamics of an M-phase-specific cytoplasmic factor in Xenopus laevis oocytes and eggs. *The Journal of cell biology*.
Glotzer, M., A.W. Murray, and M.W. Kirschner. 1991. Cyclin is degraded by the ubiquitin pathway. *Nature*.

Gray, S., and P.E. Cohen. 2016. Control of Meiotic Crossovers: From Double-Strand Break Formation to Designation. *Annual review of genetics*. 50:175-210.
Griswold, M.D. 2016. Spermatogenesis: The Commitment to Meiosis. *Physiological reviews*. 96:1-17.
Gui, L., and H. Homer. 2012. Spindle assembly checkpoint signalling is uncoupled from chromosomal position in mouse oocytes. *Development (Cambridge, England)*. 139:1941-1946.
Gunbin, K.V., V.V. Suslov, I.I. Turnaev, D.A. Afonnikov, and N.A. Kolchanov. 2011. Molecular evolution of cyclin proteins in animals and fungi. *BMC evolutionary biology*. 11:224.
Hached, K., S.Z. Xie, E. Buffin, D. Cladière, C. Rachez, M. Sacras, P.K. Sorger, and K. Wassmann. 2011. Mps1 at kinetochores is essential for female mouse meiosis I. *Development (Cambridge, England)*. 138:2261-2271.
Hamer, G., K. Gell, A. Kouznetsova, I. Novak, R. Benavente, and C. Höög. 2006. Characterization of a novel meiosis-specific protein within the central element of the synaptonemal complex. *Journal of cell science*. 119:4025-4032.
Hartwell, L.H., J. Culotti, and B. Reid. 1970. Genetic control of the cell-division cycle in yeast. I. Detection of mutants. *Proceedings of the National Academy of Sciences of the United States of America*. 66:352-359.
Hedges, S.B., J. Marin, and M. Suleski. 2015. Tree of life reveals clock-like speciation and diversification. *Molecular biology and evolution*.
Heim, A., B. Rymarczyk, and T.U. Mayer. 2017. Regulation of Cell Division. *Advances in experimental medicine and biology*. 953:83-116.
Hellmuth, S., F. Böttger, C. Pan, M. Mann, and O. Stemmann. 2014. PP2A delays APC/C-dependent degradation of separase-associated but not free securin. *The EMBO journal*. 33:1134-1147.
Henderson, K.A., K. Kee, S. Maleki, P.A. Santini, and S. Keeney. 2006. Cyclin-dependent kinase directly regulates initiation of meiotic recombination. *Cell*. 125:1321-1332.
Herbert, M., D. Kalleas, D. Cooney, M. Lamb, and L. Lister. 2015. Meiosis and maternal aging: insights from aneuploid oocytes and trisomy births. *Cold Spring Harbor perspectives in biology*. 7.
Herbert, M., M. Levasseur, H. Homer, K. Yallop, A. Murdoch, and A. McDougall. 2003. Homologue disjunction in mouse oocytes requires proteolysis of securin and cyclin B1. *Nature cell biology*. 5:1023-1025.
Herrán, Y., C. Gutiérrez-Caballero, M. Sánchez-Martín, T. Hernández, A. Viera, J.L.L. Barbero, E. de Álava, D.G. de Rooij, J.Á.Á. Suja, E. Llano, and A.M. Pendás. 2011. The cohesin subunit RAD21L functions in meiotic synapsis and exhibits sexual dimorphism in fertility. *The EMBO journal*. 30:3091-3105.
Hilioti, Z., Y.S. Chung, Y. Mochizuki, C.F. Hardy, and O. Cohen-Fix. 2001. The anaphase inhibitor Pds1 binds to the APC/C-associated protein Cdc20 in a destruction box-dependent manner. *Current biology : CB*. 11:1347-1352.

Hochegger, H., A. Klotzbücher, J. Kirk, M. Howell, K. le Guellec, K. Fletcher, T. Duncan, M. Sohail, and T. Hunt. 2001. New B-type cyclin synthesis is required between meiosis I and II during Xenopus oocyte maturation. *Development (Cambridge, England)*. 128:3795-3807.

Holt, J.E., S.I. Lane, and K.T. Jones. 2013. The control of meiotic maturation in mammalian oocytes. *Current topics in developmental biology*. 102:207-226.

Holt, J.E., J. Weaver, and K.T. Jones. 2010. Spatial regulation of APCCdh1-induced cyclin B1 degradation maintains G2 arrest in mouse oocytes. *Development (Cambridge, England)*. 137:1297-1304.

Holt, L.J., A.N. Krutchinsky, and D.O. Morgan. 2008. Positive feedback sharpens the anaphase switch. *Nature*. 454:353-357.

Howard, A., and S.R. Pelc. 1986. Synthesis of desoxyribonucleic acid in normal and irradiated cells and its relation to chromosome breakage. *International Journal of Radiation Biology and Related Studies in Physics, Chemistry and Medicine*.

Ishiguro, K.-i., J. Kim, S. Fujiyama-Nakamura, S. Kato, and Y. Watanabe. 2011. A new meiosis-specific cohesin complex implicated in the cohesin code for homologous pairing. *EMBO reports*. 12:267-275.

Ivanov, E.L., V.G. Korolev, and F. Fabre. 1992. XRS2, a DNA repair gene of Saccharomyces cerevisiae, is needed for meiotic recombination. *Genetics*. 132:651-664.

Jacobs, H.W., J.A. Knoblich, and C.F. Lehner. 1998. Drosophila Cyclin B3 is required for female fertility and is dispensable for mitosis like Cyclin B. *Genes & development*. 12:3741-3751.

Jain, D., M.R. Puno, C. Meydan, N. Lailler, C.E. Mason, C.D. Lima, K.V. Anderson, and S. Keeney. 2018. ketu mutant mice uncover an essential meiotic function for the ancient RNA helicase YTHDC2. *eLife*. 7.

Jan, S.Z., G. Hamer, S. Repping, D.G. de Rooij, A.M.M. van Pelt, and T.L. Vormer. 2012. Molecular control of rodent spermatogenesis. *Biochimica et biophysica acta*. 1822:1838-1850.

Jeffrey, P.D., A.A. Russo, K. Polyak, E. Gibbs, J. Hurwitz, J. Massagué, and N.P. Pavletich. 1995. Mechanism of CDK activation revealed by the structure of a cyclinA-CDK2 complex. *Nature*. 376:313-320.

Johzuka, K., and H. Ogawa. 1995. Interaction of Mre11 and Rad50: two proteins required for DNA repair and meiosis-specific double-strand break formation in Saccharomyces cerevisiae. *Genetics*. 139:1521-1532.

Kanatsu-Shinohara, M., R.M. Schultz, and G.S. Kopf. 2000. Acquisition of meiotic competence in mouse oocytes: absolute amounts of p34(cdc2), cyclin B1, cdc25C, and wee1 in meiotically incompetent and competent oocytes. *Biology of reproduction*. 63:1610-1616.

Kauppi, L., M. Barchi, F. Baudat, P.J. Romanienko, S. Keeney, and M. Jasin. 2011. Distinct properties of the XY pseudoautosomal region crucial for male meiosis. *Science (New York, N.Y.)*. 331:916-920.

Kauppi, L., M. Barchi, J. Lange, F. Baudat, M. Jasin, and S. Keeney. 2013. Numerical constraints and feedback control of double-strand breaks in mouse meiosis. *Genes & development*. 27:873-886.
Kee, K., R.U. Protacio, C. Arora, and S. Keeney. 2004. Spatial organization and dynamics of the association of Rec102 and Rec104 with meiotic chromosomes. *The EMBO journal*. 23:1815-1824.
Keeney, S. 2008. Spo11 and the Formation of DNA Double-Strand Breaks in Meiosis. *Genome dynamics and stability*. 2:81-123.
Keeney, S., C.N. Giroux, and N. Kleckner. 1997. Meiosis-specific DNA double-strand breaks are catalyzed by Spo11, a member of a widely conserved protein family. *Cell*. 88:375-384.
Kishimoto, T. 1988. Regulation of Metaphase by a Maturation-Promoting Factor: (meiosis/mitosis/cell cycle/metaphase/maturation-promoting factor). *Development*.
Kishimoto, T. 2018. MPF-based meiotic cell cycle control: Half a century of lessons from starfish oocytes. *Proceedings of the Japan Academy. Series B, Physical and biological sciences*. 94:180-203.
Kishimoto, T., K. Yamazaki, and Y. Kato. 1984. Induction of starfish oocyte maturation by maturation-promoting factor of mouse and surf clam oocytes. *Journal of Experimental Zoology*.
Ko, J., S. Humbert, R.T. Bronson, S. Takahashi, A.B. Kulkarni, E. Li, and L.H. Tsai. 2001. p35 and p39 are essential for cyclin-dependent kinase 5 function during neurodevelopment. *The Journal of neuroscience : the official journal of the Society for Neuroscience*. 21:6758-6771.
Kozar, K., M.A. Ciemerych, V.I. Rebel, H. Shigematsu, A. Zagozdzon, E. Sicinska, Y. Geng, Q. Yu, S. Bhattacharya, R.T. Bronson, K. Akashi, and P. Sicinski. 2004. Mouse development and cell proliferation in the absence of D-cyclins. *Cell*. 118:477-491.
Kreutzer, M.A., J.P. Richards, M.N. De Silva-Udawatta, J.J. Temenak, J.A. Knoblich, C.F. Lehner, and K.L. Bennett. 1995. Caenorhabditis elegans cyclin A- and B-type genes: a cyclin A multigene family, an ancestral cyclin B3 and differential germline expression. *Journal of cell science*. 108 (Pt 6):2415-2424.
Kubiak, J.Z., M. Weber, G. Géraud, and B. Maro. 1992. Cell cycle modification during the transitions between meiotic M-phases in mouse oocytes. *Journal of cell science*. 102 (Pt 3):457-467.
Kudo, N.R., K. Wassmann, M. Anger, M. Schuh, K.G. Wirth, H. Xu, W. Helmhart, H. Kudo, M. McKay, B. Maro, J. Ellenberg, P. de Boer, and K. Nasmyth. 2006. Resolution of chiasmata in oocytes requires separase-mediated proteolysis. *Cell*. 126:135-146.
Kumar, R., H.-M.M. Bourbon, and B. de Massy. 2010. Functional conservation of Mei4 for meiotic DNA double-strand break formation from yeasts to mice. *Genes & development*. 24:1266-1280.
Kumar, R., C. Oliver, C. Brun, A.B. Juarez-Martinez, Y. Tarabay, J. Kadlec, and B. de Massy. 2018. Mouse REC114 is essential for meiotic DNA double-

strand break formation and forms a complex with MEI4. *Life science alliance*. 1.
Kyogoku, H., and T.S. Kitajima. 2017. Large Cytoplasm Is Linked to the Error-Prone Nature of Oocytes. *Developmental Cell*. 41:287-2980000.
Lam, I., and S. Keeney. 2015. Mechanism and Regulation of Meiotic Recombination Initiation. *Cold Spring Harbor Perspectives in Biology*. 7.
Lane, S.I., Y. Yun, and K.T. Jones. 2012. Timing of anaphase-promoting complex activation in mouse oocytes is predicted by microtubule-kinetochore attachment but not by bivalent alignment or tension. *Development (Cambridge, England)*. 139:1947-1955.
Ledan, E., Z. Polanski, M.E. Terret, and B. Maro. 2001. Meiotic maturation of the mouse oocyte requires an equilibrium between cyclin B synthesis and degradation. *Developmental biology*. 232:400-413.
Lee, J., and T. Hirano. 2011. RAD21L, a novel cohesin subunit implicated in linking homologous chromosomes in mammalian meiosis. *The Journal of cell biology*. 192:263-276.
Li, J., G.W. Hooker, and S.G. Roeder. 2006a. S. cerevisiae Mer2, Mei4 and Rec114 form a complex required for meiotic double-strand break formation. *Genetics*.
Li, J., A. Mahajan, and T.-M.D. Biochemistry. 2006b. Ankyrin repeat: a unique motif mediating protein− protein interactions. *Biochemistry*.
Li, J., J.-X.X. Tang, J.-M.M. Cheng, B. Hu, Y.-Q.Q. Wang, B. Aalia, X.-Y.Y. Li, C. Jin, X.-X.X. Wang, S.-L.L. Deng, Y. Zhang, S.-R.R. Chen, W.-P.P. Qian, Q.-Y.Y. Sun, X.-X.X. Huang, and Y.-X.X. Liu. 2018. Cyclin B2 can compensate for Cyclin B1 in oocyte meiosis I. *The Journal of cell biology*.
Li, X.C., X. Li, and J.C. Schimenti. 2007. Mouse pachytene checkpoint 2 (trip13) is required for completing meiotic recombination but not synapsis. *PLoS genetics*. 3.
Libby, B.J., R. De La Fuente, M.J. O'Brien, K. Wigglesworth, J. Cobb, A. Inselman, S. Eaker, M.A. Handel, J.J. Eppig, and J.C. Schimenti. 2002. The mouse meiotic mutation mei1 disrupts chromosome synapsis with sexually dimorphic consequences for meiotic progression. *Developmental biology*. 242:174-187.
Lim, S., and P. Kaldis. 2013. Cdks, cyclins and CKIs: roles beyond cell cycle regulation. *Development (Cambridge, England)*. 140:3079-3093.
Lischetti, T., and J. Nilsson. 2015. Regulation of mitotic progression by the spindle assembly checkpoint. *Molecular & cellular oncology*. 2.
Littlepage, E., and J. Ruderman. 2002. Identification of a new APC/C recognition domain, the A box, which is required for the Cdh1-dependent destruction of the kinase Aurora-A during mitotic exit. *Genes & development*.
Liu, D., M.M. Matzuk, W.K. Sung, Q. Guo, P. Wang, and D.J. Wolgemuth. 1998. Cyclin A1 is required for meiosis in the male mouse. *Nature genetics*. 20:377-380.
Lozano, J.-C.C., E. Perret, P. Schatt, C. Arnould, G. Peaucellier, and A. Picard. 2002. Molecular cloning, gene localization, and structure of human cyclin B3. *Biochemical and biophysical research communications*. 291:406-413.

Lozano, J.-C.C., V. Vergé, P. Schatt, J.L. Juengel, and G. Peaucellier. 2012. Evolution of cyclin B3 shows an abrupt three-fold size increase, due to the extension of a single exon in placental mammals, allowing for new protein-protein interactions. *Molecular biology and evolution*. 29:3855-3871.

Madgwick, S., D.V. Hansen, M. Levasseur, P.K. Jackson, and K.T. Jones. 2006. Mouse Emi2 is required to enter meiosis II by reestablishing cyclin B1 during interkinesis. *The Journal of Cell Biology*. 174:791-801.

Mahadevaiah, S.K., J.M. Turner, F. Baudat, E.P. Rogakou, P. de Boer, J. Blanco-Rodríguez, M. Jasin, S. Keeney, W.M. Bonner, and P.S. Burgoyne. 2001. Recombinational DNA double-strand breaks in mice precede synapsis. *Nature genetics*. 27:271-276.

Maleki, S., M.J. Neale, C. Arora, K.A. Henderson, and S. Keeney. 2007. Interactions between Mei4, Rec114, and other proteins required for meiotic DNA double-strand break formation in Saccharomyces cerevisiae. *Chromosoma*. 116:471-486.

Malone, R.E., D.L. Pittman, and J.J. Nau. 1997. Examination of the intron in the meiosis-specific recombination gene REC114 in Saccharomyces. *Molecular & general genetics : MGG*. 255:410-419.

Malumbres, M., and M. Barbacid. 2001. To cycle or not to cycle: a critical decision in cancer. *Nature reviews. Cancer*. 1:222-231.

Malumbres, M., and M. Barbacid. 2005. Mammalian cyclin-dependent kinases. *Trends in biochemical sciences*. 30:630-641.

Malumbres, M., and M. Barbacid. 2009. Cell cycle, CDKs and cancer: a changing paradigm. *Nature reviews. Cancer*. 9:153-166.

Malumbres, M., E. Harlow, T. Hunt, T. Hunter, J.M. Lahti, G. Manning, D.O. Morgan, L.-H.H. Tsai, and D.J. Wolgemuth. 2009. Cyclin-dependent kinases: a family portrait. *Nature cell biology*. 11:1275-1276.

Malumbres, M., R. Sotillo, D. Santamaría, J. Galán, A. Cerezo, S. Ortega, P. Dubus, and M. Barbacid. 2004. Mammalian cells cycle without the D-type cyclin-dependent kinases Cdk4 and Cdk6. *Cell*. 118:493-504.

Margolin, G., P.P. Khil, J. Kim, M.A. Bellani, and R.D. Camerini-Otero. 2014. Integrated transcriptome analysis of mouse spermatogenesis. *BMC genomics*. 15:39.

Martinerie, L., M. Manterola, S.S. Chung, S.K. Panigrahi, M. Weisbach, A. Vasileva, Y. Geng, P. Sicinski, and D.J. Wolgemuth. 2014. Mammalian E-type cyclins control chromosome pairing, telomere stability and CDK2 localization in male meiosis. *PLoS genetics*. 10.

Masui, Y., and C.L. Markert. 1971. Cytoplasmic control of nuclear behavior during meiotic maturation of frog oocytes. *The Journal of experimental zoology*. 177:129-145.

Matsuno, K., M. Kumano, Y. Kubota, Y. Hashimoto, and H. Takisawa. 2006. The N-terminal noncatalytic region of Xenopus RecQ4 is required for chromatin binding of DNA polymerase alpha in the initiation of DNA replication. *Molecular and cellular biology*. 26:4843-4852.

Meijer, L., A. Borgne, O. Mulner, J.P. Chong, J.J. Blow, N. Inagaki, M. Inagaki, J.G. Delcros, and J.P. Moulinoux. 1997. Biochemical and cellular effects

of roscovitine, a potent and selective inhibitor of the cyclin-dependent kinases cdc2, cdk2 and cdk5. *European journal of biochemistry*. 243:527-536.
Menees, T.M., and G.S. Roeder. 1989. MEI4, a yeast gene required for meiotic recombination. *Genetics*. 123:675-682.
Mikolcevic, P., R. Sigl, V. Rauch, M.W. Hess, K. Pfaller, M. Barisic, L.J. Pelliniemi, M. Boesl, and S. Geley. 2012. Cyclin-dependent kinase 16/PCTAIRE kinase 1 is activated by cyclin Y and is essential for spermatogenesis. *Molecular and cellular biology*. 32:868-879.
Miles, D.C., J.A. van den Bergen, A.H. Sinclair, and P.S. Western. 2010. Regulation of the female mouse germ cell cycle during entry into meiosis. *Cell cycle (Georgetown, Tex.)*. 9:408-418.
Miller, M.P., E. Unal, G.A. Brar, and A. Amon. 2012. Meiosis I chromosome segregation is established through regulation of microtubule-kinetochore interactions. *eLife*. 1.
Miyata, H., J.M. Castaneda, Y. Fujihara, Z. Yu, D.R. Archambeault, A. Isotani, D. Kiyozumi, M.L. Kriseman, D. Mashiko, and T. Matsumura. 2016. Genome engineering uncovers 54 evolutionarily conserved and testis-enriched genes that are not required for male fertility in mice. *Proceedings of the National Academy of Sciences*. 113:7704-7710.
Miyoshi, T., M. Ito, K. Kugou, S. Yamada, and F.-M. cell. 2012. A central coupler for recombination initiation linking chromosome architecture to S phase checkpoint. *Molecular cell*.
Moens, P.B., N.K. Kolas, M. Tarsounas, E. Marcon, P.E. Cohen, and B. Spyropoulos. 2002. The time course and chromosomal localization of recombination-related proteins at meiosis in the mouse are compatible with models that can resolve the early DNA-DNA interactions without reciprocal recombination. *Journal of cell science*. 115:1611-1622.
Morgan, D.O. 1997. Cyclin-dependent kinases: engines, clocks, and microprocessors. *Annual review of cell and developmental biology*. 13:261-291.
Morgan, D.O. 2007. The cell cycle: principles of control. *The cell cycle: principles of control*.
Möröy, T., and C. Geisen. 2004. Cyclin E. *The international journal of biochemistry & cell biology*. 36:1424-1439.
Mueller, A.C., M.A. Keaton, and A. Dutta. 2011. DNA replication: mammalian Treslin-TopBP1 interaction mirrors yeast Sld3-Dpb11. *Current biology : CB*. 21:40.
Murakami, H., and S. Keeney. 2014. Temporospatial Coordination of Meiotic DNA Replication and Recombination via DDK Recruitment to Replisomes. *Cell*. 158:861-873.
Murphy, M., M.G. Stinnakre, C. Senamaud-Beaufort, N.J. Winston, C. Sweeney, M. Kubelka, M. Carrington, C. Bréchot, and J. Sobczak-Thépot. 1997. Delayed early embryonic lethality following disruption of the murine cyclin A2 gene. *Nature genetics*. 15:83-86.

Murray, A.W. 1989. Cyclin synthesis and degradation and the embryonic cell cycle. *Journal of cell science. Supplement*. 12:65-76.
Murray, A.W. 2004. Recycling the cell cycle: cyclins revisited. *Cell*. 116:221-234.
Musacchio, A., and K.G. Hardwick. 2002. The spindle checkpoint: structural insights into dynamic signalling. *Nature reviews. Molecular cell biology*. 3:731-741.
Musacchio, A., and E.D. Salmon. 2007. The spindle-assembly checkpoint in space and time. *Nature reviews. Molecular cell biology*. 8:379-393.
Nguyen, T.B., K. Manova, P. Capodieci, C. Lindon, S. Bottega, X.-Y.Y. Wang, J. Refik-Rogers, J. Pines, D.J. Wolgemuth, and A. Koff. 2002. Characterization and expression of mammalian cyclin b3, a prepachytene meiotic cyclin. *The Journal of biological chemistry*. 277:41960-41969.
Niault, T., K. Hached, R. Sotillo, P.K. Sorger, B. Maro, R. Benezra, and K. Wassmann. 2007. Changing Mad2 levels affects chromosome segregation and spindle assembly checkpoint control in female mouse meiosis I. *PloS one*. 2.
Nickerson, H.D., A. Joshi, and D.J. Wolgemuth. 2007. Cyclin A1-deficient mice lack histone H3 serine 10 phosphorylation and exhibit altered aurora B dynamics in late prophase of male meiosis. *Developmental biology*. 306:725-735.
Nigg, E.A. 2001. Cell cycle regulation by protein kinases and phosphatases. *Ernst Schering Research Foundation workshop*:19-46.
Nikalayevich, E., N. Bouftas, and K. Wassmann. 2018. Detection of Separase Activity Using a Cleavage Sensor in Live Mouse Oocytes. *Methods in molecular biology (Clifton, N.J.)*. 1818:99-112.
Nurse, P. 1990. Universal control mechanism regulating onset of M-phase. *Nature*. 344:503-508.
Nurse, P., and P. Thuriaux. 1980. Regulatory genes controlling mitosis in the fission yeast Schizosaccharomyces pombe. *Genetics*. 96:627-637.
Odorisio, T., T.A. Rodriguez, E.P. Evans, and C.-A.R. Nature …. 1998. The meiotic checkpoint monitoring sypapsis eliminates spermatocytes via p53-independent apoptosis. *Nature …*.
Ortega, S., I. Prieto, J. Odajima, A. Martín, P. Dubus, R. Sotillo, J.L. Barbero, M. Malumbres, and M. Barbacid. 2003. Cyclin-dependent kinase 2 is essential for meiosis but not for mitotic cell division in mice. *Nature genetics*. 35:25-31.
Page, S.L., and R.S. Hawley. 2003. Chromosome choreography: the meiotic ballet. *Science (New York, N.Y.)*. 301:785-789.
Parisi, T., A.R. Beck, N. Rougier, T. McNeil, L. Lucian, Z. Werb, and B. Amati. 2003. Cyclins E1 and E2 are required for endoreplication in placental trophoblast giant cells. *The EMBO journal*. 22:4794-4803.
Peters, J.-M.M. 2006. The anaphase promoting complex/cyclosome: a machine designed to destroy. *Nature reviews. Molecular cell biology*. 7:644-656.
Petronczki, M., M.F. Siomos, and K. Nasmyth. 2003. Un ménage à quatre: the molecular biology of chromosome segregation in meiosis. *Cell*. 112:423-440.

Pfleger, C.M., and M.W. Kirschner. 2000. The KEN box: an APC recognition signal distinct from the D box targeted by Cdh1. *Genes & development*.
Pines, J. 2011. Cubism and the cell cycle: the many faces of the APC/C. *Nature reviews. Molecular cell biology*. 12:427-438.
Pines, J., and T. Hunter. 1990. Human cyclin A is adenovirus E1A-associated protein p60 and behaves differently from cyclin B. *Nature*. 346:760-763.
Polański, Z. 1997. Genetic background of the differences in timing of meiotic maturation in mouse oocytes: a study using recombinant inbred strains. *Journal of reproduction and fertility*. 109:109-114.
Polański, Z., H. Homer, and J.Z. Kubiak. 2012. Cyclin B in mouse oocytes and embryos: importance for human reproduction and aneuploidy. *Results and problems in cell differentiation*. 55:69-91.
Polanski, Z., E. Ledan, S. Brunet, S. Louvet, M.H. Verlhac, J.Z. Kubiak, and B. Maro. 1998. Cyclin synthesis controls the progression of meiotic maturation in mouse oocytes. *Development (Cambridge, England)*. 125:4989-4997.
Prieto, I., J.A. Suja, N. Pezzi, L. Kremer, C. Martínez-A, J.S. Rufas, and J.L. Barbero. 2001. Mammalian STAG3 is a cohesin specific to sister chromatid arms in meiosis I. *Nature cell biology*. 3:761-766.
Primorac, I., and A.J. Musacchio. 2013. Panta rhei: the APC/C at steady state. *J Cell Biol*.
Qiao, R., F. Weissmann, M. Yamaguchi, N.G. Brown, R. VanderLinden, R. Imre, M.A. Jarvis, M.R. Brunner, I.F. Davidson, G. Litos, D. Haselbach, K. Mechtler, H. Stark, B.A. Schulman, and J.-M.M. Peters. 2016. Mechanism of APC/CCDC20 activation by mitotic phosphorylation. *Proceedings of the National Academy of Sciences of the United States of America*. 113:8.
Rattani, A., P.K. Vinod, J. Godwin, K. Tachibana-Konwalski, M. Wolna, M. Malumbres, B. Novák, and K. Nasmyth. 2014. Dependency of the spindle assembly checkpoint on Cdk1 renders the anaphase transition irreversible. *Current biology : CB*. 24:630-637.
Ravnik, S.E., and D.J. Wolgemuth. 1996. The developmentally restricted pattern of expression in the male germ line of a murine cyclin A, cyclin A2, suggests roles in both mitotic and meiotic cell cycles. *Developmental biology*. 173:69-78.
Refik-Rogers, J., K. Manova, and A. Koff. 2006. Misexpression of cyclin B3 leads to aberrant spermatogenesis. *Cell cycle (Georgetown, Tex.)*. 5:1966-1973.
Reis, A., H.-Y.Y. Chang, M. Levasseur, and K.T. Jones. 2006. APCcdh1 activity in mouse oocytes prevents entry into the first meiotic division. *Nature cell biology*. 8:539-540.
Revenkova, E., M. Eijpe, C. Heyting, C.A. Hodges, P.A. Hunt, B. Liebe, H. Scherthan, and R. Jessberger. 2004. Cohesin SMC1 beta is required for meiotic chromosome dynamics, sister chromatid cohesion and DNA recombination. *Nature cell biology*. 6:555-562.
Robert, T., A. Nore, C. Brun, C. Maffre, B. Crimi, H.M.M. Bourbon, and B. de Massy. 2016. The TopoVIB-Like protein family is required for meiotic DNA double-strand break formation. *Science (New York, N.Y.)*. 351:943-949.

Romanienko, P.J., J. Giacalone, J. Ingenito, Y. Wang, M. Isaka, T. Johnson, Y. You, and W.H. Mark. 2016. A Vector with a Single Promoter for In Vitro Transcription and Mammalian Cell Expression of CRISPR gRNAs. *PloS one*. 11.

Russell, P., and P. Nurse. 1986. Schizosaccharomyces pombe and Saccharomyces cerevisiae: a look at yeasts divided. *Cell*. 45:781-782.

Sachdeva, U.M., and J.M. O'Brien. 2012. Understanding pRb: toward the necessary development of targeted treatments for retinoblastoma. *The Journal of clinical investigation*. 122:425-434.

Sanchez-Pulido, L., J.F. Diffley, and C.P. Ponting. 2010. Homology explains the functional similarities of Treslin/Ticrr and Sld3. *Current biology : CB*. 20:10.

Sangrithi, M.N., J.A. Bernal, M. Madine, A. Philpott, J. Lee, W.G. Dunphy, and A.R. Venkitaraman. 2005. Initiation of DNA replication requires the RECQL4 protein mutated in Rothmund-Thomson syndrome. *Cell*. 121:887-898.

Santaguida, S., A. Tighe, A.M. D'Alise, S.S. Taylor, and A. Musacchio. 2010. Dissecting the role of MPS1 in chromosome biorientation and the spindle checkpoint through the small molecule inhibitor reversine. *The Journal of cell biology*. 190:73-87.

Santamaría, D., C. Barrière, A. Cerqueira, S. Hunt, C. Tardy, K. Newton, J.F. Cáceres, P. Dubus, M. Malumbres, and M. Barbacid. 2007. Cdk1 is sufficient to drive the mammalian cell cycle. *Nature*. 448:811-815.

Saredi, G., H. Huang, C.M. Hammond, C. Alabert, S. Bekker-Jensen, I. Forne, N. Reverón-Gómez, B.M. Foster, L. Mlejnkova, T. Bartke, P. Cejka, N. Mailand, A. Imhof, D.J. Patel, and A. Groth. 2016. H4K20me0 marks post-replicative chromatin and recruits the TONSL–MMS22L DNA repair complex. *Nature*. 534:714-718.

Sasanuma, H., K. Hirota, T. Fukuda, N. Kakusho, K. Kugou, Y. Kawasaki, T. Shibata, H. Masai, and K. Ohta. 2008. Cdc7-dependent phosphorylation of Mer2 facilitates initiation of yeast meiotic recombination. *Genes & development*. 22:398-410.

Satyanarayana, A., and P. Kaldis. 2009. Mammalian cell-cycle regulation: several Cdks, numerous cyclins and diverse compensatory mechanisms. *Oncogene*. 28:2925-2939.

Scherthan, H. 2001. A bouquet makes ends meet. *Nature reviews. Molecular cell biology*. 2:621-627.

Schramm, S., J. Fraune, R. Naumann, A. Hernandez-Hernandez, C. Höög, H.J. Cooke, M. Alsheimer, and R. Benavente. 2011. A novel mouse synaptonemal complex protein is essential for loading of central element proteins, recombination, and fertility. *PLoS genetics*. 7.

Schulman, B.A., D.L. Lindstrom, and E. Harlow. 1998. Substrate recruitment to cyclin-dependent kinase 2 by a multipurpose docking site on cyclin A. *Proceedings of the National Academy of Sciences of the United States of America*. 95:10453-10458.

Schultz, N., and H.-F. K. 2003. A multitude of genes expressed solely in meiotic or postmeiotic spermatogenic cells offers a myriad of contraceptive targets. *Proceedings of the …*.

Session, D.R., M.P. Fautsch, R. Avula, W.R. Jones, A. Nehra, and E.D. Wieben. 2001. Cyclin-dependent kinase 5 is expressed in both Sertoli cells and metaphase spermatocytes. *Fertility and sterility*. 75:669-673.

Sherr, C.J. 1994. G1 phase progression: cycling on cue. *Cell*. 79:551-555.

Sherr, C.J., and R.-J. M. 1999. CDK inhibitors: positive and negative regulators of G1-phase progression. *Genes & development*.

Sherr, C.J., and J.M. Roberts. 1999. CDK inhibitors: positive and negative regulators of G1-phase progression. *Genes & development*. 13:1501-1512.

Shindo, N., K. Kumada, and T. Hirota. 2012. Separase sensor reveals dual roles for separase coordinating cohesin cleavage and cdk1 inhibition. *Developmental cell*. 23:112-123.

Shinohara, A., and M. Shinohara. 2004. Roles of RecA homologues Rad51 and Dmc1 during meiotic recombination. *Cytogenetic and genome research*. 107:201-207.

Shoji, S., N. Yoshida, M. Amanai, M. Ohgishi, T. Fukui, S. Fujimoto, Y. Nakano, E. Kajikawa, and A.C.F. Perry. 2006. Mammalian Emi2 mediates cytostatic arrest and transduces the signal for meiotic exit via Cdc20. *The EMBO Journal*. 25:834-845.

Sicinska, E., I. Aifantis, L. Le Cam, W. Swat, C. Borowski, Q. Yu, A.A. Ferrando, S.D. Levin, Y. Geng, H. von Boehmer, and P. Sicinski. 2003. Requirement for cyclin D3 in lymphocyte development and T cell leukemias. *Cancer cell*. 4:451-461.

Sicinski, P., J.L. Donaher, Y. Geng, S.B. Parker, H. Gardner, M.Y. Park, R.L. Robker, J.S. Richards, L.K. McGinnis, J.D. Biggers, J.J. Eppig, R.T. Bronson, S.J. Elledge, and R.A. Weinberg. 1996. Cyclin D2 is an FSH-responsive gene involved in gonadal cell proliferation and oncogenesis. *Nature*. 384:470-474.

Sicinski, P., J.L. Donaher, S.B. Parker, T. Li, A. Fazeli, H. Gardner, S.Z. Haslam, R.T. Bronson, S.J. Elledge, and R.A. Weinberg. 1995. Cyclin D1 provides a link between development and oncogenesis in the retina and breast. *Cell*. 82:621-630.

Sigrist, S., H. Jacobs, R. Stratmann, and C.F. Lehner. 1995. Exit from mitosis is regulated by Drosophila fizzy and the sequential destruction of cyclins A, B and B3. *The EMBO journal*. 14:4827-4838.

Sigrist, S.J., and C.F. Lehner. 1997. Drosophila fizzy-related down-regulates mitotic cyclins and is required for cell proliferation arrest and entry into endocycles. *Cell*. 90:671-681.

Sivakumar, S., and G.J. Gorbsky. 2015. Spatiotemporal regulation of the anaphase-promoting complex in mitosis. *Nature Reviews Molecular Cell Biology*.

Smith, L.D., and R.E. Ecker. 1971. The interaction of steroids with Rana pipiens Oocytes in the induction of maturation. *Developmental biology*. 25:232-247.

Snowden, T., K.-S.S. Shim, C. Schmutte, S. Acharya, and R. Fishel. 2008. hMSH4-hMSH5 adenosine nucleotide processing and interactions with homologous recombination machinery. *The Journal of biological chemistry*. 283:145-154.

Solc, P., R.M. Schultz, and J. Motlik. 2010. Prophase I arrest and progression to metaphase I in mouse oocytes: comparison of resumption of meiosis and recovery from G2-arrest in somatic cells. *Molecular human reproduction*. 16:654-664.

Speed, R.M. 1982. Meiosis in the foetal mouse ovary. I. An analysis at the light microscope level using surface-spreading. *Chromosoma*. 85:427-437.

Stanzione, M., M. Baumann, F. Papanikos, I. Dereli, J. Lange, A. Ramlal, D. Tränkner, H. Shibuya, B. de Massy, Y. Watanabe, M. Jasin, S. Keeney, and A. Tóth. 2016. Meiotic DNA break formation requires the unsynapsed chromosome axis-binding protein IHO1 (CCDC36) in mice. *Nature cell biology*. 18:1208-1220.

Stemmann, O., I.H. Gorr, and D. Boos. 2006. Anaphase topsy-turvy: Cdk1 a securin, separase a CKI. *Cell cycle (Georgetown, Tex.)*. 5:11-13.

Stuart, D., and C. Wittenberg. 1998. CLB5 and CLB6 are required for premeiotic DNA replication and activation of the meiotic S/M checkpoint. *Genes & development*. 12:2698-2710.

Sunkara, P.S., D.A. Wright, and R.-P.N. of the. 1979. Mitotic factors from mammalian cells induce germinal vesicle breakdown and chromosome condensation in amphibian oocytes. *Proceedings of the …*.

Sutton, K.A., M.K. Jungnickel, and H.M. Florman. 2008. A polycystin-1 controls postcopulatory reproductive selection in mice. *Proceedings of the National Academy of Sciences of the United States of America*. 105:8661-8666.

Swanson, W.J., and V.-V.D. reviews genetics. 2002. The rapid evolution of reproductive proteins. *Nature reviews genetics*.

Sweeney, C., M. Murphy, M. Kubelka, S.E. Ravnik, C.F. Hawkins, D.J. Wolgemuth, and M. Carrington. 1996. A distinct cyclin A is expressed in germ cells in the mouse. *Development*. 122:53-64.

Tachibana, K., and N. Yanagishima. 1987. Preliminary characterization of maturation-promoting factor from yeast Saccharomyces cerevisiae. *Journal of cell …*.

Tanaka, S., T. Umemori, K. Hirai, S. Muramatsu, Y. Kamimura, and H. Araki. 2007. CDK-dependent phosphorylation of Sld2 and Sld3 initiates DNA replication in budding yeast. *Nature*. 445:328-332.

Tang, J.-X., D. Chen, S.-L. Deng, J. Li, Y. Li, Z. Fu, X.-X. Wang, Y. Zhang, S.-R. Chen, and Y.-X. Liu. 2018. CRISPR/Cas9-mediated genome editing induces gene knockdown by altering the pre-mRNA splicing in mice. *BMC Biotechnology*. 18.

Terret, M.E., K. Wassmann, I. Waizenegger, B. Maro, J.M. Peters, and M.H. Verlhac. 2003. The meiosis I-to-meiosis II transition in mouse oocytes requires separase activity. *Current biology : CB*. 13:1797-1802.

Tessé, S., H.-M.M. Bourbon, R. Debuchy, K. Budin, E. Dubois, Z. Liangran, R. Antoine, T. Piolot, N. Kleckner, D. Zickler, and E. Espagne. 2017. Asy2/Mer2: an evolutionarily conserved mediator of meiotic recombination, pairing, and global chromosome compaction. *Genes & development*. 31:1880-1893.

Tingen, C., A. Kim, and T.K. Woodruff. 2009. The primordial pool of follicles and nest breakdown in mammalian ovaries. *Molecular human reproduction*. 15:795-803.

Touati, S.A., E. Buffin, D. Cladière, K. Hached, C. Rachez, J.M. van Deursen, and K. Wassmann. 2015. Mouse oocytes depend on BubR1 for proper chromosome segregation but not for prophase I arrest. *Nature communications*. 6:6946.

Touati, S.A., D. Cladière, L.M. Lister, I. Leontiou, J.-P.P. Chambon, A. Rattani, F. Böttger, O. Stemmann, K. Nasmyth, M. Herbert, and K. Wassmann. 2012. Cyclin A2 is required for sister chromatid segregation, but not separase control, in mouse oocyte meiosis. *Cell reports*. 2:1077-1087.

Touati, S.A., and K. Wassmann. 2016. How oocytes try to get it right: spindle checkpoint control in meiosis. *Chromosoma*. 125:321-335.

Treen, N., T. Heist, W. Wang, and M. Levine. 2018. Depletion of Maternal Cyclin B3 Contributes to Zygotic Genome Activation in the Ciona Embryo. *Current biology : CB*. 28:1150-1156.

Tsurumi, C., S. Hoffmann, S. Geley, R. Graeser, and Z. Polanski. 2004. The spindle assembly checkpoint is not essential for CSF arrest of mouse oocytes. *The Journal of cell biology*. 167:1037-1050.

van der Voet, M., M.A. Lorson, D.G. Srinivasan, K.L. Bennett, and S. van den Heuvel. 2009. C. elegans mitotic cyclins have distinct as well as overlapping functions in chromosome segregation. *Cell cycle (Georgetown, Tex.)*. 8:4091-4102.

Viera, A., J.S. Rufas, I. Martínez, J.L.L. Barbero, S. Ortega, and J.A.A. Suja. 2009. CDK2 is required for proper homologous pairing, recombination and sex-body formation during male mouse meiosis. *Journal of cell science*. 122:2149-2159.

Vogt, E., M. Kirsch-Volders, J. Parry, and U. Eichenlaub-Ritter. 2008. Spindle formation, chromosome segregation and the spindle checkpoint in mammalian oocytes and susceptibility to meiotic error. *Mutation research*. 651:14-29.

Wan, L., H. Niu, B. Futcher, C. Zhang, K.M. Shokat, S.J. Boulton, and N.M. Hollingsworth. 2008. Cdc28-Clb5 (CDK-S) and Cdc7-Dbf4 (DDK) collaborate to initiate meiotic recombination in yeast. *Genes & development*. 22:386-397.

Wang, J., X. Chenivesse, B. Henglein, and C. Bréchot. 1990. Hepatitis B virus integration in a cyclin A gene in a hepatocellular carcinoma. *Nature*. 343:555-557.

Wassmann, K., V. Liberal, and R. Benezra. 2003. Mad2 phosphorylation regulates its association with Mad1 and the APC/C. *The EMBO journal*. 22:797-806.

Wolgemuth, D.J., M. Manterola, and A. Vasileva. 2013. Role of cyclins in controlling progression of mammalian spermatogenesis. *The International journal of developmental biology*. 57:159-168.

Wolgemuth, D.J., and S.S. Roberts. 2010. Regulating mitosis and meiosis in the male germ line: critical functions for cyclins. *Philosophical transactions of the Royal Society of London. Series B, Biological sciences*. 365:1653-1662.

Xu, H., M.D. Beasley, W.D. Warren, G.T. van der Horst, and M.J. McKay. 2005. Absence of mouse REC8 cohesin promotes synapsis of sister chromatids in meiosis. *Developmental cell*. 8:949-961.

Yamaguchi, M., R. VanderLinden, F. Weissmann, and R. Qiao. 2016. Cryo-EM of mitotic checkpoint complex-bound APC/C reveals reciprocal and conformational regulation of ubiquitin ligation. *Molecular cell*.

Yang, F., R. De La Fuente, N.A. Leu, C. Baumann, K.J. McLaughlin, and P.J. Wang. 2006. Mouse SYCP2 is required for synaptonemal complex assembly and chromosomal synapsis during male meiosis. *The Journal of cell biology*. 173:497-507.

Yang, R., R. Morosetti, and K.-H.P. Research. 1997. Characterization of a second human cyclin A that is highly expressed in testis and in several leukemic cell lines. *Cancer Research*.

Yoshinaga, K., S. Nishikawa, M. Ogawa, and H.-S. …. 1991. Role of c-kit in mouse spermatogenesis: identification of spermatogonia as a specific site of c-kit expression and function. *….*

Yu, Q., and P. Sicinski. 2004. Mammalian cell cycles without cyclin E-CDK2. *Cell cycle (Georgetown, Tex.)*. 3:292-295.

Yuan, K., and P.H. O'Farrell. 2015. Cyclin B3 is a mitotic cyclin that promotes the metaphase-anaphase transition. *Current biology : CB*. 25:811-816.

Yuan, L., J.G. Liu, J. Zhao, E. Brundell, B. Daneholt, and C. Höög. 2000. The murine SCP3 gene is required for synaptonemal complex assembly, chromosome synapsis, and male fertility. *Molecular cell*. 5:73-83.

Yufei Li, Leyun Wang, Linlin Zhang, Zhengquan He, Guihai Feng, Hao Sun, Jiaqiang Wang, Zhikun Li, Chao Liu, Jiabao Han, Junjie Mao, Xuewei Yuan, Liyuan Jiang, Ying Zhang, Qi Zhou, and W. Li. 2018. Cyclin B3 is specifically required for metaphase to anaphase transition in mouse oocyte meiosis I. *bioRxiv 390351*.

Zegerman, P., and J.F. Diffley. 2007. Phosphorylation of Sld2 and Sld3 by cyclin-dependent kinases promotes DNA replication in budding yeast. *Nature*. 445:281-285.

Zhang, T., S.-T.T. Qi, L. Huang, X.-S.S. Ma, Y.-C.C. Ouyang, Y. Hou, W. Shen, H. Schatten, and Q.-Y.Y. Sun. 2015. Cyclin B3 controls anaphase onset independent of spindle assembly checkpoint in meiotic oocytes. *Cell cycle (Georgetown, Tex.)*. 14:2648-2654.

Zickler, D., and N. Kleckner. 2015. Recombination, Pairing, and Synapsis of Homologs during Meiosis. *Cold Spring Harbor perspectives in biology*. 7.